

Final Report

DEVELOPMENT OF A LOW-NOISE, COLD-CATHODE
TRAVELING-WAVE TUBE

(25 June 1964 - 31 August 1965)

Contract No. NAS 5-9002

prepared for

National Aeronautics and Space Administration
Goddard Space Flight Center
Greenbelt, Maryland

GPO PRICE \$ _____

CFSTI PRICE(S) \$ _____

Hard copy (HC) 3.80

Microfiche (MF) .75

FF 653 July 65

Microwave Electronics Corporation

FACILITY FORM 602	N 66 35580 - 35581	
	(ACCESSION NUMBER)	(THRU)
	109	1
	(PAGES)	(CODE)
	CR-71842	09
	(NASA CR OR TMX OR AD NUMBER)	(CATEGORY)

Final Report

DEVELOPMENT OF A LOW-NOISE, COLD-CATHODE
TRAVELING-WAVE TUBE

(29 June 1964 to 31 August 1965)

prepared by
G. Foggiato

September 1965

for
National Aeronautics and Space Administration
Goddard Space Flight Center
Greenbelt, Maryland
Contract No. NAS 5-9002

CONTENTS

	<u>Page</u>
ABSTRACT	iii
I. INTRODUCTION	1
II. TECHNICAL DISCUSSION	4
A. Program Objective	4
B. Cold Cathode Development	9
C. Cathode Test Structures and Techniques	16
D. TWT, Design and Evaluation	21
E. Noise Properties of the Cold Cathode	40
CONCLUSION	52
REFERENCES	53
APPENCIX A: SRI REPORT	

ILLUSTRATIONS

<u>Figure</u>	<u>Page</u>
1. Energy diagram of Schottky barrier cathode.	10
2. Test structure design.	17
3. Basic cold cathode.	18
4. Proposed cold cathode electron gun.	20
5. Electron gun.	23
6. Low-noise electron gun incorporating thermionic cathode.	24
7. Current versus grid 1 voltage, grid 2 voltage being a constant.	26
8. Beam current profile.	27
9. Voltage profile for two sets of anode voltages.	28
10. Current density profile.	30
11. Electron gun voltage and electron beam profile.	31
12. Electron gun voltage and electron beam profile.	32
13. Noise figure versus frequency.	33
14. Noise figure versus frequency.	34
15. Small-signal gain and power output versus frequency.	36
16. Small-signal gain and power output versus frequency.	37
17. Small-signal gain versus frequency for M5282, Serials 1 and 2.	38
18. Noise figure versus frequency for M5282, Serials 1 and 2.	39
19. Spectrum of noise current in semiconductors.	44

ABSTRACT

The requirements for a practical solid-state cathode are summarized, and a review of the experimental work is presented. Semiconductors ZnO and TiO_2 were extensively studied to determine their feasibility for use in a cathode. The more recent work on GaP is presented in detail. Requirements of the metal surface film and activating materials are reviewed with emphasis on metal-semiconductor contacts and low-work-function BaO-metal photosurfaces.

Development of the traveling-wave tube is reviewed and data of two fabricated tubes are presented. Studies of processing techniques and possible methods of incorporating the cathode in the TWT are given. The noise properties of the cold cathode are discussed with emphasis on the contributions from the cathode and its operation.

I. INTRODUCTION

The program objective is to develop a traveling-wave tube utilizing a cold cathode electron source. The primary task was development of the cold cathode, then adapting this cathode to operate in a traveling-wave tube. The physical and electronic compatibility of the cold cathode structure with the traveling-wave tube was the main objective.

Development of the cold cathode was subcontracted to Stanford Research Institute (SRI). Their detailed report is included as an appendix, but the cold cathode work is discussed in the main body of the report in relation to the work being done at Microwave Electronics Corporation (MEC). The SRI task was devoted to obtaining electron emission in a vacuum; once this was accomplished, MEC would then place the cathode structure in a traveling-wave tube that has operated with a standard thermionic cathode and in which ultralow noise figures have been achieved. This would permit a comparison between the two emitter types in addition to optimizing the TWT design.

Development of the TWT and techniques of inserting the cold cathode were undertaken by MEC. The TWT design was approached from the viewpoint of developing an ultralow noise TWT utilizing a thermionic cathode, then replacing it with a cold cathode. RF performance objectives are as follows:

Frequency	5.8 to 6.6 Gc
Noise Figure	---
Thermionic Cathode	5 db
Cold Cathode	3 db
Small-Signal Gain	25 db, Min.
Saturated Power Output	Approx. 1 mW, Min.

Initially, the tube was to be solenoid-focused so an optimum design could be established. Then, a permanent magnet structure was to be designed and fabricated.

In an effort to establish the TWT design, use was made of a digital computer. Since few changes can be made on the TWT helix structure to optimize noise figure, the major effort was devoted to optimizing the electron gun. The gun configurations were "programmed" for use by the computer and calculations of the potential profiles were made. With this information, another computer program was used to calculate noise figure and electron beam profiles. This approach required less time than experimental studies and, in addition, gave more accurate results.

With the completion of a gun design, the preliminary TWT's were designed and fabricated. Changes could be incorporated as needed although it was necessary to keep the number of tubes to a minimum since the major effort was oriented towards development of the cold cathode. Each tube was tested at different current levels, both to determine its RF characteristics and to minimize the cathode current. Since initial studies cannot predict current densities obtainable from cold cathodes, preliminary tests were conducted at low current densities.

Preliminary comparisons between noise properties of a cold and thermionic cathode show that both structures have noise performance advantages, but the cold cathode emitter appears to be capable of lower noise figures since it is inherently thermally cool. With a small difference between the Schottky barrier height and work function into vacuum, a narrow velocity spread of emitted electrons could also be achieved, thus further enhancing the noise figure.

The additional task pursued by MEC was to study the noise properties of a cold cathode. The study would essentially parallel the approach

taken on the tunnel cathode: in that case the barrier is a thin insulator instead of the Schottky barrier established by the metal semiconductor junction. Other effects, such as beam ripple, random electron emission, etc., all enhance the noise generated in the beam-type amplifiers. Due to the tasks required for completion, only the latter effects were studied.

II. TECHNICAL DISCUSSION

A. Program Objective

This technical discussion is directed toward identifying the tasks completed toward meeting the contract objectives. The broad objectives of the program provide for:

- Development of the Schottky cold cathode by SRI, structurally and electrically suitable for use in an ultralow-noise C-band TWT. In addition, SRI would develop the techniques for fabricating, processing and analyzing the cold cathode.
- Development by MEC of a C-band ultralow-noise TWT, having 1-milliwatt power output and 3-db noise figure objective. The effort would include studies of cathode life and noise properties of the cold cathode, cold-cathode processing in a TWT vacuum envelope and evaluating cold-cathode performance in an ultralow noise traveling-wave tube having a capability of ultralow noise operation with a thermionic cathode.

The discussion has been separated into four areas of study and experimental work, with a brief summary of the cathode development comprising the initial discussion. A more detailed description is given in the appended SRI report. Two areas are concerned with the TWT and its development with particular emphasis on adaptation to the cold cathode. The noise properties of cold cathodes and their relation to low noise traveling-wave tubes are described in the final section.

The development of a hot-electron cold cathode was undertaken by SRI as a subcontractor to MEC. The operational basis of the cold cathode consists of generating hot electrons in a thin metal surface film by forward biasing a rectifying semiconductor metal diode. Under forward bias, electrons diffuse through the semiconductor to the metal surface

film. As the electrons enter the metal films, they are accelerated to very high velocities; some of these hot electrons arrive at the metal vacuum interface with sufficient energy and momentum to enter the vacuum.

Successful operation of this cathode depends upon achieving a vacuum barrier lower than the semiconductor metal barrier. The mean free path of hot electrons in metals increases with a decrease in energy, thus to achieve the highest possible hot-electron current into the vacuum, it is desirable to make the vacuum barrier as low as possible. Therefore, the highest efficiency is achieved with the lowest possible vacuum work function.

Numerous materials have a low work function and could be used to "activate" the cathode, but many of these are impractical due to their low melting points and high vapor pressures. Thermionic work functions of metal films activated with BaO have been measured by Moore and Allison.^{1*} Their results indicate that values of approximately 1 ev are achievable, independent of the metal used. Activating the metal surface film of the cold cathode with BaO would then yield a stable 1-ev work function.

The choice of suitable materials for the semiconductor and metal surface film is dictated primarily by the requirement for a high barrier at the metal surface film interface. By using a large band-gap semiconductor with a carefully selected metal, a high barrier height may be achieved. The large band-gap semiconductor also ensures that hole currents will be negligible compared to electron currents. Many semiconductor materials meet these requirements, but careful study of the metal semiconductor junction must be undertaken to ensure a blocking contact and high barrier height with each combination of metal and semiconductor.

Materials which provide low work function into vacuum include cesium and barium, both of which are impractical because they have low melting

*All references are listed in the last section of this report.

points and high vapor pressures. Effort was expended in evaluating BaO; both to develop techniques for deposition and to achieve the lowest work function possible. BaO appears to be satisfactory in every respect and activation is more practical than with the alkali metals. Work functions down to 1.35 ev have been obtained, and it is believed possible to achieve lower values with improved processing techniques. During this program, a number of photo-tubes were fabricated, utilizing a variety of metals, namely, Ag, Pt, Mo, Ta, and W. Work function measurements were made with photo-response techniques. Up to the present time, BaO deposited on Ag has yielded the low value of 1.35 ev.

It has been found that the optimum conditions for achieving low work functions comprise slow processing and ultra-high vacuums. Evaporating source temperature is also critical since it must be kept below the disassociation temperature of barium and oxygen. Ultrahigh vacuums of 10^{-9} Torr or better using Vac-Ion systems must be achieved to prevent evaporation of any contaminating materials on the metal surface film. Better results are also obtained when the substrate is heated.

Initial experimental work on developing a cold cathode was concentrated on ZnO with silver being used for the metal film. Much difficulty was encountered when constructing ZnO cathodes using a variety of metals. Preliminary problems were the selection of low vapor pressure metals which would yield a high barrier with polycrystalline ZnO, thus leading to the study of single-crystal material. As a result of these studies, a new theory of metal semiconductor contacts was formulated to predict which metal semiconductor combinations would yield a blocking contact.

In the case of ZnO, the theory predicts (and experiments show) a blocking contact would be made with metals having a valence of one. Since the alkali metals are unsuitable, only copper, silver or gold could be used. In turn, properties such as low agglomeration temperatures would exclude

copper, gold and silver for a cathode which must withstand a high bake-out temperature cycle. A more serious problem was that Schottky barriers on single-crystal ZnO in excess of 1 ev could not be obtained.

It was therefore necessary to study other semiconductors, primarily those whose metal constituent had a higher valence than zinc (valence 2). The valence theory predicts that a much larger choice of metals for the counter electrode would be available. Based on this theory, SiC and TiO_2 were selected for study. Due to the difficulties encountered in SiC technology, TiO_2 was chosen for evaluation as the cathode semiconductor. An additional advantage of TiO_2 is its adaptability to any size and configuration of cathode desired.

Investigation of the suitability of TiO_2 was commenced by using Pt as the metal surface film. Several TiO_2 -Pt cathodes deteriorated to a short circuit during fabrication, processing and testing. Two of the cathodes yielded some Schottky barrier emission, although this could have been thermionic emission occurring from a hot spot where the short circuit existed.

A modified design utilizing a glass substrate was fabricated to establish the cause of the short circuit and possible methods of eliminating it. Several cathodes were fabricated and tested but again the I-V characteristics deteriorated to a short circuit. With further resistance measurements, it was concluded that the cathode itself became a short circuit. In the case of one cathode, some Schottky barrier emission is believed to have occurred.

Due to the poor diode characteristics and many variables associated with constructing a cathode directly, a major effort was reverted to fabricating a "good" diode, then incorporating this in a cathode. Some very pure titanium was obtained and techniques and processes were optimized to produce the best diodes obtainable. Data from measurements on TiO_2 -Pt diodes could not confirm the existence of a Schottky barrier. Very good diodes were fabricated, but since the barrier height was unknown, no meaningful information on the required vacuum work function could be acquired. Therefore,

work was discontinued with TiO_2 and other semiconductors were selected. From this effort, a considerable amount of technology was developed for surface preparation to obtain a Schottky barrier.

Another large band-gap material which has good possibilities is GaP, this being readily obtainable in large crystals. Previous investigations with GaP-Pt diodes have confirmed the existence of Schottky barriers of 1.45 eV^2 . Techniques have been developed for preparing the surfaces of GaP crystals. In addition, a good ohmic-contact material, namely, Te-doped silver, has been found and is more satisfactory as a vacuum tube material than the lead initially used.

Continuance of the cathode development is being pursued under another program. The brief summary above described the work performed to develop a cold cathode. In the following paragraphs the work performed at MEC is summarized. MEC's responsibility dealt with developing the TWT and analyzing the noise properties of the cold cathode.

A TWT was designed to give the RF performance characteristics stated above. This tube would initially utilize a thermionic cathode and optimization of the tube would be completed with this cathode. Upon successful operation of a cold cathode, the thermionic cathode would be replaced and further RF tests would be performed. Accordingly, the tube was designed to facilitate replacement of the cathode and to provide the desired characteristics at low current levels.

A digital computer was used to establish the electron gun design. Calculations were made of potential profiles to be used in noise figure calculations. Upon establishing the gun design, several tubes were fabricated and tested. As indicated later, sufficient gain was obtained even at current levels near 100 microamperes. Noise figures near 9 db were measured and further refinement of the gun design could reduce these to near 5 db. With the lower temperature associated with the cold cathode, noise figures near 3 db may be achieved. Due to the major effort being

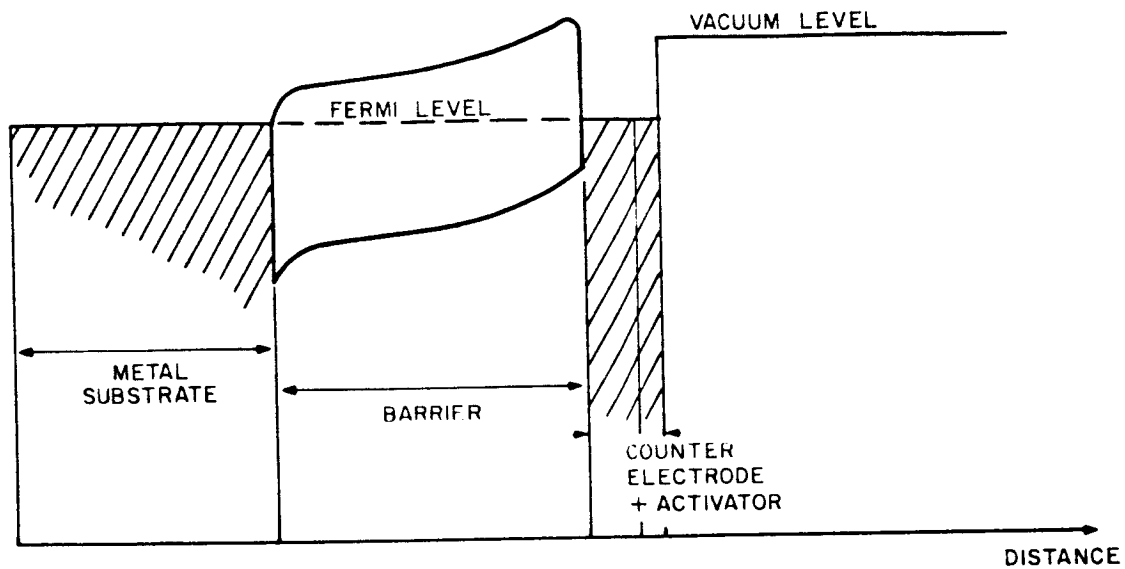
concentrated on developing an operational cold cathode, further work on the tubes was terminated. Several diodes were constructed for use upon realization of a cold cathode.

Considering the low temperature of a cold cathode, its noise properties should be enhanced appreciably over those of a thermionic cathode. One disadvantage is the velocity spread which is obtained unless the Schottky barrier height and vacuum work function are nearly the same. Some noise contributions may also be attributed to the lack of a space charge region above the cathode. This provides some velocity smoothing and may be realized by biasing the electron-gun anodes to form a potential minimum. Furthermore, the noise figure will still be nearly the same as that established by the cathode temperature, this being the ambient temperature of the structure.

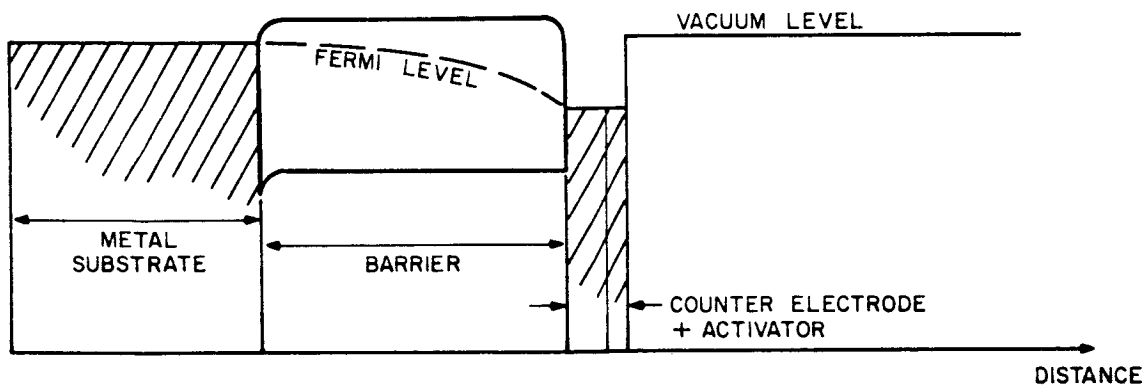
This concludes the program objectives and brief summary of the work done on this program. The following sections will describe in more detail how this work was performed and give more detailed results from the test performed. Work accomplished by SRI is summarized in the first section, with details thoroughly described in the appended SRI report. Subsequent sections describe MEC's efforts.

B. Cold Cathode Development

A brief description of the cold cathode development will be given here, with more details being described in the SRI report included as an appendix. The objective of this phase was the development of a hot-electron cold cathode for a low-level traveling-wave tube. Hot electrons, generated in a thin metal film by forward biasing a rectifying semiconductor metal diode, are accelerated to very high velocities. Those possessing sufficient energy and momentum enter the vacuum upon overcoming the potential barrier at the metal-vacuum interface. Figure 1 is an energy diagram illustrating the energy levels required for an electron to be emitted. Upon application of



a. Energy versus distance of Schottky barrier cathode without bias.



b. Energy versus distance of Schottky barrier cathode with bias.

Fig. 1. Energy diagram of Schottky barrier cathode.

a bias, the Schottky barrier is lowered thus permitting diffusion of "hot-electrons" to the thin metal film. The electrons essentially are transmitted through the metal film and those having sufficient energy to overcome the metal-vacuum barrier are emitted into vacuum.

To achieve an operational cathode, a vacuum barrier lower than the semiconductor metal barrier must be obtained. To accomplish this, materials with low work functions must be deposited on the metal surface film. A number of materials having low work functions may be used to "activate" the cathode; however, many of these are impractical for vacuum tubes due to their low melting points and high vapor pressures.

Measurements by Moore and Allison¹ indicate that work functions of 1 ev may be obtained with depositions of thin layers of BaO, independent of the metal used. They also concluded that no heat treatment of the BaO layer is required to achieve the 1-ev work function. Activating the metal surface film with BaO will result in a stable work function of approximately 1 ev. Such activation should be far more practical than using the alkali metals as an "activator".

During this program, an effort was made to measure the work function of evaporated BaO on Ag, Pt, Mo, and W. Initially, work functions of 1.55 ev were obtained on Pt, but no lower values were measured in further experiments. Evaluations of BaO evaporated on Ag gave work functions as low as 1.35 ev, but due to low-temperature agglomeration properties, this metal is unsuitable for a cathode that must withstand a high bake-out temperature cycle. Work with Mo and W was somewhat hampered when the need for a better vacuum system was decided upon. A considerable amount of work was expended to fabricate the system, and initial evaporations of Mo and W were being completed during the final phases of this program. However, preliminary measurements on Mo yielded work functions of 1.4 ev. Data thus far indicate

that the lower work functions could possibly be obtained with multiple layer films, the layer adjacent to the semiconductor forming the blacking contact and highest Schottky barrier, then a covering layer of metal to obtain the lower work functions upon evaporation of BaO. Some inconclusive data on a Ta and Pt photodiode gave work functions as low as 1.32 ev, but two intercepts were found in the Fowler plot. This indicated a work function for Pt on Ta and that of Ta only, both of which were covered with BaO.

Preliminary investigations were concentrated on utilizing ZnO as the semiconductor material. According to simple Schottky theory, many metals should form a blacking contact with ZnO, but in reality most form an ohmic or near-ohmic contact instead. Silver was found to form a blacking contact and was used for the metal surface film. Low work functions of BaO on Ag seemed very desirable, but with silver having a high vapor pressure in addition to low-agglomeration temperatures, other metals were investigated. However, after an intensive study of Schottky barriers formed by ZnO in combination with a variety of metals, the only other acceptable metals were copper and gold, and these metals, having properties similar to silver, are not suitable for this application; furthermore, copper and gold would not yield Schottky barriers greater than 1 ev, this being too low to match with a metal-vacuum barrier.

Work on ZnO was terminated and investigations on other semiconductors showed those having higher valence than zinc (valence 2) would give higher barriers. In the case of a metal oxide (or sulfide) semiconductor, the valence of the metal constituent is the important criterion. Two semiconductors were chosen for study, namely SiC and TiO_2 , both have large band gaps and are more refractory than ZnO. Due to difficulties associated with SiC technology, TiO_2 was chosen for an extensive evaluation. Additional advantages of TiO_2 are the availability of titanium and its adaptability to many mechanical configurations.

Several TiO_2 -Pt cathodes were fabricated and tested, utilizing the complete metal-ceramic substrate described in the SRI report. In every case, the I-V characteristics of the cathode deteriorated to a short circuit during fabrication, processing or testing. The short circuits occurred at small "pit" holes in the semiconductor layer. However, two cathodes apparently did give some Schottky barrier emission before becoming a complete short circuit. Both cathodes exhibited very good diode characteristics initially, but during test either heating or high voltage gradients caused the semiconductor surfaces to deteriorate.

To investigate the causes of the short circuit, a modified design utilizing glass as the substrate was fabricated and tested. In this case, the blocking contacts (Schottky barrier) deteriorated to an ohmic-contact during fabrication, processing and/or testing. Resistance measurements showed that the cathode itself became a short circuit. During initial testing, all the cathodes "emitted", but with the high bias levels required, the emission could have been either thermionic or a transverse field effect. In the case of one cathode, some Schottky emission is believed to have occurred. Transverse field emission is not desirable for low-noise tubes due to the large electron velocity spread in the beam.

An ultrahigh vacuum system was required because of the poor test data obtainable and because ultraclean semiconductor surfaces are required to yield good Schottky barriers. A system utilizing a 400 L/S titanium booster pump was constructed, thus alleviating the problem of slow pumping speeds during processing and also enhancing the vacuum obtainable. The additional pumping speed would alleviate the occluded gases being liberated from the experimental device during processing. Also, no heat is required for seal-in processes, thus reducing the deteriorating effects during processing. Much cleaner substrates could be prepared in addition to keeping the evaporants very pure. An electron beam evaporator was also purchased to provide rapid clean material depositions.

In conjunction with the work mentioned above, work was continued in evaluating TiO_2 . Further inconclusive data concerning the barrier height of TiO_2 and Pt led to the investigation of TiO_2 diodes. No barrier heights could be measured using either spectrographic methods or $1/C^2$ versus V techniques. It was thus concluded that either no barrier actually exists or that some other effects dominate when measurements are made. The work on TiO_2 was concluded and other semiconductors were introduced as possibilities. As mentioned before, SiC was considered, but very small amounts of SiC single crystal material are available, thus investigations were diverted to GaP.

Cowley and Sze² have measured the barrier heights produced by evaporating metals onto single crystals of GaP. Barriers up to 1.5 ev have been measured, the highest being obtained with Pt. Reducing the work function of Pt below 1.5 ev would give suitable materials for a cold cathode. Initially, indium or lead were to be used for ohmic contacts, but a more refractory metal was desirable. A good ohmic contact could be obtained with Te-doped silver, this being a suitable material with respect to vapor pressure.

Initial work consisted of preparing the surface of GaP crystals, this including lapping, polishing and etching. Additional experiments were performed with several metals evaporated on GaP. Final work consisted of measuring barrier heights on crystals which were carefully prepared.

From the research conducted in this phase, certain conclusive data on material requirements were found. Requirements for the semiconductor surface film, and the vacuum are presented in detail.

1. Metal Surface Film

- It must be possible to activate the film with a low-work-function coating so that the vacuum barrier is low ($\lesssim 1.3$ ev).
- The surface film must make a blocking contact with a high barrier ($\gtrsim 1.3$ ev) with the semiconductor used.

- The hot-electron mfp (mean-free-path) should be as long as possible.
- It must be possible to deposit a continuous film on the order of 100 Å in thickness.
- The sheet resistance of the film should be as low as possible.

2. Semiconductor

- A large band-gap ($\gtrsim 2$ eV) is required to minimize hole injection from the metal surface film.
- It must be possible to make an ohmic contact, which means it is necessary to dope the crystal n-type to a reasonably low resistivity.
- The semiconductor must be available in reasonably large single crystals.

3. Vacuum

- An oil-free vacuum system is required to produce a clean metal/semiconductor junction and a clean vacuum surface for the cathode.
- A vacuum of $\sim 10^{-9}$ to 10^{-10} torr is believed necessary during, and at all times subsequent to, fabrication of the cathode structure. This is necessary to achieve and maintain a low vacuum work function.

Continued study and further understanding of metal semiconductor barrier must also be pursued. In conclusion, these investigations have led to the further understanding of metal semiconductor properties in addition to almost realizing an operational Schottky barrier cathode.

C. Cathode Test Structures and Techniques

The basic requirements of the cathode test structure are a very good vacuum and some method of activating the cathode with BaO. Since BaO becomes contaminated with exposure to moisture, the most feasible method of activating the cathode is in the vacuum provided by the external test structure. Additional requirements include the bias electrodes and collector for the emitted hot-electrons. During this program, the major effort was expended towards developing the techniques for constructing and activating the cathode.

The initial test structure design is shown in Fig. 2. A barium oxide source is provided for activating the cold cathode which in this case may be a standard thermionic cathode. Figure 2 also shows the vacuum pump tubulation located near the BaO source since a major portion of the gases are occluded from this area during the conversion of BaCO_3 to BaO. In addition, these gases are pumped so that contamination of the cold cathode is kept to a minimum. Anodes 1 and 2 are provided for biasing the cold cathode with Anode 3 being the collector of any emitted hot electrons. A heater is provided for barium carbonate conversion to BaO and to evaporate BaO onto the cold cathode. In order to be used on a traveling-wave tube, this structure is modified; more anodes are needed and the barium oxide source must have a hole for passing the electron beam.

The cathode structure of Fig. 3 consists of a molybdenum base upon which a platinum rod is attached. An aluminum oxide insulation is installed around the platinum rod for mechanical rigidity and heat dissipation. The cold cathode consists of a semiconductor material bonded electrically and mechanically to the platinum rod and upon this semiconductor is deposited a thin surface film. Barium oxide is evaporated onto the thin film to yield a low work function into vacuum. To provide an external connection for applying the bias voltage, a Kovar cup is attached as shown in Fig. 3. Also, the

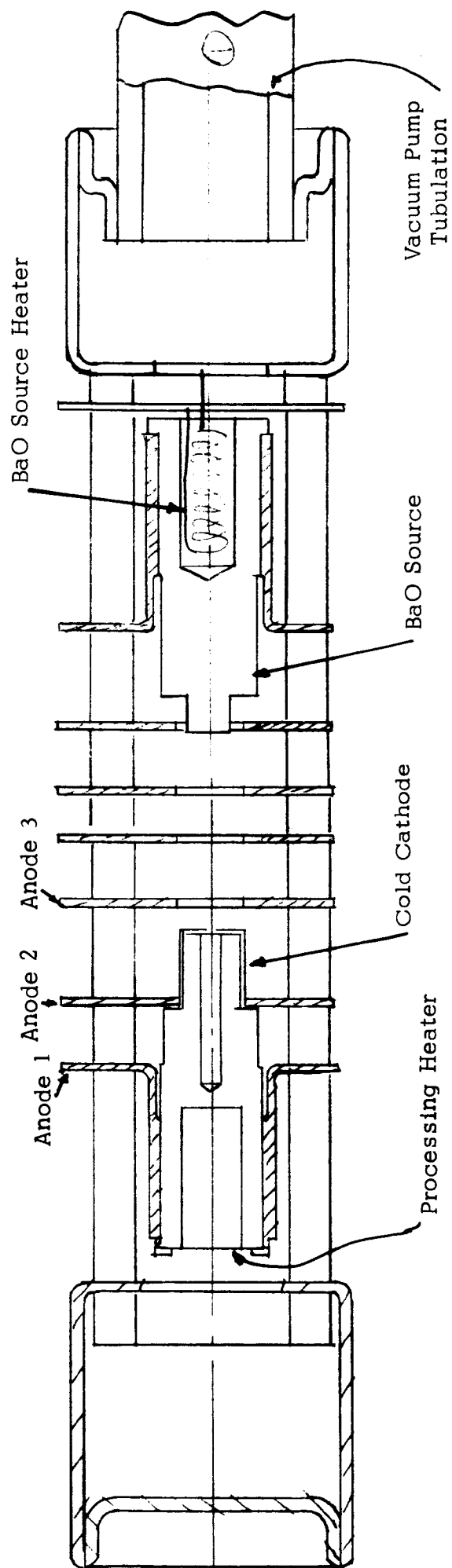


Fig. 2. Test structure design.

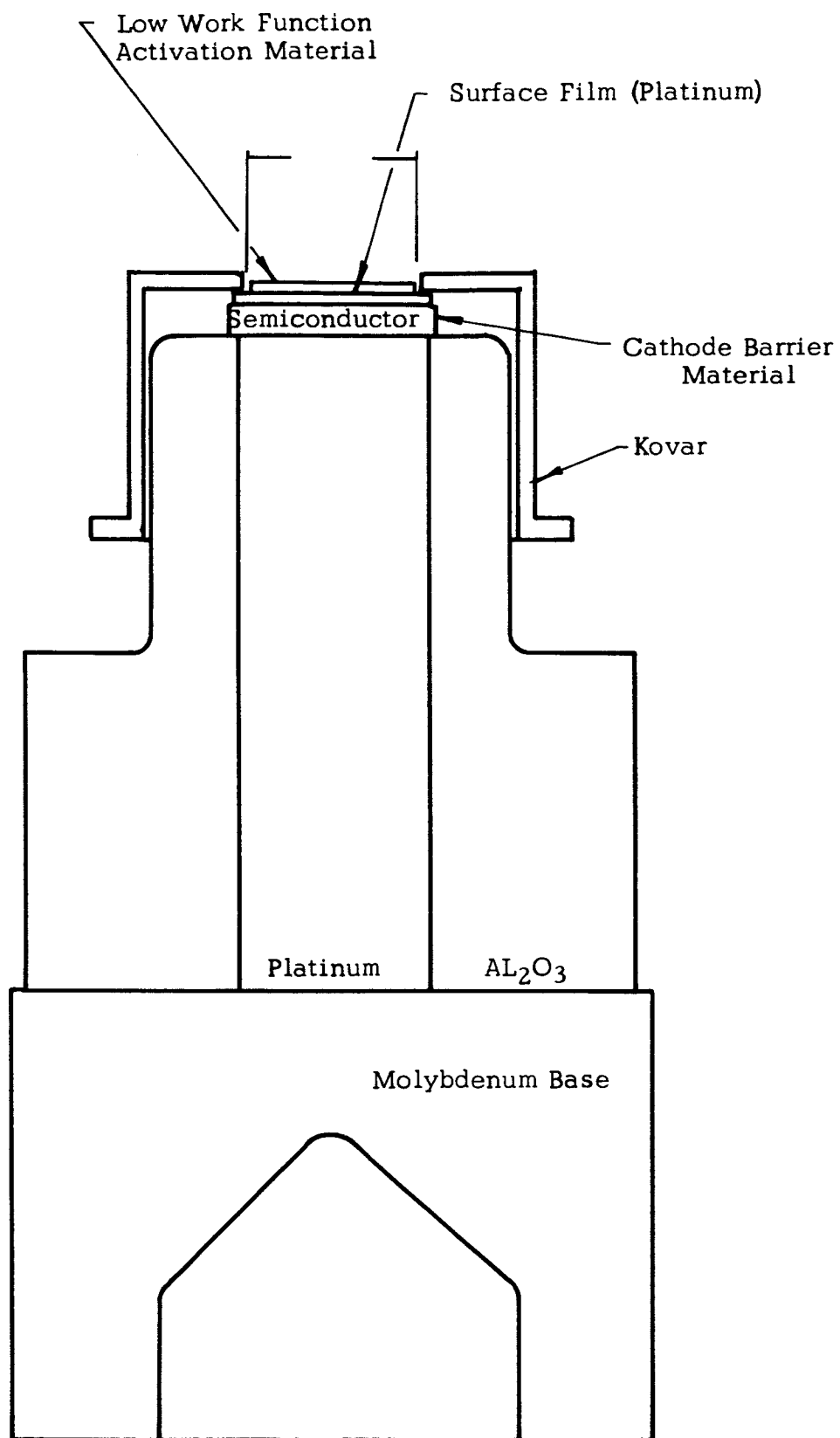


Fig. 3 . Basic cold cathode. The relative thicknesses of the various cathode materials are exaggerated.

cup helps keep the cathode correctly positioned. For additional mechanical rigidity, the Al_2O_3 insulator is brazed to the molybdenum base. To operate the cathode, two volts bias is applied across the cathode barrier material by use of the Kovar cup and molybdenum base as electrodes.

Upon realizing an operational cold cathode, it will be inserted in an electron gun structure as shown in Fig. 4. This in turn will be attached to the remainder of the traveling-wave tube vacuum envelope. A BaO source is provided for activating the cold cathode within this structure since external activation would present numerous difficulties. The processing heater will heat the cold cathode structure, thus ensuring a more uniform BaO surface layer. After a thorough bake out, the TWT will be ready for test.

With successful processing of the cold cathode, testing will be pursued, initially on a pulsed basis with increasing duty cycles until CW operation is attained. Preliminary tests on a pulsed basis will prevent cathode heating and possible deterioration of emission characteristics. The TWT RF characteristics will be determined in addition to the dc properties of the cathode. Life tests would begin on the best cathodes available to determine reliability and possible means of improving it. Further testing would be continued in a TWT which would be delivered.

Cathode fabricating and processing techniques which have been developed include the construction of a cathode and processes of activation. Construction of the cathode has been described in the previous section and the supplementary SRI report; thus only the activation processes will be described.

Experimental work by Moore and Allison, and others, have shown that work functions of 1 ev may be obtained with the proper processing techniques. Further work at SRI indicated that values near this could only be obtained with very controlled conditions, namely slow processing with ultrahigh vacuums and temperature control on both substate and evaporatant source. Meaningful quantitative data on time and temperature were not obtained due to difficulties encountered when evaporating Pt. The final experiments

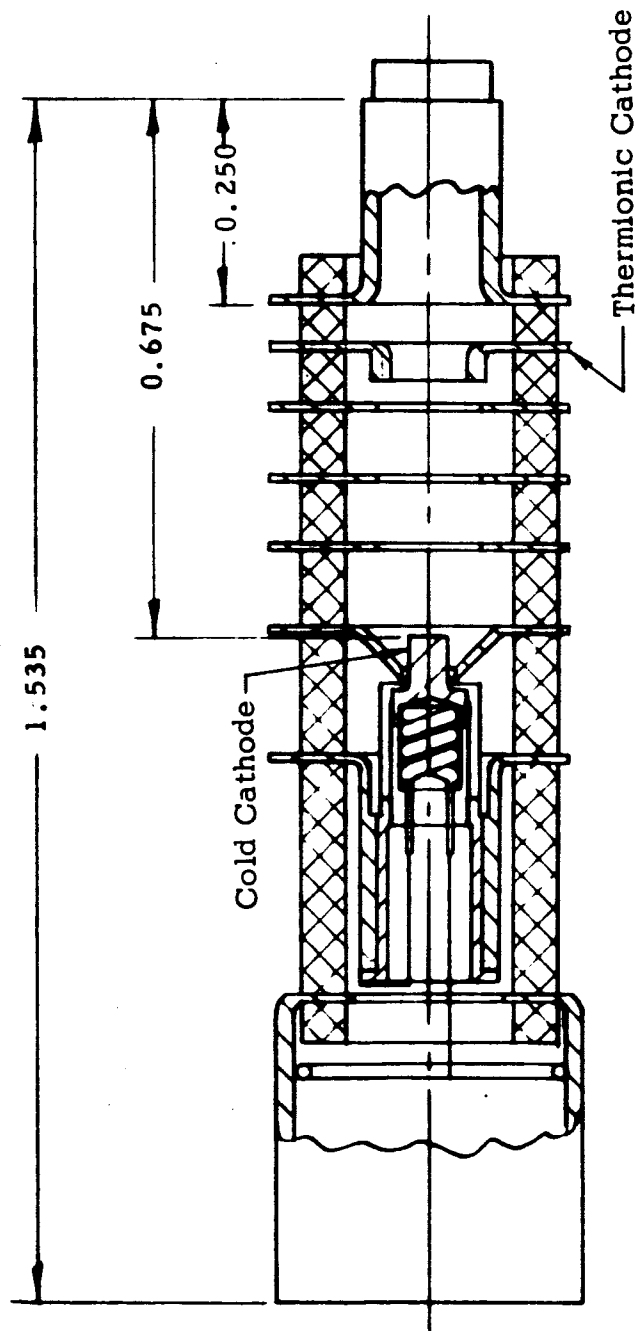


Fig. 4. Proposed cold cathode electron gun.

utilized RF heating to evaporate Pt, then, upon evaporating BaO through numerous time and temperature cycles, work functions near 1.5 ev were obtained. Temperature must be carefully controlled due to the disassociation of barium and oxygen.

This concludes the description of processing techniques and the cathode test structure. Further refinements on techniques will come about as more knowledge is acquired concerning low work function processes and technology. Areas of concern include techniques of deposition, what work function may be obtained with a variety of metals, stability of such materials, and other possible activating materials.

D. TWT, Design and Evaluation

The TWT specifications were given previously and are repeated here.

At 6 Gc, the RF characteristics are to be as follows:

Small Signal Gain	30 db
Saturated Power Output	3 dbm
Noise Figure (Thermionic Cathode)	5 db
Noise Figure (objective) with cold cathode	3 db

With a combination of previous experience and concern of maximum cathode current density, a beam current of 150 microamperes was chosen. To yield the required output power with efficiencies obtainable at these current levels, the beam voltage was chosen at 600 volts. On the basis of these parameters, the remaining physical dimensions were calculated and are presented below.

Cathode Diameter (emitter)	0.050 inch
Helix Mean Diameter	0.060 inch
Helix Turns per Inch	88.5
Helix Length	10.388 inches
Method of RF Coupling	Pin match
Number of Gun Electrodes	5

utilized RF heating to evaporate Pt, then, upon evaporating BaO through numerous time and temperature cycles, work functions near 1.5 ev were obtained. Temperature must be carefully controlled due to the disassociation of barium and oxygen.

This concludes the description of processing techniques and the cathode test structure. Further refinements on techniques will come about as more knowledge is acquired concerning low work function processes and technology. Areas of concern include techniques of deposition, what work function may be obtained with a variety of metals, stability of such materials, and other possible activating materials.

D. TWT, Design and Evaluation

The TWT specifications were given previously and are repeated here.

At 6 Gc, the RF characteristics are to be as follows:

Small Signal Gain	30 db
Saturated Power Output	3 dbm
Noise Figure (Thermionic Cathode)	5 db
Noise Figure (objective) with cold cathode	3 db

With a combination of previous experience and concern of maximum cathode current density, a beam current of 150 microamperes was chosen. To yield the required output power with efficiencies obtainable at these current levels, the beam voltage was chosen at 600 volts. On the basis of these parameters, the remaining physical dimensions were calculated and are presented below.

Cathode Diameter (emitter)	0.050 inch
Helix Mean Diameter	0.060 inch
Helix Turns per Inch	88.5
Helix Length	10.388 inches
Method of RF Coupling	Pin match
Number of Gun Electrodes	5

Drift Tube Length	0.260 inch
Distance (cathode to drift tube)	0.435 inch
Outside Diameter (vacuum envelope, helix)	0.175 inch
Outside Diameter (vacuum envelope, gun)	0.335 inch
Over-all Length (vacuum envelope)	13.770 inches
Vacuum Envelope Material	Monel-Alumina

Figure 5 illustrates the mechanical assembly of the TWT. In turn, this vacuum envelope would be inserted in the TWT package which consists of RF matching assemblies and the magnetic beam focusing structure.

Since few changes may be incorporated on the helix to improve noise figure, no further modifications were made to this structure. The major effort was continued toward improving the electron gun for optimization of noise figure and cathode to interacting circuit impedance transformation. The ensuing paragraphs describe the work pursued in this direction.

Ultralow noise gun designs are based on empirical design and experimental results obtained from different designs. Based on this concept, a search of the literature showed that an electron gun structure designed by Standard Telephone and Cables (STC) in England³ yielded noise figures of almost 2.5 db in S-band. Therefore, as an initial design a scaled version was adapted to the different cathode size and the frequency range in which this tube would be operating. For comparison, the STC electron gun operated at S-band with beam current and voltage of 40 microamperes and 150 volts respectively; parameters for the MEC TWT are 150 microamperes and 600 volts.

Two major modifications were thus required; the gun length was increased and a larger inner diameter was chosen. The modified gun is shown in Fig. 6 with some typical dimensions indicated. Multiple electrodes provide a gradual increase in beam potential to the helix voltage, thus transforming the initial beam impedance to that of the beam within the helix region.

Low noise figures are obtained under conditions of forming a virtual cathode in the cathode second-grid region. Data presented by STC and reproduced

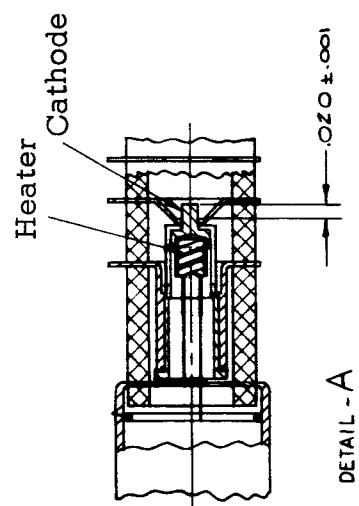
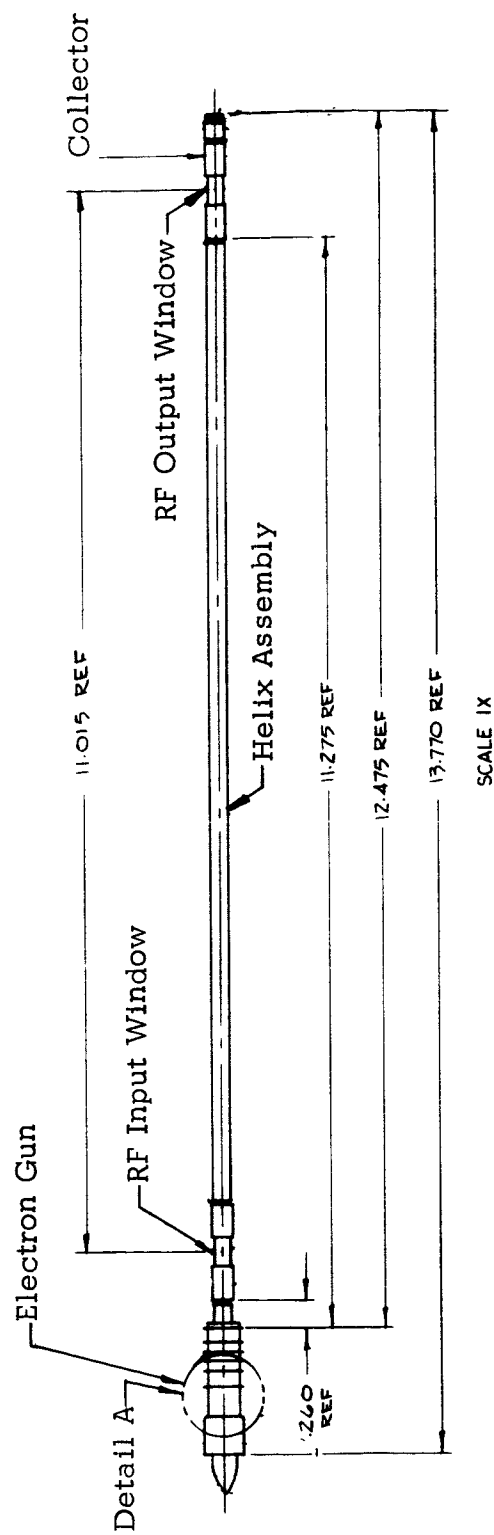


Fig. 5. Vacuum envelope assembly.

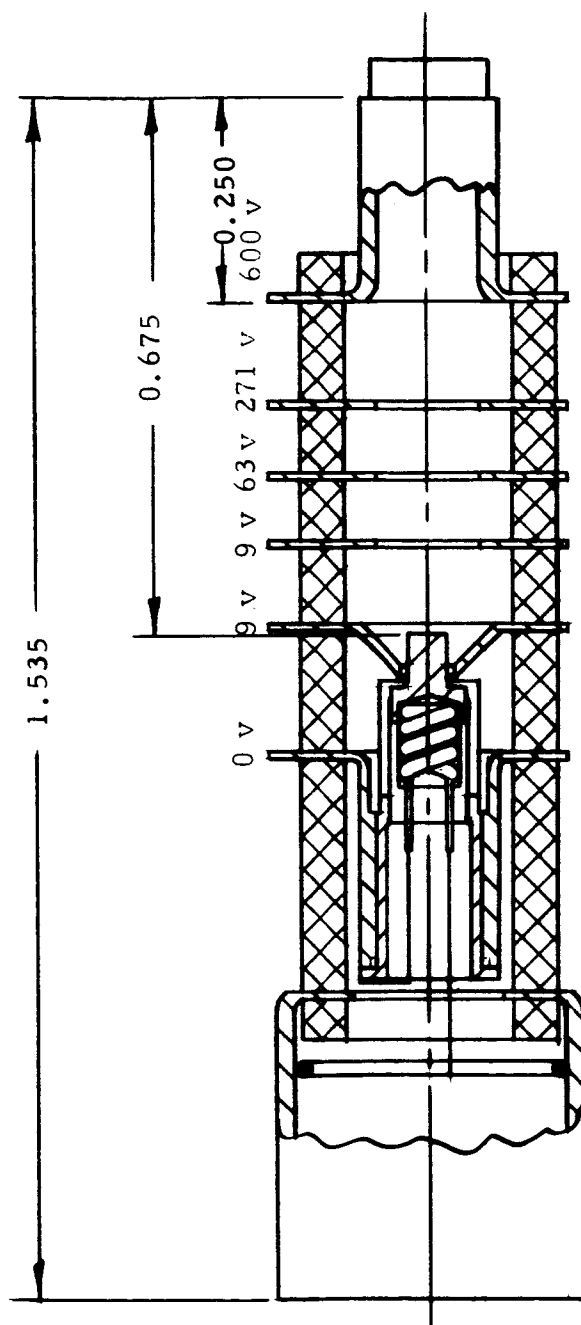


Fig. 6. Low-noise electron gun incorporating thermionic cathode.

in Fig. 7 show that as the virtual cathode was formed by increasing V_{g1} (the grid voltage), the noise factor varied smoothly. This indicated that good noise performance was not connected with the virtual cathode, but with the general situation of a low velocity region in which nonlinear effects could become important. It is evident that the basic noise quantities, particularly those associated with the electron velocity spread, may be manipulated in the very low potential region of the gun. To study this region, some potential profile calculations, which are described later, were made to determine the electrode configurations which are required.

Another phenomena related to good noise performance is the current density profile. The STC profile shown in Fig. 8 introduces the concept of linear edge current as being an important design parameter for low-noise guns. This mechanism tends to reduce the initial kinetic noise voltage, thus causing a reduction in the noise wave amplitude. In relation to the cold-cathode structure, edge emission would be feasible and very advantageous. The cold cathode bias current creates heating, principally in the center of the semiconductor. A hollow cathode providing a hollow beam, thus simulating edge emission, would allow removal of this heat by properly mounting the cathode to a heat sink. Application of the bias voltage causes current to flow through the semiconductor. Due to ohmic losses, the entire cold cathode is heated, causing additional noise generation and possible deterioration of the cathode.

A considerable effort was expended to find the proper electrode configuration near the cathode. Utilization of the computer allowed calculations of the potential profile with a variety of electrode potentials and electrode shapes. Briefly, the computer initially solves Laplace's equation for the electrode configuration and potentials chosen, then through a reiterative process includes the presence of an electron beam. Continuing, the potential profile is corrected for space charge, then the cathode current density is calculated.

Two of the most interesting cases are presented in Figs. 9 through 12. Figures 8 and 9 present the voltage and current density profiles for the operating

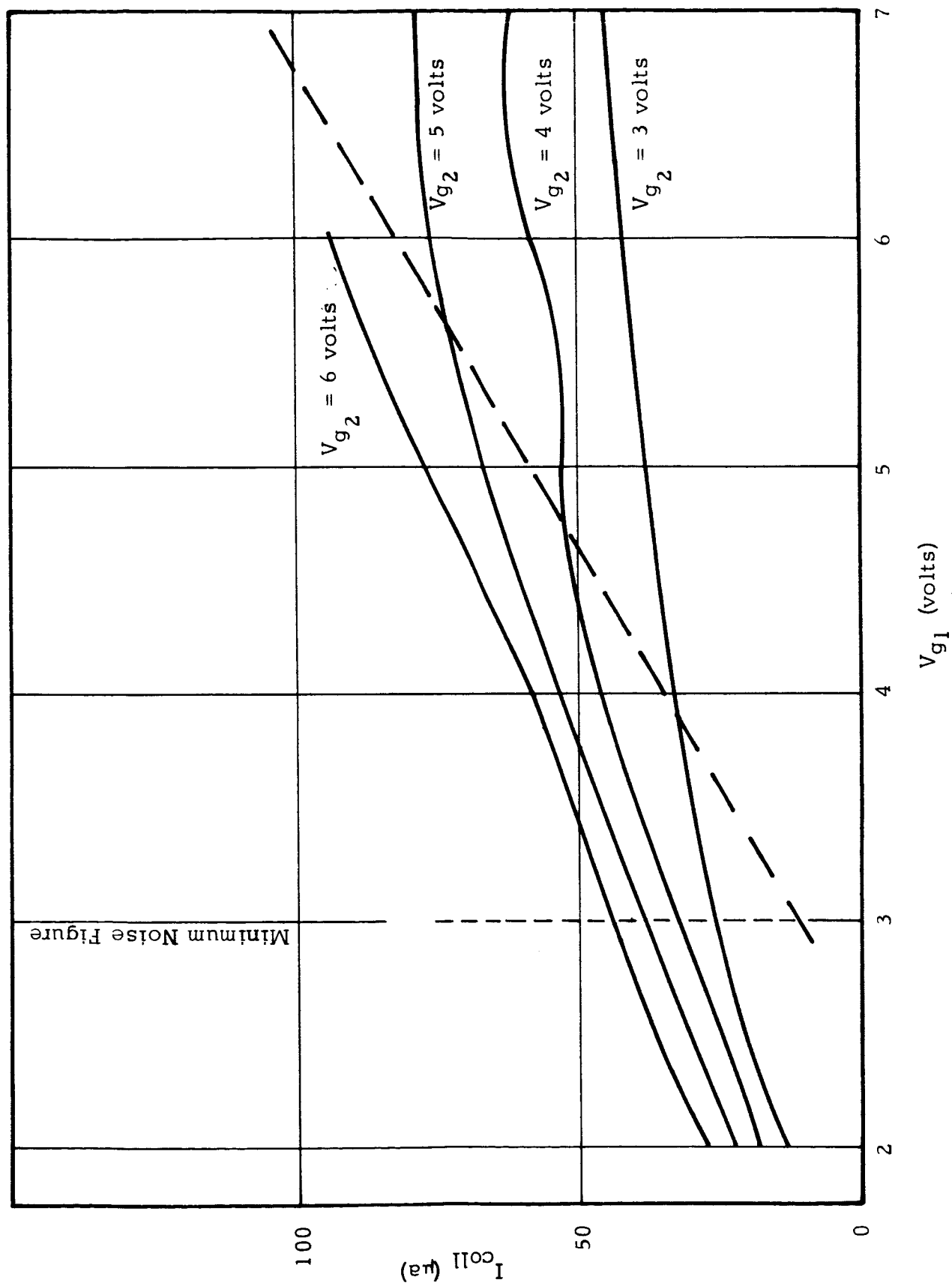


Fig. 7 . Current versus grid 1 voltage, grid 2 voltage being a constant.

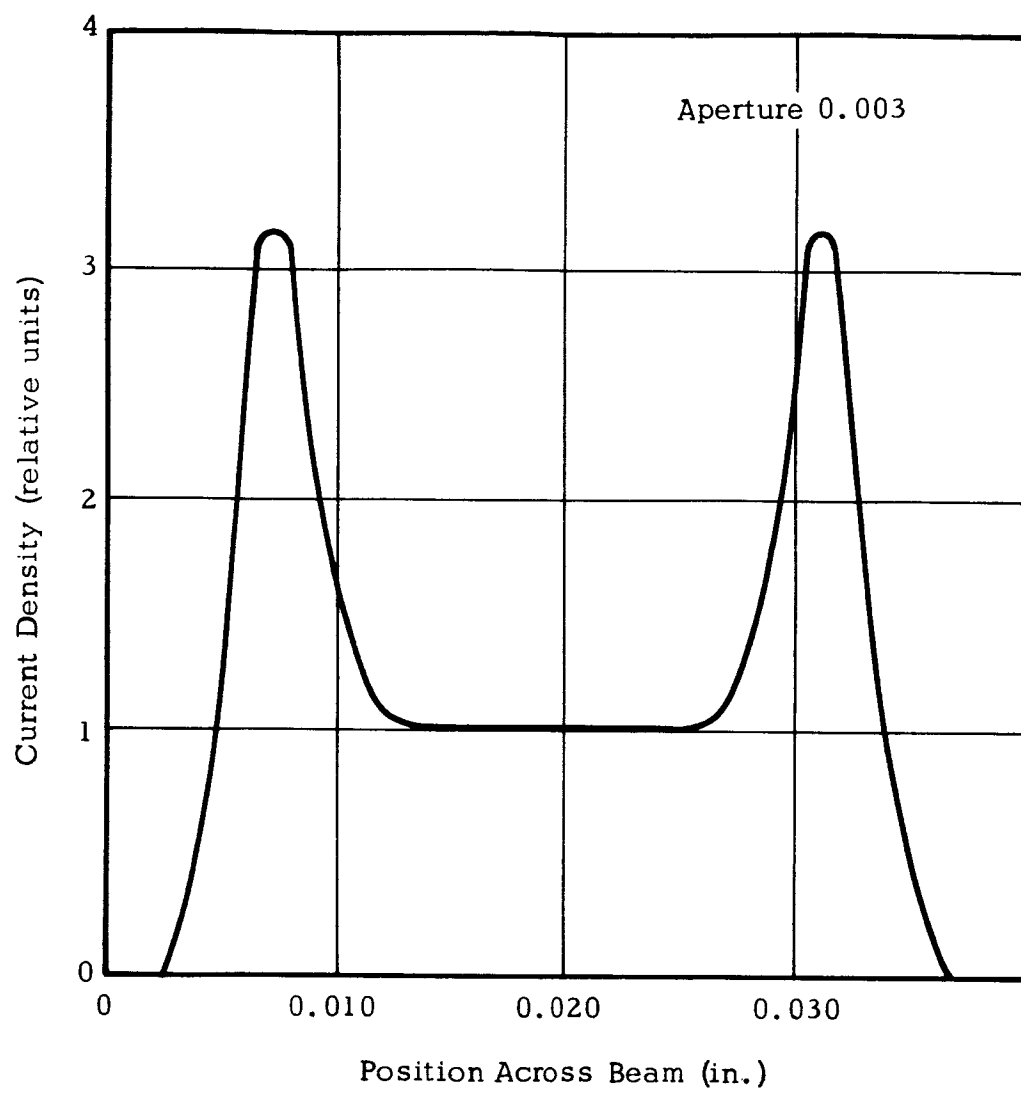


Fig. 8 . Beam current profile.

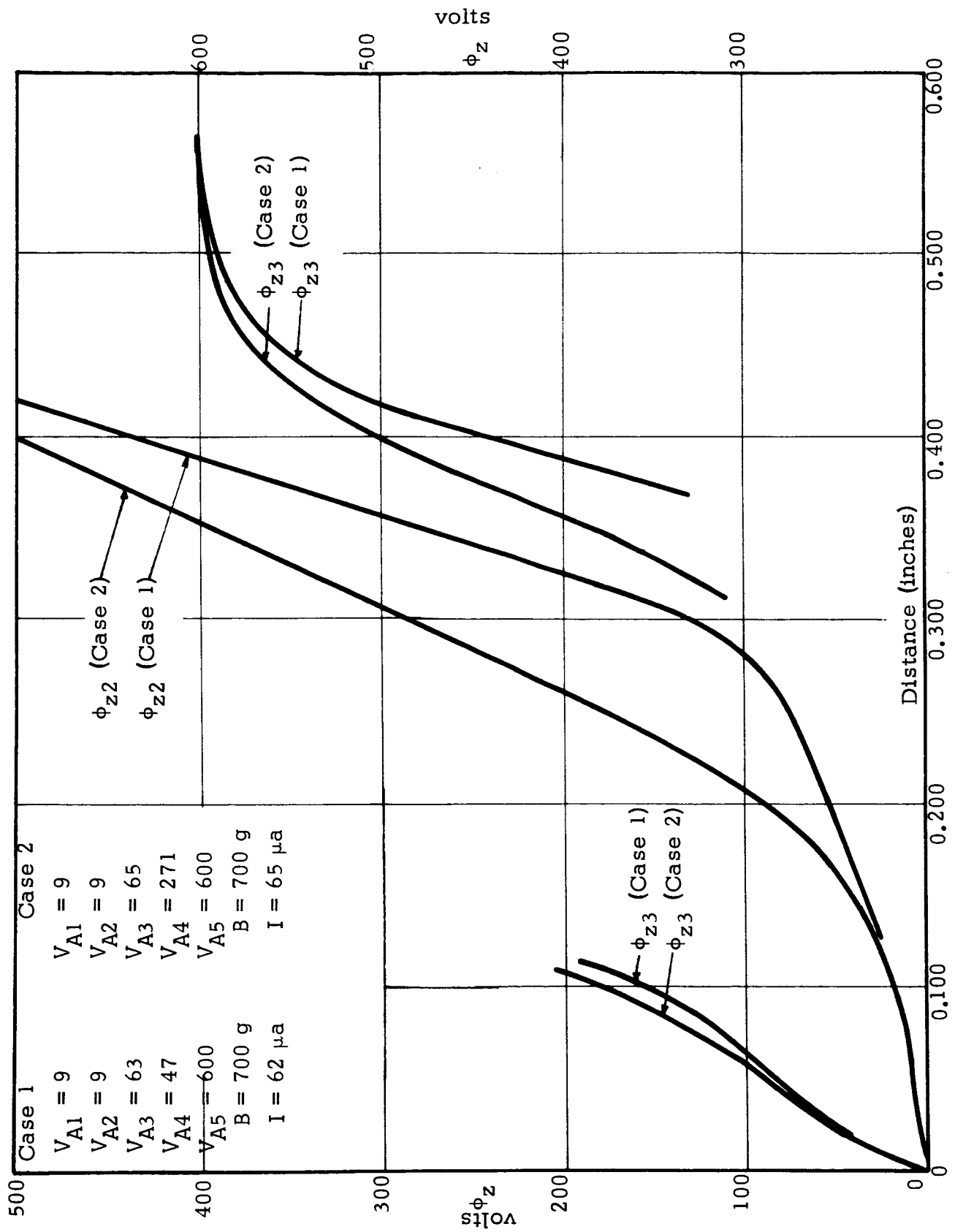


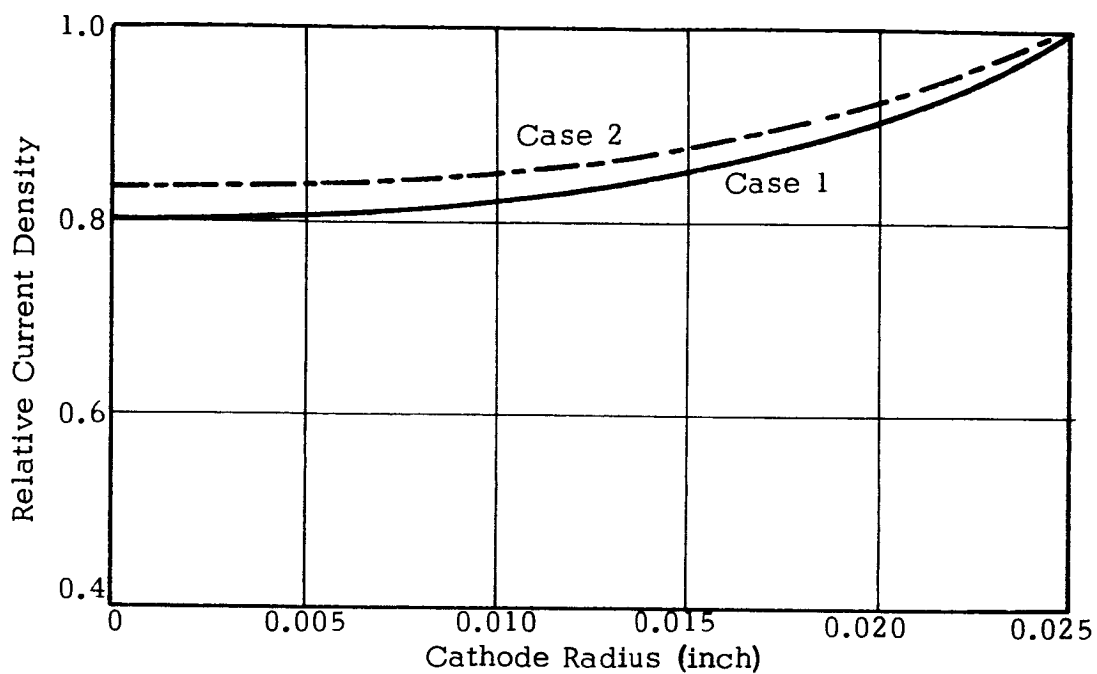
Fig. 9. Voltage profile for two sets of anode voltages.

conditions stated. Note is made of the gradual increase in potential near the cathode, this being the space charge region where, as discussed before, the important noise properties of the electron beam are formulated. Beyond this region the potential increases rapidly; then gradually tapers to the helix potential. It is throughout the increasing potential where the noise waves created by fluctuations at the cathode are transformed to an impedance as seen at the interacting circuit. Figure 10 shows the current density profile obtained with the indicated grid and anode voltages. As may be seen, the edge emission is larger, this being attributed to the anode-to-cathode proximity and potential depression in the center region due to space charge.

Another source of information on noise properties of electron beams is the beam profile, i.e., the beam configuration and nonuniformities due to magnetic or electric lens effects. From the computer calculations, two beam profiles were derived. With the first case shown in Fig. 11, a potential depression tends to form an electric lens effect which distorts the profile. The decrease in axial potential caused by Anode 3 tends to contract the beam, then an expansion occurs due to space charge repulsion. Case 2 demonstrates the effect of varying the anode potential; a much smoother beam is created and lens effects are kept to a minimum.

Beam ripple⁴ is caused by lens effects, either magnetic or electric. Nonuniform magnetic fields or abrupt transitions between fields of different magnitude tend to distort the electron path, causing both beam ripple and possible electron interception at the electrodes. Both of these enhance noise generation, beam ripple through noise wave amplification, and beam interception through randomizing effects. The same phenomena are created by an electric lens, in this case the dc electric fields causing a deviation in the electron path.

Two TWTs were fabricated and evaluated; the data is presented in Fig. 13 through 16. RF tests include measurements of noise figures, small-signal gain and saturated output power. Figures 13 and 14 show the noise figure



Case 2	Case 1
$V_{A1} = 9 \text{ v}$	$V_{A1} = 9 \text{ v}$
$V_{A2} = 9 \text{ v}$	$V_{A2} = 9 \text{ v}$
$V_{A3} = 63 \text{ v}$	$V_{A3} = 63 \text{ v}$
$V_{A4} = 271 \text{ v}$	$V_{A4} = 47 \text{ v}$
$V_{A5} = 600 \text{ v}$	$V_{A5} = 600 \text{ v}$
Magnetic Field = 700 gauss	

Fig. 10. Current density profile.

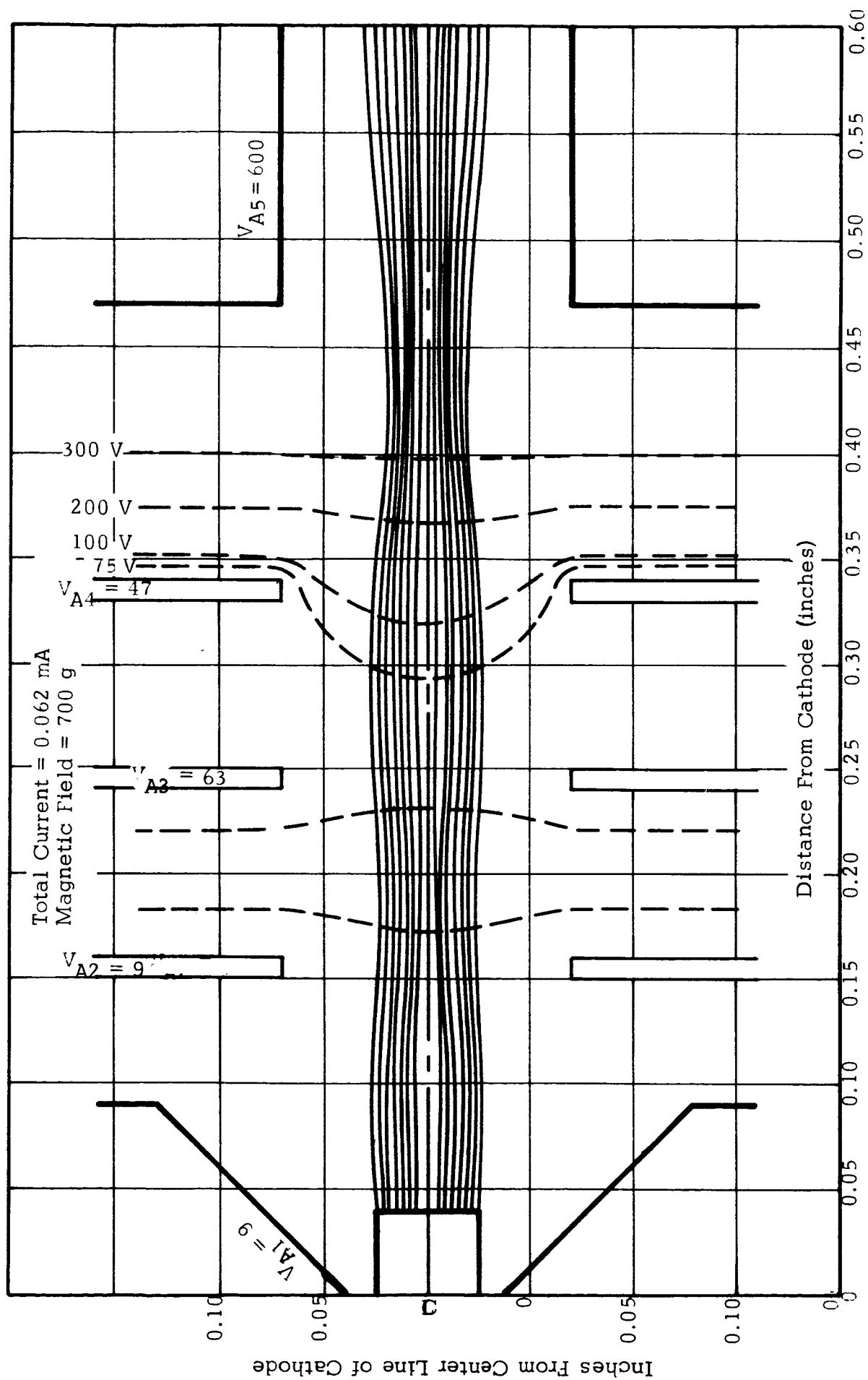


Fig. 11. Electron gun voltage and electron beam profile.

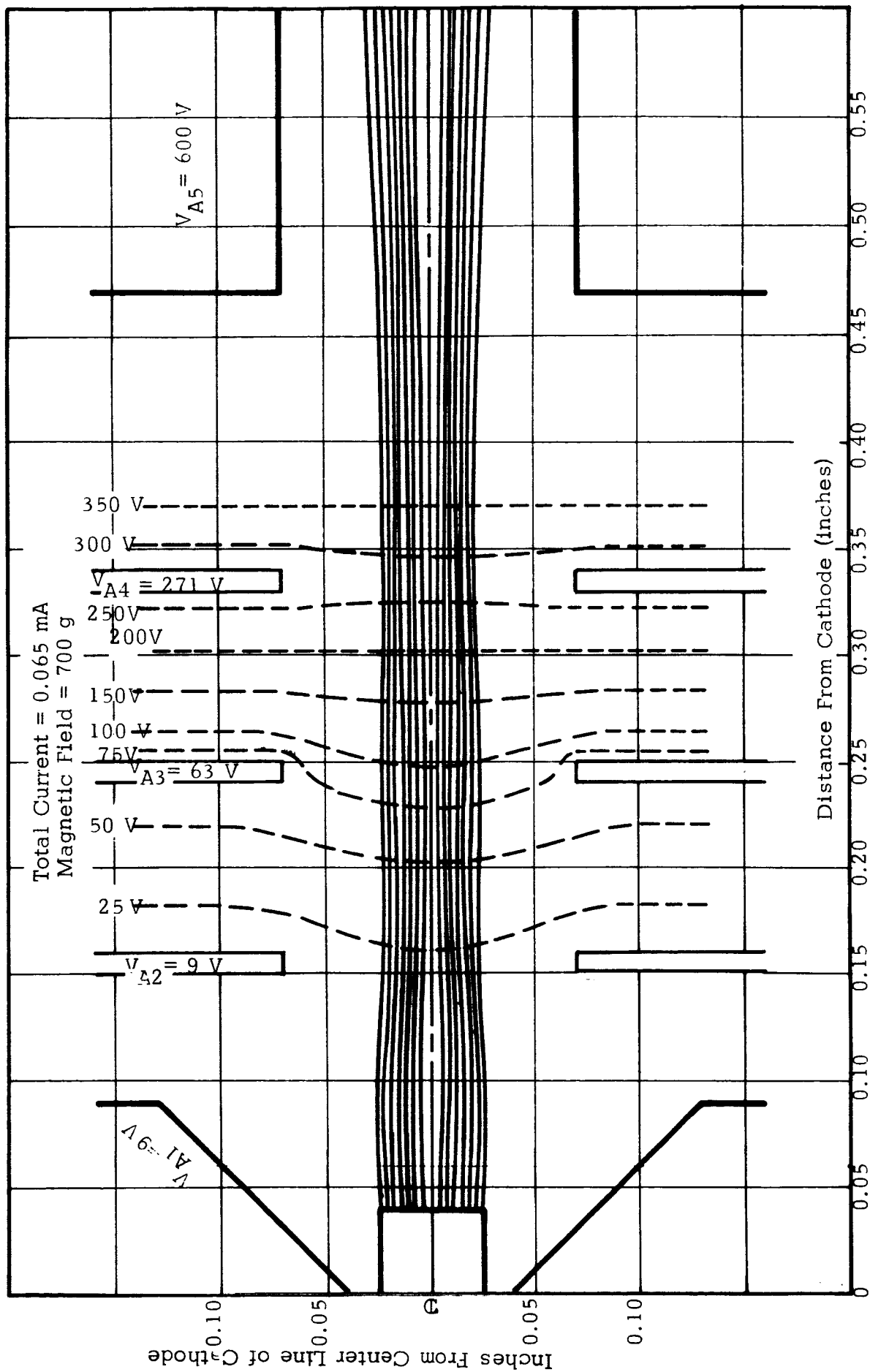


Fig. 12. Electron gun voltage and electron beam profile.

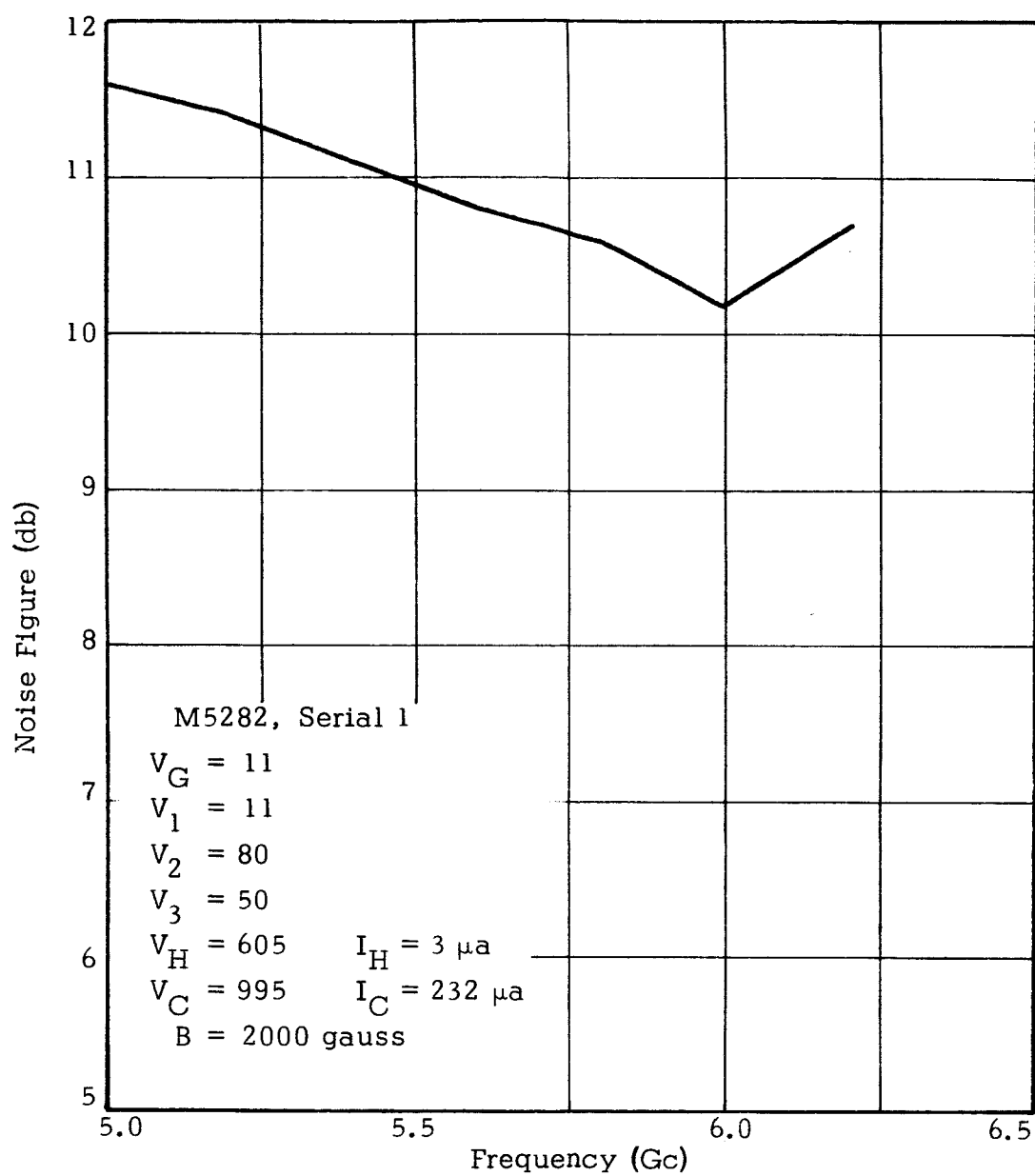


Fig. 13. Noise figure versus frequency.

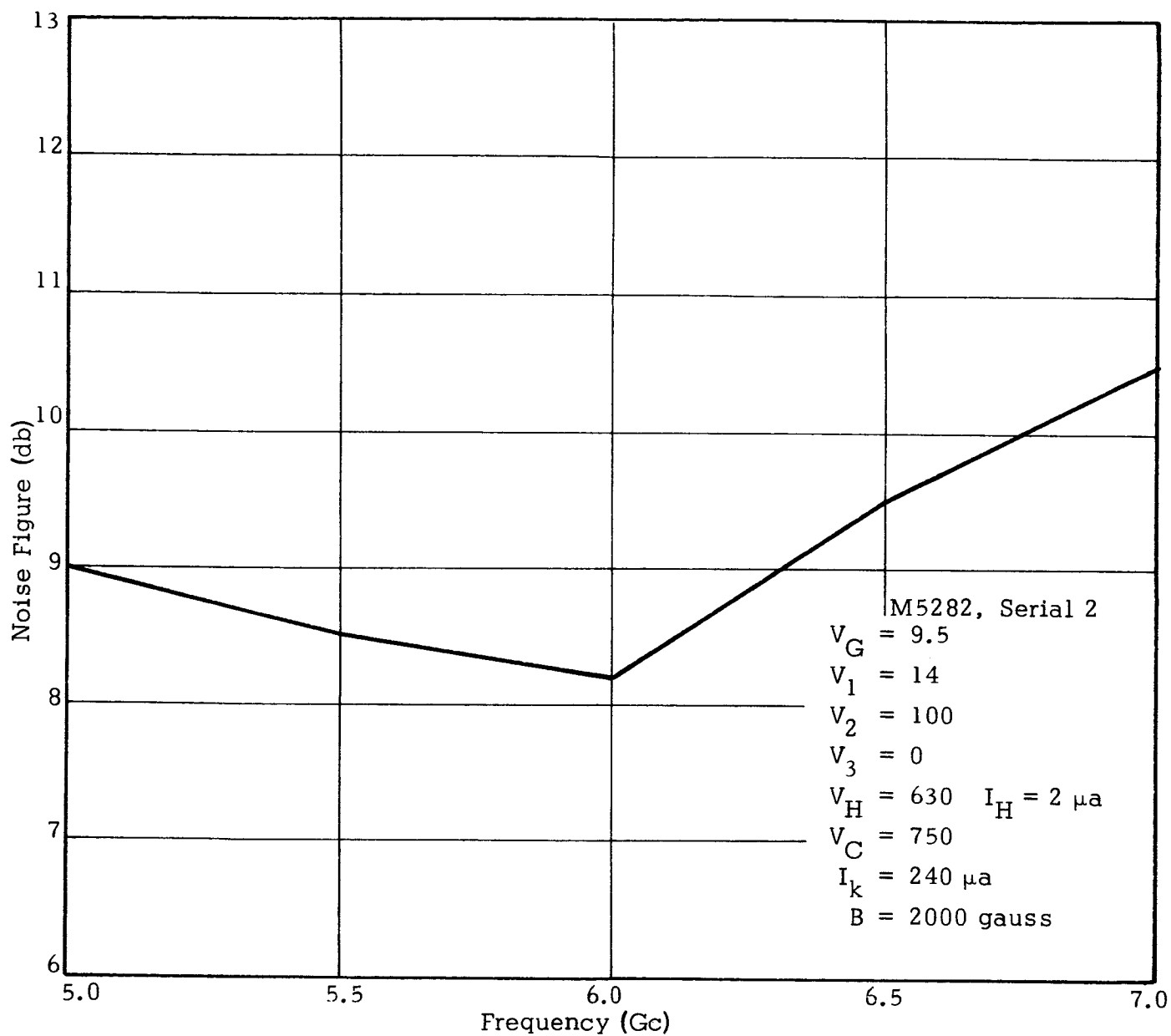


Fig. 14. Noise figure versus frequency.

characteristics of Tubes 1 and 2 respectively. High magnetic fields (2000 gauss) were required to keep current interception to a minimum and also obtain the optimum noise figures. Further refinement of the gun design was to be continued to improve these noise characteristics.

With the cathode current levels indicated in Figs. 13 and 14, the TWT gain was enough to present problems with oscillations. Therefore further testing was continued at lower current levels. Noise figure was decreased slightly, thus only small-signal gain (SSG) and power output (P_o) of Serial 2 were measured since its characteristics were better than those of Serial 1. As seen in Fig. 15, a decrease in SSG and P_o were experienced with increasing frequency, both indicating the tube characteristics are "centered" at the lower band edge. A significant decrease in SSG and P_o is found when the current is decreased to 50 microamperes. However, Fig. 16 clearly indicates some meaningful data may be obtained at this current level.

To improve the TWT RF characteristics, two design modifications were incorporated. Figures 11 and 12 show the proximity of equipotential lines, indicating rapid voltage change from one anode to the next. This provides a rapid change in beam velocity which intensifies noise generation and beam ripple, both of which increase the TWT noise figure. To remedy this situation the electron gun was redesigned with smaller anode inner diameters to improve the potential profile. Another significant contribution to decreasing noise figure is the potential profile formulated by the cathode and grid. It has been found by experiment that a cathode-to-grid spacing of 0.20 inch is optimum for low-noise figure. The second set of tubes were therefore fabricated with cathode-to-grid spacings of 0.018 and 0.020 inch.

Due to tube length, difficulties were encountered when focusing this TWT. As noted in the data presented, the magnetic field was 2000 gauss for optimum noise figure. A subsequent test at 1200 gauss was made, and these data are presented in Figs. 17 and 18. The noise figure has degraded by

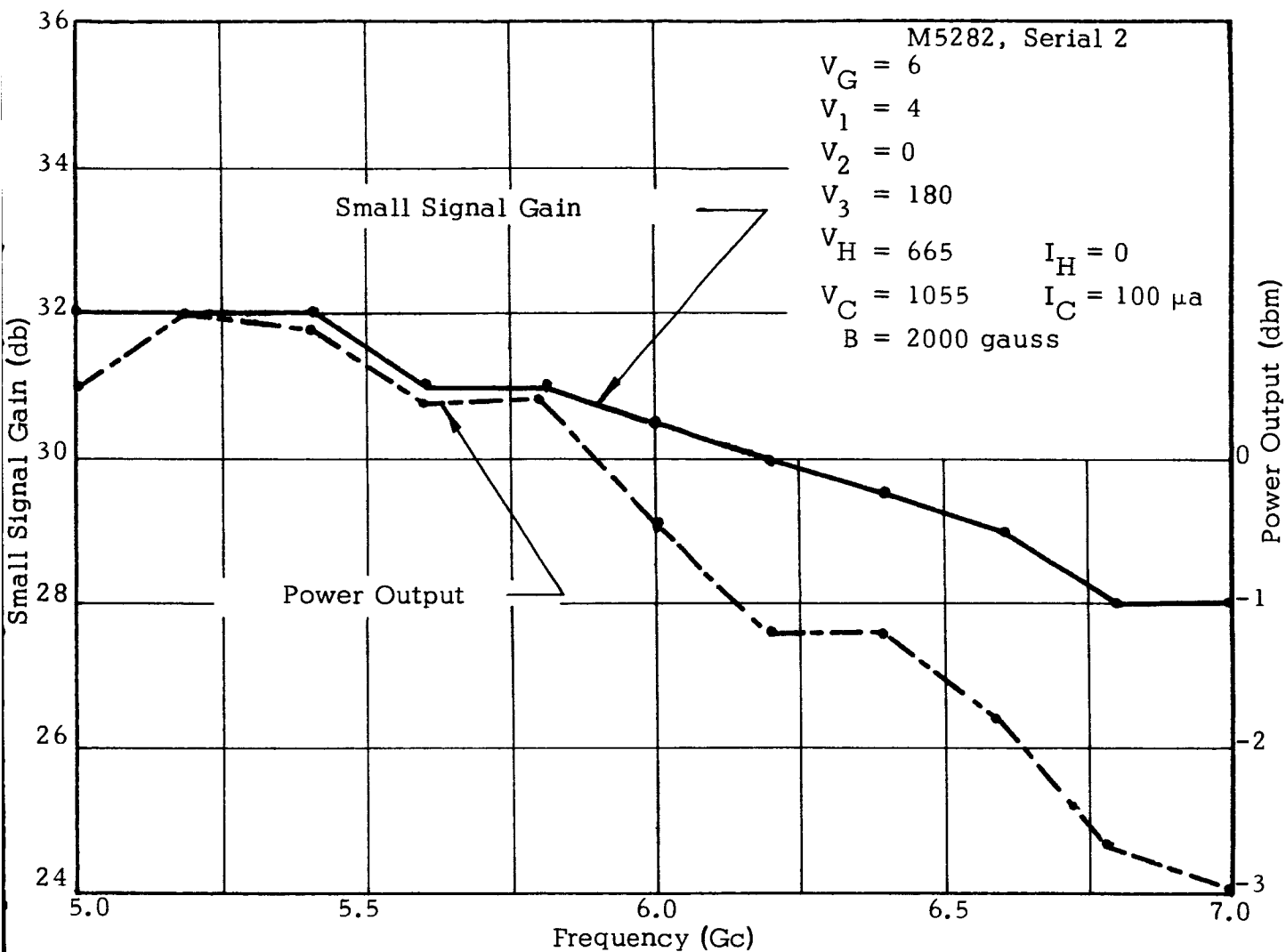


Fig. 15. Small-signal gain and power output versus frequency.

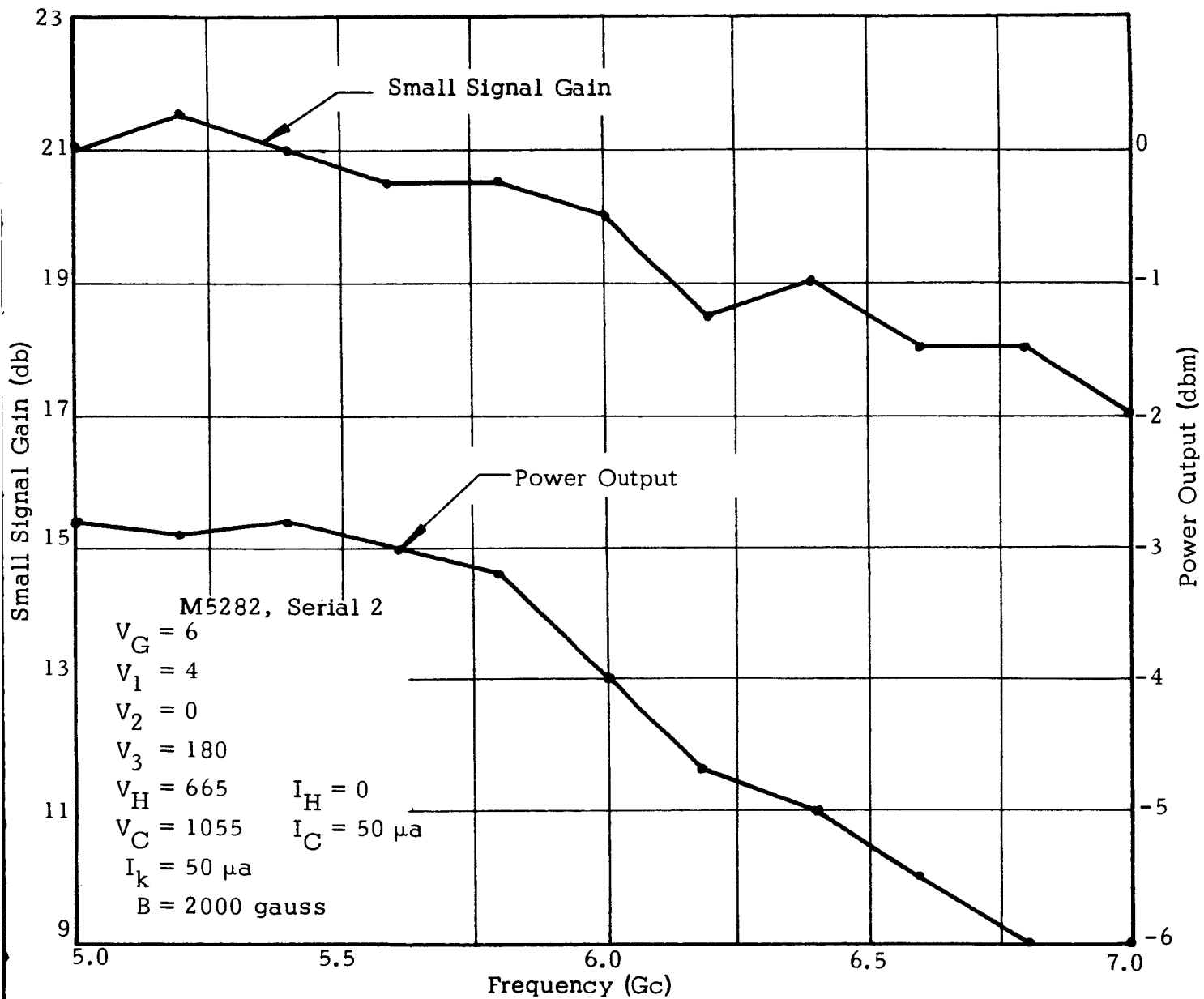


Fig. 16. Small-signal gain and power output versus frequency.

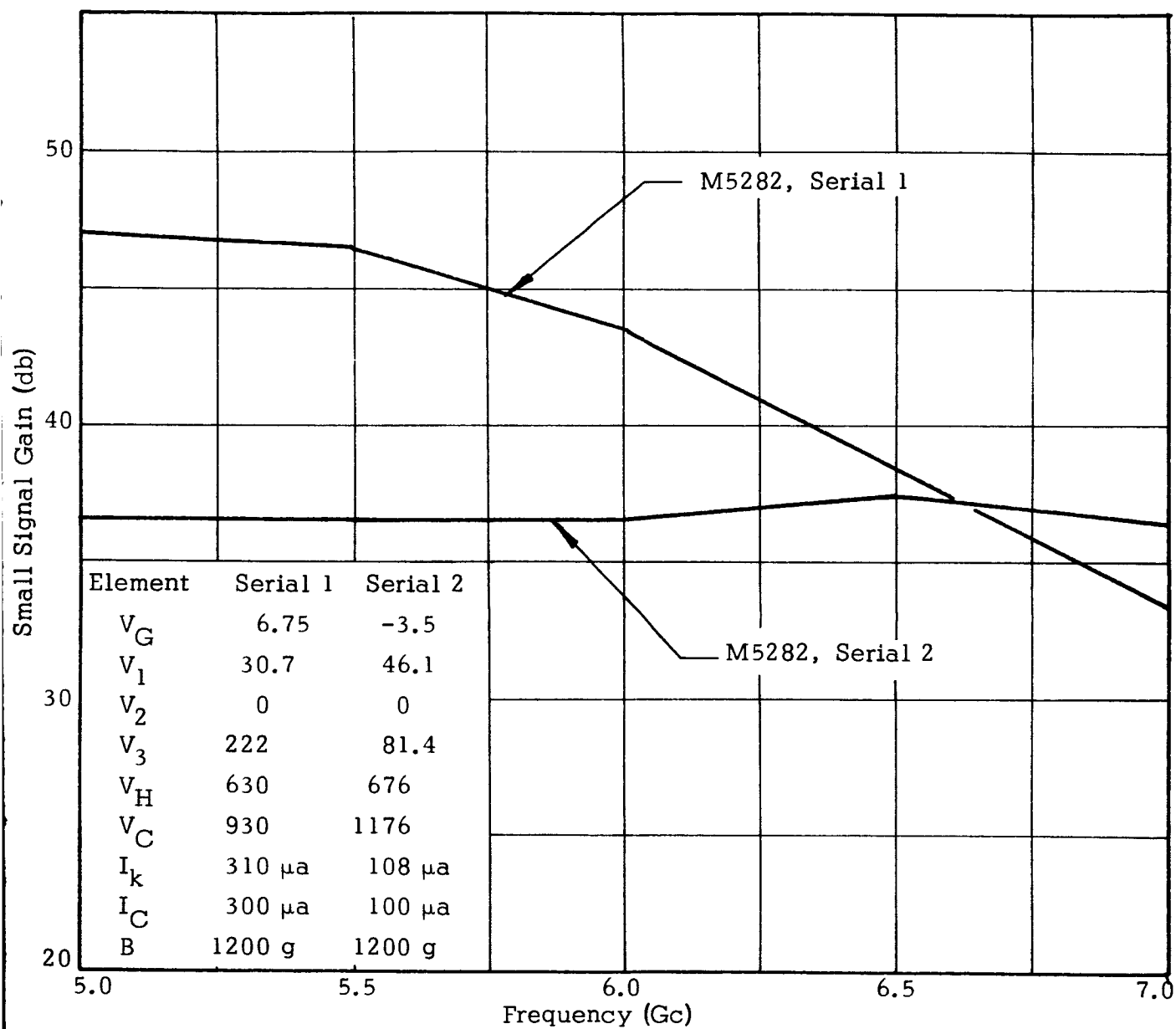


Fig. 17. Small-signal gain versus frequency for M5282, Serials 1 and 2.

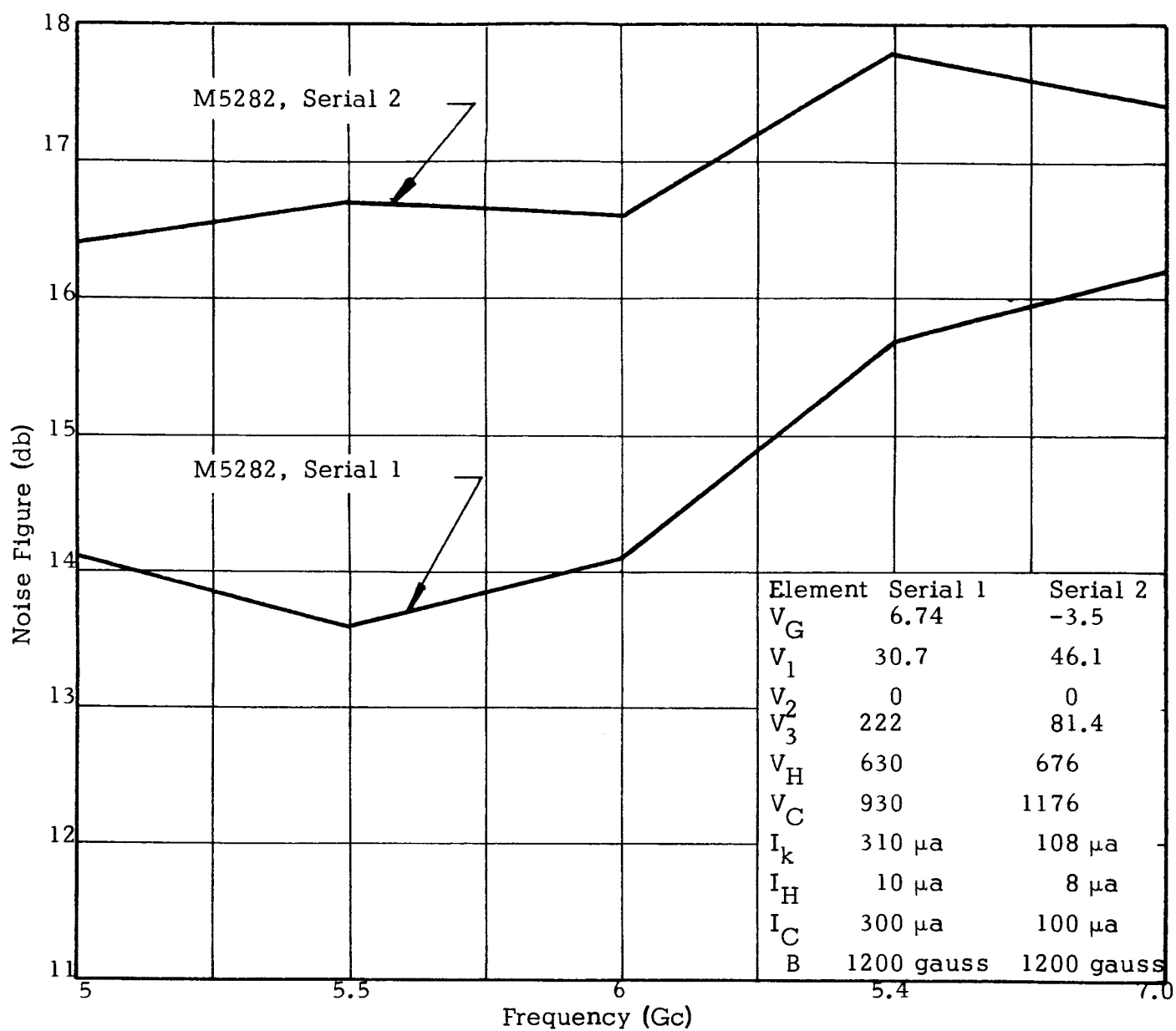


Fig. 18. Noise figure versus frequency for M5282, Serials 1 and 2.

4 to 6 db due to current interception by the helix. With the large cathode diameter being used, the beam-to-helix radius ratio is 0.833, thus the beam is very close to the helix. Any transverse magnetic field or lens effect due to electric field will enhance current interception.

Modifications to a 0.030-inch cathode were incorporated in subsequent tubes since the cold cathode could be fabricated to a smaller size. With a cathode 0.030-inch in diameter, the cathode loading at 75 microamperes is 4.1 mA/cm^2 this being a low current-density value for low-noise TWTs and also for a cold cathode. The present tube provides sufficient gain, even at 75 microamperes such that cathode loading will not be a hazard.

Two tubes were fabricated incorporating the modifications mentioned above when it was decided that MEC's efforts should be expended toward assisting the development of the cold cathode. Further work on the tube aspect was terminated with the intention of resuming when a cold cathode was available. Some diodes structures were fabricated for initial tests on the cathode.

This concluded the section on the TWT aspect of the contract. To this end, the TWT vacuum envelope is available upon realizing an operational cathode.

E. Noise Properties of the Cold Cathode

When comparing the noise figure of a cold cathode with that of the thermionic cathode, the latter's higher noisiness is the result of two phenomena. First, the cold cathode is inherently cooler, and second, the electron-velocity fluctuations may be lower. The latter point has not been proven but is inferred from theory.

Traveling-wave tube noise figures depend on the noise level generated in the diode region and the transformation of that noise to the helix region by means of accelerating elements. Other noise contributions which must be accounted for include excess noise due to beam transmission defects, secondary emission, and ion oscillations. The following paragraphs will discuss the former phenomenon first, then deal with emission and velocity fluctuation noise later.

Excess noise due to beam transmission defects may be grouped in two major categories;⁵ those which tend to restore full randomness and those which tend to amplify noise over its random value. The defects categorized in the first group include:

- Nonuniformity of the dc velocity across the electron beam due to space charge depression of the potential.
- Lens effects causing transverse acceleration of electrons.
- Nonuniform current density across the beam.
- Electron interception on gun electrodes or interacting circuit.

The second group includes the mechanisms which tend to amplify any perturbation on the beam beyond complete randomness. Of such mechanisms, there are several:

- Scalloping-beam and rippled wall amplification.
- Slipping stream amplification.
- Beam instability in axial magnetic focusing field.

Beam transmission defects may be avoided by careful gun and amplifier design. Randomizing effects are reduced by operating with a low space charge density beam and by elimination of beam velocity discontinuities. Current interception due to a poor magnetic focusing structure design also enhances noise generation. Ion deflections of electrons may be eliminated by operating the tube under hard vacuum.

Current interception and ion deflections may be eliminated by using a well focused beam. With this approach, the magnetic focusing structure must be well designed and may have to include the cathode region.

Secondary emission is caused by secondary electrons liberated by primary electrons from intercepting electrodes and, particularly, from the collector. To reduce this phenomenon, a transverse magnetic field may be applied or electrodes may be coated with a material of low secondary-emission coefficient.

Ion oscillation noise is caused by plasma oscillation of ions in the electron beam. This effect is a primary contribution and is due to modulation of the beam. To keep this phenomenon to a minimum, requirements for a high vacuum must be observed and a design that avoids ion traps is essential.

In relation to the cold cathode, the defects described above essentially pertain to the beam beyond the emission area. Velocity fluctuations from the cathode may be enhanced by nonuniform magnetic fields. Since the velocity spread from a cold cathode is still unknown, the randomizing defects cannot be studied from the standpoint of noise enhancement. Some interception noise from the metal film grid or surface film of the cold cathode may be a serious cause of noise-figure degradation and would need to be evaluated.

The primary area of concern pertains to cold-cathode emission and operation. Emission is dependent upon achieving a vacuum barrier lower than the semiconductor metal barrier and the diffusion of electrons through the semiconductor and metal film.

Due to the finite conductivity of the semiconductor, a bias current will flow with the bias voltage applied. This current, in addition to generating thermal noise from power dissipation, also generates current noise; this generation mechanism will be described later. Another source of noise in semiconductors is generation-recombination (gr) noise. Both noise sources mentioned above premodulate the electron flow before the beam is formulated. Since the electrons need to pass through the metal surface film and activating semiconductor, some randomness will be eliminated due to collision processes and electron absorption. With the cold cathode not operating as a space charge limited device, reduction of randomness is not experienced. Furthermore, the electron velocity may be larger than for a comparable thermionic emitter.

In the following discussion, the noise sources will be exploited to determine their influence on the noise properties of the cold cathode.^{6,7} Noise

generation in the semiconductor will be discussed first; then a qualitative discussion of noise caused by transmission of electrons through the metal film and activating layer of semiconductor. Further discussion on the absence of the space charge "cloud" will be given.

The total mean square noise current in semiconductor has been found experimentally to follow a law of the form:

$$i_N^2 = \left[\frac{K_1 I^a}{f^\beta} + \frac{K_2 I^2}{1 + \left(\frac{f}{f_1}\right)^2} + \frac{4 kT}{R} \right] \Delta f \quad (1)$$

where K , K_2 , f_1 , d , and β are constants chosen empirically to fit experimental data. Equation (1) is shown in Fig. 19. Three distinct regions of the frequency spectrum can be seen. At high frequencies, the dominant noise is thermal noise or Johnson noise and is given by the third term of Eq.(1). At low frequencies, the principal source of noise is due to current flow and is characterized by a $1/f^\beta$ spectral dependence, where β lies between 1.0 and 1.5. At intermediate frequencies a third form of noise appears dominant, a type described in terms of a characteristic frequency f_1 .

Thermal noise existing at all frequencies is predominant at high frequencies and the mechanism of generation is the random motion of charge carriers. This phenomenon exists even in the absence of current flow through the semiconductor. The expression for noise power derived upon thermodynamic considerations is given by:

$$P_n = k T \Delta f$$

The principal source of noise at low frequencies in many semiconductors has been called current noise, contact noise, and modulation noise. The noise power spectrum in this case is approximately dependent upon the

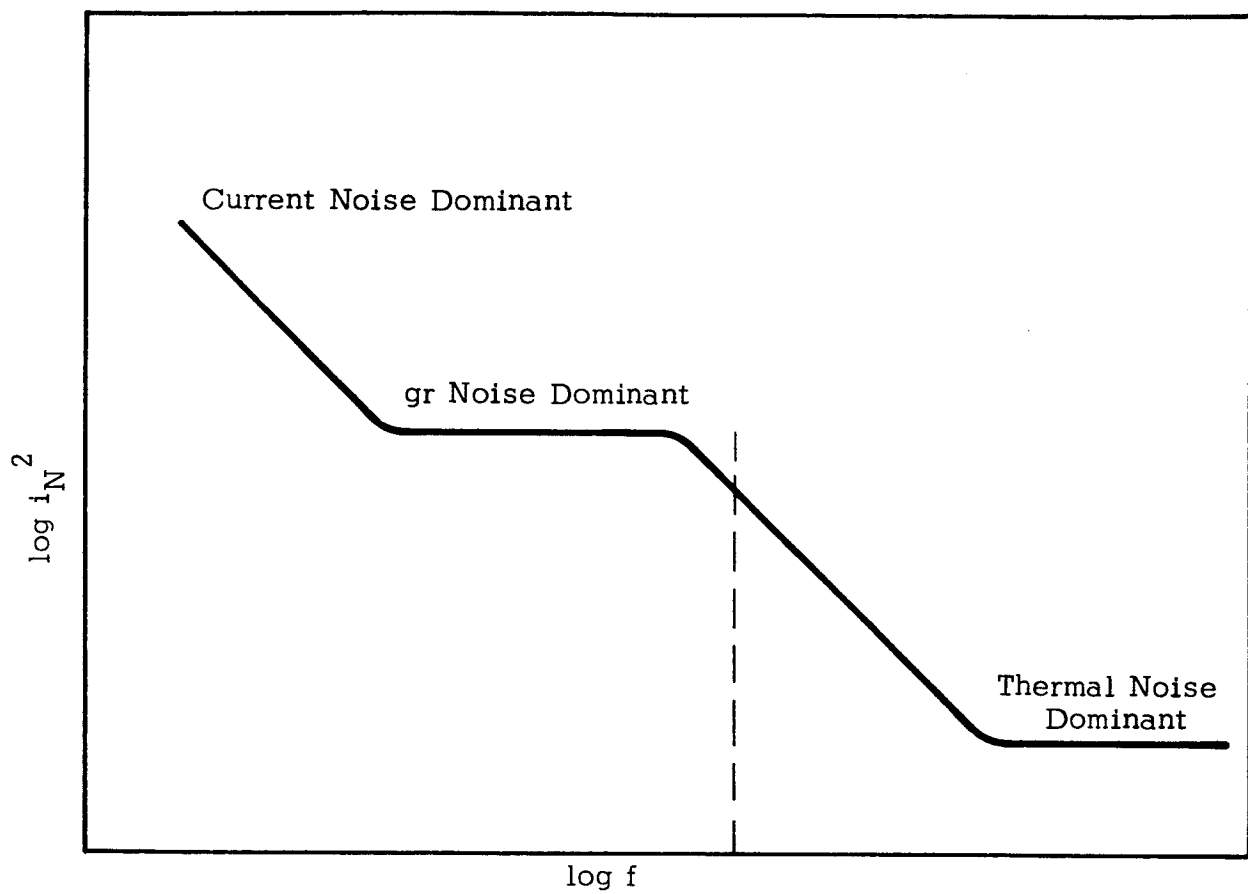


Fig. 19. Spectrum of noise current in semiconductors.

reciprocal of the frequency and the square of the current. Since the generation mechanism is not sufficiently understood, several present day theories will be discussed.

The third type of noise, designated as shot noise by some authors and generation-recombination or "gr" noise by others, is found at frequencies intermediate between those dominated by current noise or thermal noise. The power spectrum may be described in terms of an upper characteristic frequency, beyond which thermal noise predominates. Fluctuations in instantaneous free carrier densities due to random character of the generation, recombination, and trapping processes are the principal contribution to the noise power.

1. Current Noise

The power spectrum of current noise is of the form:

$$I_N^2 = \frac{K_1 I^\alpha \Delta f}{f^\beta}$$

where $\alpha \approx 2$, $\beta \approx 1$ and K_1 is a proportionality factor. Several theories have been suggested and will be briefly described.

Some authors² have postulated that current noise is associated with potential barriers, whether they exist at intergranular contacts, at rectifying electrodes, at the semiconductor surface, at dislocations, or at point contacts. Numerous experiments have demonstrated noise generation when a potential barrier exists.

The dependence of noise voltage upon bias current suggests that current noise is the result of fluctuations in conductivity of the material which in turn modulates the bias current. Petritz⁹ has introduced the term "modulation noise" indicating that current noise is due to some effect which modulates the carrier densities and thus the conductivity of the material.

Current noise may be characterized by the summation of a number of processes having a distribution of time constants all having a form

$$f(\tau) = \frac{a \tau}{(1 + \omega^2 \tau^2)}$$

If each process is multiplied by a weighting factor inversely proportional to τ , the integrated functions have a $1/f$ dependence. To interpret this, it is proposed that the noise form is due to ions having a distribution of energies for diffusion, migrating to a barrier, and modulating the barrier. Rose has proposed that the barrier modulation is attributed to presence of electronic charges coming from trapping states distributed in energy over the forbidden band, the lifetime of these trapped charges being an approximately exponential function of the trap depth. However, van Vliet¹¹ postulates that the noise spectrum is determined by the mean free time of charges, and long trapping times cannot account for the noise currents at low frequencies. Furthermore, Rollin and Templeton have observed $1/f$ noise down to 2×10^{-4} cps, necessitating lifetimes of hours. This phenomenon thus cannot be resolved to give a finite noise power since a lower and upper frequency limit does not seem to exist.

In contrast to the situation for thermal noise, the current-noise voltage depends upon the dimensions of the semiconducting material. It has been shown that for a material of given resistivity the mean square current noise voltage varies inversely with the cube of the cross-sectional area and therefore with the cube of the thickness. This implies that thin films of semiconducting materials will be more likely to be limited by current noise than will bulk materials. This latter point is significant with the cold cathode since its physical makeup consists of a thin semiconductor film. Further correlation of the above phenomena and their relation to the cold cathode will be presented later.

2. Generation-Recombination Noise

The dominant source of noise in semiconductors at intermediate frequencies is generation-recombination (gr) noise. Its power spectrum is constant at low frequencies but decreases rapidly beyond a characteristic frequency, f_1 , related to the inverse of the carrier lifetime. Generation-recombination noise in a semiconductor is due to the statistical fluctuation in the concentration of carriers. It is analogous to shot noise in electron tubes.

The complete analysis of "gr" noise must consider several discrete areas in semiconductors, namely those which are extrinsic, near intrinsic and intrinsic. Additional consideration must be given to areas in which the carrier transit time due to the applied field is either less than, equal to, or greater than the carrier lifetime. Furthermore, the recombination mechanisms enters in since an adequate description depends on whether it is monomolecular or bimolecular.

Van Vliet¹¹ has shown that the power spectrum in extrinsic semiconductors may be expressed as:

$$P(f) = \frac{4 I_o^2 \tau}{\bar{N} (1 + \omega^2 \tau^2)} \quad (2)$$

Examination of Eq. (2) shows the "gr" noise to be proportional to the square of the current through the semiconductor and inversely proportional to \bar{N} , the total number of carriers. Thus, a heavily doped semiconductor will exhibit less "gr" noise than a pure sample with the same lifetime and equal bias current. Also, it may be seen that the spectrum is flat to a characteristic frequency related to the reciprocal of the carrier lifetime.

In relation to the cold cathode, the two major phenomena described above generate noise which will modulate the electron flow through the semiconductor material. This in turn will be carried over to the electron beam except for the attenuation experienced when the electrons diffuse through

the metal film and activating semiconductor. Assuming the noise is random, thus having a positive and equal negative velocity contributions, some electrons will not have sufficient energy to overcome the Schottky barrier. The electron will in turn dissipate its energy in the semiconductor causing heating and, in effect, raising the inherent cathode temperature. Additional noise will be contributed at the metal semiconductor junction since a potential barrier is present.

The total contribution of these noise sources may be determined upon realization of an operational cathode. Measurements of the electron velocity distribution may be pursued in addition to determining the noise contributions of the semiconductor material. Better understanding of electron transmission through thin metal films is essential before these measurements can be related to the noise generation in the semiconductor and at the potential barrier.

At this point, some discussion of the noise contributions due to thin metal films is appropriate. Other than the Johnson noise associated with the temperature, the noise-contributing events are electron-electron collisions in which carriers lose sufficient energy to make emission impossible. Two mechanisms for noise generation in these metal films which have been considered are

- that the film is of a granular structure, and
- that the film is continuous but so thin that it has not developed a full metallic structure.

These mechanisms are associated with very thin films, i.e., thickness less than the mean free path of the conduction electrons. With the metals which are being used for the cold cathode, mean free paths of 100 to 500° A have been measured. Since the metal surface film thickness of 100 to 200° A is less than a mean free path, noise may be generated by the scattering of electrons when they meet the film surface, thus reducing their mean free path.

Concerning the first point mentioned, an analysis suggested by A. Rose¹² shows that the noise current will be

$$I = \frac{\bar{n} a}{\tau} = Fa \quad (3)$$

where

τ = smallest time unit in the device,

\bar{n} = number of events that contribute to current flow, each with a charge contribution a .

Letting F equal \bar{n}/τ , the average rate of current-causing events, Eq. (3) becomes

$$I = Fa \quad (4)$$

Events distributed according to the Poisson distribution have an rms deviation from the mean of $(\bar{n})^{1/2}$, thus the rms fluctuation or "noise" current I_n has a value

$$I_n = \frac{(\bar{n})^{1/2} a}{\tau} \quad (5)$$

Equation (5) may be manipulated to

$$I_n^2 = \frac{Fa^2}{\tau} \quad (6)$$

For the electron-electron collision processes, the rate of such events F is given by

$$F = \frac{I T_{tr}}{q \tau_{ec}}$$

where

T_{tr} = free-carrier transit time, and

τ_{ec} = mean time to an electron-electron collision.

The charge contribution per event is q , the electron charge, so that from Eq. (6)

$$I_n^2 = \frac{I T_{tr} q^2}{V \tau_{ec} \tau} = \frac{q I \tau}{\tau \lambda} = \frac{q I d}{\tau \lambda} \quad (7)$$

where

d = metal-layer thickness

V = velocity of the electrons through the metal

λ = mean-free-path for an electron-electron collision.

From the results of Sze¹³, it is estimated that $\lambda \cong 300^\circ \text{A}$. Hence, if the film thickness is nearly the same, the noise contribution, calculated from Eq. (7), is approximately

$$I_n^2 \cong 10^{-27} (\text{amp})^2$$

where I_n is the current per unit area (cm^2). This current may not be significant in comparison to the noise currents due to the semiconductor.

The latter phenomena, namely granular or film discontinuities, introduce noise because the energy bands do not overlap, thus the films do not contain a conduction band in the normal sense of the word. It has been suggested that thin films are less dense than the bulk metal, and the larger spacing between atoms prevent the formation of normal conduction bands. To substantiate this postulation further, in practice semiconducting properties are observed in thin metal films, indicating that conductivity is dependent upon film thickness. Further investigation of these phenomena must be undertaken to define the mechanisms of noise generation.

Present-day theories appear to be established as follows:

- Very thin films are granular and possess semiconducting properties due to the transfer of electrons between grain boundaries.

- The transfer mechanism is not understood, but requires excitation energies of a millivolt or so.
- However, continuous films which are thin enough may have resistivities much greater than the bulk material without having semiconducting properties. Such films may be used in noise-free applications.

Further noise contributions will be made by current noise generated at the rectifying barrier and shot noise, corresponding to the passage of current through the barrier by means of injected carriers. Shot noise is described in numerous texts, and is characterized by a flat spectrum over the frequencies at which transit time is insignificant and by proportionality to current. Additional noise due to these phenomena will tend to premodulate the electron beam and tend to have the same effects as the semiconductor noise contributions.

In conclusion, the predescribed sources of noise will be significant in determining the ultimate noise figure of the cold cathode. Further quantitative analysis is needed to determine the significance of each contribution and this would involve a search in itself. In addition, the emission properties of the cathode (velocity spread, electron energy) would be another study of significance since preliminary indications show little correlation between this cathode and an equivalent thermionic emitter.

CONCLUSION

Major progress was made towards evaluating suitable materials for a cold cathode and techniques for fabricating the cathode and its associated structure. The important conclusive evidence of the feasibility of constructing a cathode is detailed in the appended SRI report.

A test structure, namely the TWTs and diodes, has been completed, and is available upon realization of a cold cathode. Preliminary TWTs have achieved satisfactory noise figures and RF characteristics for initial testing of the cathode. Techniques have been explored to activate and transfer the cathode to a test structure.

The noise generating mechanisms of the cold cathode have been briefly studied to determine the relative improvement over a thermionic cathode. No quantitative analysis has been made since this would involve a search in itself. From preliminary studies, the cold cathode should have a lower noise figure due to its lower temperature and its surmised lower electron velocity spread. No evidence to substantiate the latter point, however, has been found.

Concluding, further work can be pursued since to date, there has been no concrete evidence that the cold cathode cannot be practically realized. Furthermore, the major impact in the electronics industry of an operational cold cathode would warrant further research.

REFERENCES

1. G. E. Moore and H. W. Allison, *Phys. Rev.*, 77, 1950, p. 246.
2. M. Cowley and S. Sze, paper to be published.
3. J. G. Armstrong, "Study of an Ultralow-Noise Traveling-Wave Tube Gun," STC Values, Standard Telephone and Cables Limited.
4. C. K. Birdsall, "Rippled Wall and Rippled Stream Amplifiers," *Proc. IRE*, Vol. 42, pp. 1628-35; November 1954.
5. Smullin, L.D. and Haus, H.A., "Noise in Electron Devices," Technology Press of MIT and John Wiley and Sons, Inc., New York, New York.
6. P.W. Kruse, L.D. McGlauchlin and R.B. McQuistan, "Elements of Infrared Technology, Generation, Transmission, and Detection," John Wiley and Sons, Inc., New York, New York; 1963.
7. D.A. Bell, "Electrical Noise Fundamentals and Physical Mechanism," D. Van Nostrand Company, Ltd., London, England; 1960.
8. C.J. Christenson and G.L. Pearson, *Bell Syst. Tech. J.*, 15, 197 (1936)
R.W. Smith and A. Rose, *Phys. Rev.*, 92, 857 (1953).
L. Bess, *Phys. Rev.*, 91, 1569 (1953).
S.R. Morrison, *Phys. Rev.*, 104, 619 (1956).
9. R.L. Petritz, *Proc. IRE*, 40, 1440 (1952).
10. A. Rose, Photoconductivity Conference, John Wiley and Sons, New York (1956), p. 3.
11. K. M. van Vliet, *Proc. IRE*, 46, 1004 (1958).
12. A. Rose, "Concepts in Photo Conductivity and Allied Problems," Interscience, New York, New York; 1963.
13. S. M. Sze, "Hot electrons in Gold Films," Technical Report No. 1659-4, April 1963, Stanford Electronics Laboratories, Stanford University.



September 1965

Final Report

N66 35581

COLD CATHODES FOR LOW-NOISE TWT APPLICATIONS

Prepared for:

MICROWAVE ELECTRONICS CORPORATION
3165 PORTER DRIVE
STANFORD INDUSTRIAL PARK
PALO ALTO, CALIFORNIA


CONTRACT SRI 010165

By: D. V. GEPPERT B. V. DORE

SRI Project 5175

Approved: PHILIP J. RICE, MANAGER
PHYSICAL ELECTRONICS LABORATORY

J. D. NOE, EXECUTIVE DIRECTOR
ENGINEERING SCIENCES AND INDUSTRIAL DEVELOPMENT

Copy No. 

ABSTRACT

The requirements for a practical substrate for the surface-barrier cathode are summarized, and a review of the various substrate designs is presented. The requirements for the semiconductor for the cathode are summarized, followed by a review of the efforts expended on the semiconductors ZnO and TiO_2 . The more recent work on GaP is presented in greater detail. The requirements for the metal surface film are summarized, and a discussion is given of the status of metal/semiconductor contacts. The activation requirements are summarized, followed by a review of the measurements to date on evaporated BaO. The experimental results of the program are then reviewed. Emphasis is laid on the stability and long life that have been demonstrated for surface-barrier diodes under dynamic life test and for low-work-function BaO/metal photo-surfaces.

CONTENTS

ABSTRACT	ii
LIST OF ILLUSTRATIONS	iv
LIST OF TABLES	v
I INTRODUCTION	1
II TECHNICAL DISCUSSION	3
A. Substrates	3
1. Summary of Requirements	3
2. Review of Designs	4
B. Semiconductor Layers	7
1. Summary of Requirements	7
2. Summary of Zinc Oxide Effort	8
3. Summary of Titanium Dioxide Effort	9
4. Gallium Phosphide	9
C. Surface Film	20
1. Summary of Requirements	20
2. Metal/Semiconductor Contacts	23
D. Activation	24
1. Summary of Requirements	24
2. Measurements	25
E. Experimental Results	26
III SUMMARY AND CONCLUSIONS	37
Appendix--DETAILS OF TiO_2 Investigation	38
REFERENCES	41

ILLUSTRATIONS

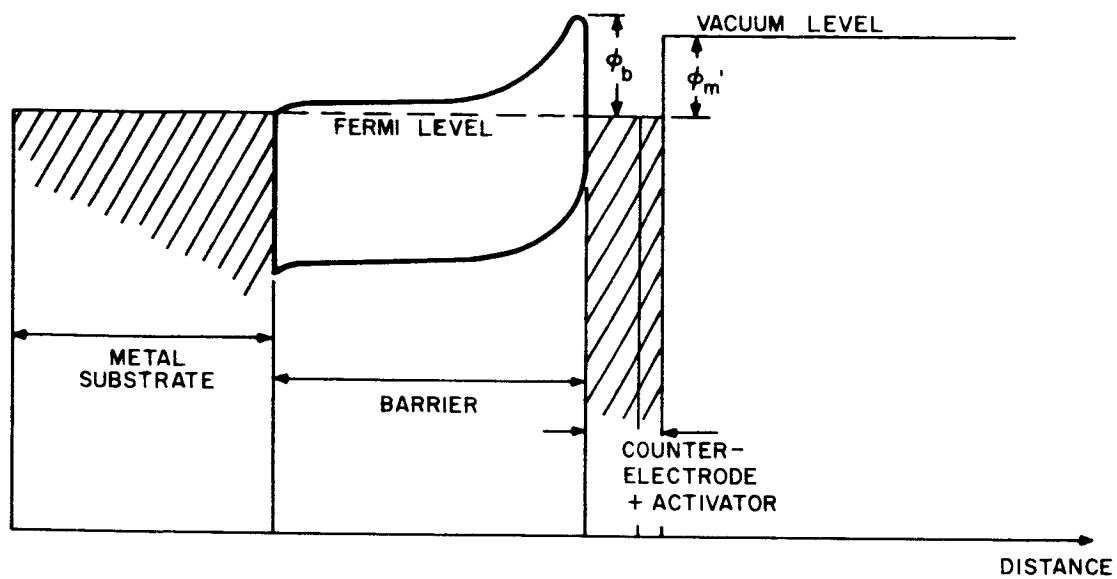
Fig. 1	Energy Diagram of Surface Barrier Cathode	2
Fig. 2	Cross Section of Assembled Cathode Structure	6
Fig. 3	Normalized Transmission of Monsanto Gallium Phosphide . . .	13
Fig. 4	Normalized Transmission of Stanford Gallium Phosphide . . .	14
Fig. 5	Relative Absorption of Monsanto Gallium Phosphide	15
Fig. 6	Relative Absorption of Stanford Gallium Phosphide	16
Fig. 7	Tracing of Spectrometer Data	19
Fig. 8	Dissociation Pressure of Gallium Phosphide	21
Fig. 9	Square Root of Photoresponse vs. Photon Energy for Gallium Phosphide/Tungsten Diode	25
Fig. 10	Square Root of Photoresponse vs. Photon Energy for Platinum/Barium Oxide Photocathode	28
Fig. 11	Fowler Plot for Platinum/Barium Oxide Phototube	29
Fig. 12	I-V Characteristic of Single-Crystal Zinc Oxide/Silver Paint Diode After 7500 Hours of Operation	30
Fig. 13	I-V Characteristic of Gallium Phosphide/ Evaporated Platinum Diode After 2200 Hours of Operation	31
Fig. 14	I-V Characteristic of Titanium Dioxide/ Evaporated Platinum Diode	32
Fig. 15	Square Root of Photoresponse vs. Photon Energy for Gallium Phosphide/Evaporated Platinum Diode	33
Fig. 16	I-V Characteristic of Gallium Phosphide/ Evaporated Tungsten Diode	34
Fig. 17	Log I vs. V Plot for Gallium Phosphide/ Evaporated Tungsten Diode	35
Fig. 18	Photograph of Multiport, Oil-Free Vacuum Station	36

LIST OF TABLES

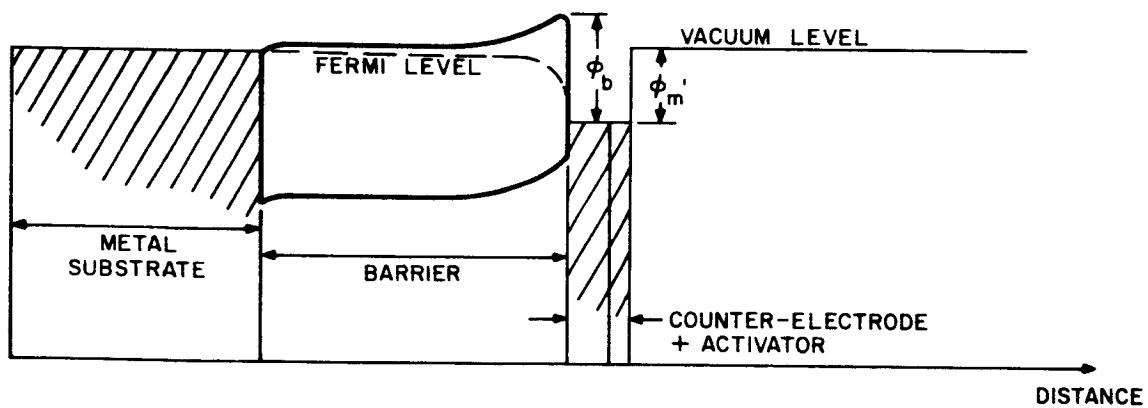
Table I	Summary of Results of Barium Oxide Activation Experiments	27
---------	--	----

I INTRODUCTION

The objective of this program was the development of a hot-electron surface barrier cathode for application to a low-level traveling-wave tube. The hot electrons are generated in a thin metal surface film by forward-biasing a rectifying semiconductor/metal diode. The metal film is on the order of 100\AA in thickness and is activated by a low-work-function coating to reduce the vacuum barrier below the semiconductor/metal barrier. Energy diagrams for the cathode, with and without bias, are shown in Figs. 1(a) and 1(b). The dimensions of the structure are not drawn to scale. The thickness of the metal film is exaggerated for reasons of clarity. Referring to Fig. 1(b), a portion of the hot electrons emitted over the top of the barrier into the metal film traverse the film ballistically and enter the vacuum. Most of those electrons that become scattered in the metal film are lost, however, and these electrons create a bias current for the device.



(a) ENERGY vs DISTANCE OF SURFACE BARRIER CATHODE WITHOUT BIAS



(b) ENERGY vs DISTANCE OF SURFACE BARRIER CATHODE WITH BIAS

TA-5175-19

FIG. 1 ENERGY DIAGRAM OF SURFACE BARRIER CATHODE

II TECHNICAL DISCUSSION

A. SUBSTRATES

1. Summary of Requirements

A number of requirements for a substrate structure have evolved during the course of this investigation and in previous studies of a similar type. These requirements were considered in some detail in the First Quarterly Report^{1*} and will be summarized here.

a. Electrical Contacts

The operation of a Schottky barrier cathode requires the application of a bias of about 1.5 v across the semiconductor layer. Since the cathode current should not exceed a few milliamperes, thin metallic films are usually adequate conductors. The critical areas in the bias circuit are the transitions from these films to the active cathode area, and from the films to the electrical leads. In order to limit the current density in these areas, the bias voltage should be applied by means of massive contacts with no interconnecting films or wires. It has been found that the contact to the surface electrode should completely surround the active area to minimize the possibility of burnout in this region.

b. Heat Dissipation

A uniform cathode structure 1 mm in diameter would have to dissipate about 1 watt/cm². Unfortunately, it is very difficult to fabricate a completely uniform structure, even of these small dimensions. It is important then to be able rapidly to dissipate the additional heat developed in the nonuniform areas of the cathode. For this reason the use of completely insulating substrates--such as glass or sapphire--is not recommended.

* References are listed at the end of the report.

c. Vacuum Properties

A thermionic cathode is self-cleaning in the sense that the heat removes any surface contamination that accumulates between operating periods. A thin-film cold cathode does not have this capability and thus must operate in a higher vacuum than the thermionic cathode. Therefore, it is important to use materials in the cathode and the substrate that can be processed at sufficiently high temperatures to minimize subsequent outgassing during the operation of the tube. Only refractory materials with good vacuum properties capable of withstanding a high-temperature bakeout should be considered.

d. Adaptability

The physical support for the cathode structure should be readily adaptable to mounting in TWT gun structures. The design should be such that it can replace the thermionic cathode with only minor adjustments to existing gun structures. The need for concave emitting surfaces in convergent flow guns should also be considered, so planar, insulating substrates are unsuitable for several reasons.

2. Review of Designs

A substrate design was developed early in the program that appeared to meet most of the preceding requirements. Before going into the details of this design a number of preliminary designs will be reviewed.

In a study for Microwave Electronics Corporation in 1963, a cylindrical substrate was designed that would replace the thermionic cathode in MEC's stacked-gun structure. The substrate was sapphire with fired gold contact areas, which proved to be unreliable. Another deficiency in this design was the lack of any form of heat sink.

The next design used a metal shank of molybdenum in place of the sapphire. This provided a good heat sink; however, it was necessary to use an insulating cap of glaze to isolate the contact areas for the surface film. When it was found that pin holes in the glaze could not be eliminated, this approach was abandoned.

A coaxial design incorporating a Kovar pin and a Kovar outer cylinder separated by 7052 glass was more successful. The end of the coaxial structure was ground and polished so that the inner Kovar pin provided the base electrode for the cathode. The exposed edge of the outer Kovar cylinder contacted the evaporated counter electrode. Although the electrical contacts were reliable and the heat sink was adequate, this structure could not be subjected to high temperature processing.

A platinum/alumina structure was designed in the first quarter of this study and was modified slightly to meet additional requirements that became apparent as the work progressed. A cross section of the final design is shown in Fig. 2. The steps in fabricating the structure are outlined below.

- (1) Semi-fired or "green" alumina ceramic is machined oversize to allow for approximately 20-percent shrinkage in a final high-temperature firing.
- (2) The platinum pin is inserted in the oversize center hole in the ceramic and the assembly is fired at approximately 1550°C. The ceramic shrinks, forming a hermetically tight seal between the platinum and the ceramic.
- (3) The molybdenum shank is machined to dimension, the ceramic is metallized and brazed to the molybdenum with gold.
- (4) The structure is chucked up on the molybdenum shank, the ceramic is cut to length with a diamond wheel and ground to final dimensions.
- (5) The monel hat is machined and pressed down on the alumina-platinum post after the cathode structure is in place.

The monel ring shown in Fig. 2 was added to locate accurately the Ti-TiO₂ cathode structures on the support. An additional feature not shown in the drawing is a small conical-shaped shim of beryllium copper placed between the cathode structure and the platinum post. The apex of the cone is toward the platinum and ensures a reliable pressure contact between cathode structure and the platinum.

Although time did not permit the actual testing of gallium phosphide (GaP) cathode structures, this substrate is ideally suited for mounting single-crystal GaP with previously-prepared contacts. In this case the

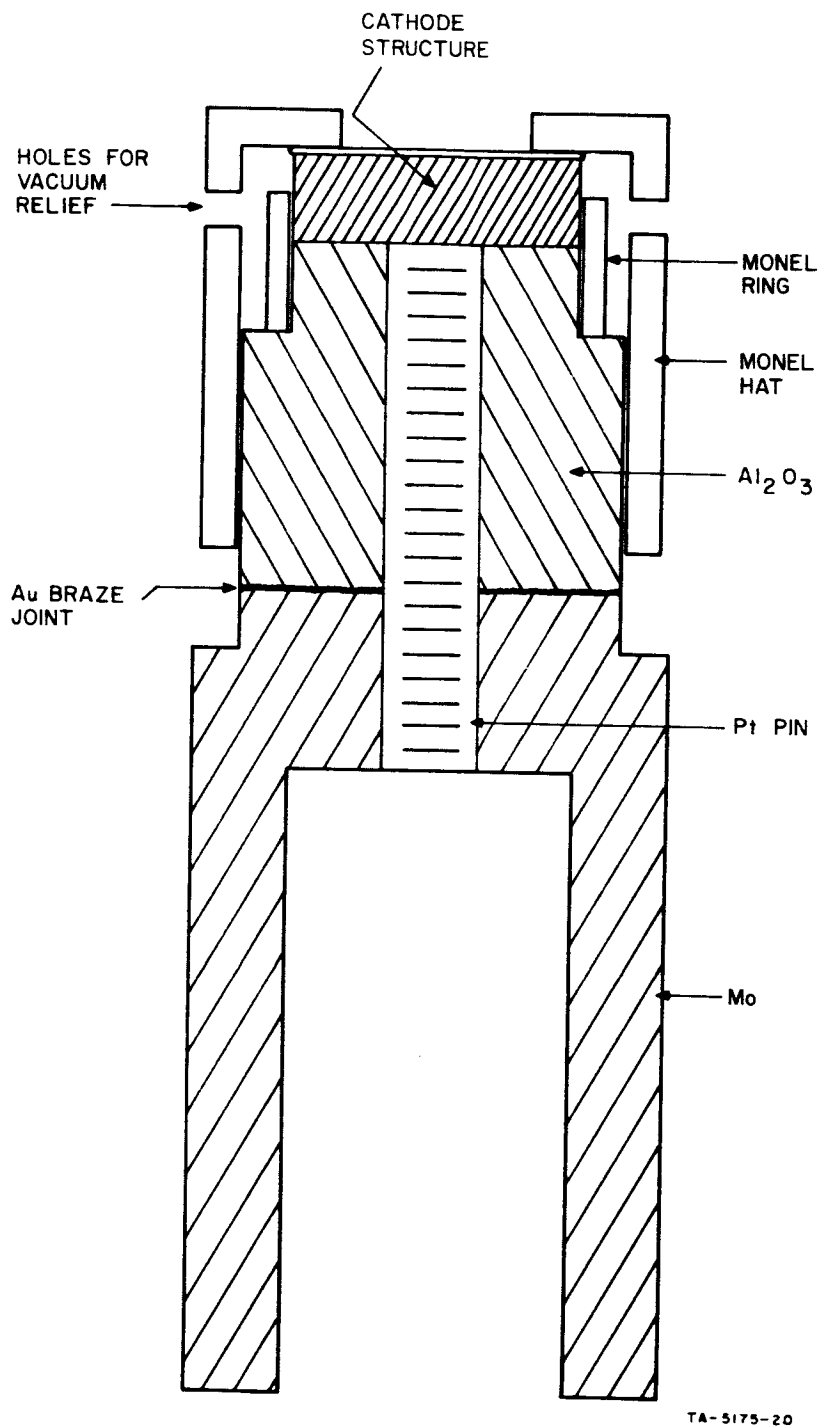


FIG. 2 CROSS SECTION OF ASSEMBLED CATHODE STRUCTURE

monel ring may not be required, but the monel hat would be used to make a positive electrical contact from the cathode electrode of the gun to an evaporated film on the GaP crystal.

The recess in the molybdenum shank is included to provide for the insertion of a conventional cathode heater. This would be used for additional outgassing of the assembled structure, and to facilitate transferring the cathode to the traveling wave tube.

B. SEMICONDUCTOR LAYERS

1. Summary of Requirements

The semiconductor for the surface-barrier cathode must produce a high barrier in combination with the metal surface film. In particular, the surface barrier ϕ_b must be greater than the work function of the metal surface film ϕ'_m after activation with evaporated barium oxide (BaO). Inasmuch as work functions between 1.3 and 1.75 ev have been achieved with evaporated BaO on several metals, metal/semiconductor surface barriers of this magnitude are required for the cathode. Although the theory of metal/semiconductor contacts is still being developed, there does appear to be correlation between metal/semiconductor barrier height and the electron affinity of the semiconductor. Theory and experiment both indicate that low values of electron affinity produce high values of surface barriers. Thus the semiconductor for the cold cathode should have a low electron affinity. Unfortunately, values of electron affinity have been measured for only a few semiconductors, thus making it necessary to employ a cut-and-try approach in finding a suitable semiconductor.

One theory of metal/semiconductor contacts that appeared in the literature during the course of the work correlated metal/semiconductor barrier height with the band gap of the semiconductor.² In particular, this theory indicated that the barrier height should be two-thirds of the band gap. Thus, for a barrier of, say, 1.5 ev, a band gap equal to or greater than 2.25 ev would be required. This theory was of no appreciable help in the search for a suitable semiconductor, however, inasmuch

as we had been restricting our investigations to semiconductors with a band gap of about 2.5 ev or higher, to avoid hole injection from the metal into the semiconductor under normal forward bias conditions.

Another requirement that the semiconductor must meet is that it must be possible to make an ohmic contact to the material for electrons from the substrate metal. It is not necessarily easy to meet this requirement, inasmuch as the semiconductor must necessarily make a high blocking contact to most metals.

It is desirable that the semiconductor be available in large, single crystals having good crystalline perfection, and it should be possible to suitably dope the crystals n-type down to a reasonable resistivity, say in the range 0.1 to 10 ohm-cm.

2. Summary of Zinc Oxide Effort

Some effort was devoted to investigating the suitability of zinc oxide (ZnO) as the semiconductor. Its band gap was known to be suitably large (about 3.2 ev). Its electron affinity had not been measured, but it had been estimated by Wright³ to be on the order of 3 ev. It was known to be possible to make ohmic contact to the material. It was known that it could be prepared in the form of sintered polycrystalline layers, and it was also available in single-crystal form from Minnesota Mining and Manufacturing Company.

Both sintered polycrystalline layers and single crystals were investigated. It appeared at one time that barriers of about 2.5 ev were being obtained. This came about as a result of large $1/C^2$ vs. V intercepts. We know now that such large values of intercepts can be caused by a contaminating layer between the semiconductor and the metal, such as could be caused by oil from the diffusion pump used to evacuate the bell jar used at that time. The best estimate of actual barrier heights on single-crystal ZnO is about 1 ev with silver electrodes.

3. Summary of Titanium Dioxide Effort*

Titanium Dioxide (TiO_2) was selected for study primarily because published I-V characteristics of TiO_2 /metal rectifiers appeared to indicate surface barrier heights of about 1.5 ev. The TiO_2 was prepared by oxidizing sheet titanium in steam, followed by a wet anodization process. This procedure automatically produced an ohmic contact between the metal and the oxide. The electron affinity of TiO_2 is unknown, and the band gap is disputable, but probably about 3.0 ev.

Excellent rectifiers were prepared using evaporated counter-electrodes of several metals, but attempts to measure the resulting barrier heights were unsuccessful. The $1/C^2$ vs. V curves did not behave properly, and no hot-electron spectrometer data could be obtained. Several attempts at securing vacuum emission from TiO_2 /metal/BaO structures were made, and some of these appeared to be partially successful. Difficulties were encountered, however, in retaining good I-V characteristics during the various steps involved in fabricating and processing a tube for test. In general, the I-V curves tended to degenerate into an ohmic condition during processing and testing.

Excellent cold emission was obtained on special structures wherein the contact to the surface film was itself a thin metallic film. When large voltages and currents were applied to the diodes, the resistance became very high as a result of the thin contact film opening up. The resulting hot-electron emission was doubtless of the transverse-field type. This emission was stable, but gradually decreased to negligible values in a few hours time as the metal film eventually disintegrated.

4. Gallium Phosphide

a. Availability of Gallium Phosphide Single Crystals

The majority of experimental work on GaP has been done using small crystals that were broken from polycrystalline clusters. In

* For a detailed description of TiO_2 investigation, see Appendix A.

general, these crystals appeared to have large impurity and imperfection concentrations. During the last quarter, better-quality single crystals of larger size have been obtained.

One crystal, approximately 10 mm in diameter and 0.5 mm thick was obtained from Monsanto Chemical Company. This crystal represents the results of the latest techniques developed at Monsanto and is of the highest purity and resistivity currently available. It is n-type, doped with tellurium, and with the (111) crystal faces coinciding with the large-area sides. The free-carrier concentration is reported to be about $7 \times 10^{17} \text{ cm}^{-3}$ and the resistivity is about 0.08 ohm-cm. The crystal contains up to 2 percent of arsenic, presumably due to the techniques used for its growth. It appears that sufficient crystals will be available from Monsanto; however, the cost is fairly high (\$240 per crystal). It is also possible to obtain crystals containing lower concentrations of arsenic, but the cost rises very rapidly as the arsenic concentration is lowered; the practical lower limit of arsenic is not known at present.

A second crystal, approximately 15 mm square and 0.5 mm thick was obtained from Stanford University. This crystal is of interest because of its higher resistivity and apparently greater purity and perfection. It is an n-type crystal and is doped with sulfur with the (111) crystal faces coinciding with the large-area sides. The resistivity is about 0.6 ohm-cm, although this has not been confirmed. This crystal was produced by a process developed at Stanford University, which is presumably different from the process used by Monsanto. As the supply of crystals available at the University is very small, additional crystals of this type would have to be grown at SRI, should the evaluation show definite advantages. This could be done, since all the process details are available; however, it appears that the quantity of material in the single crystal is sufficient to complete the objectives of the present phase of the program.

b. Preparation of Crystals

Preparation of the small crystals used in the beginning of the program consisted simply of breaking a suitable single crystal from a

polycrystalline cluster and etching in hot aqua regia (the sizes were so small that control of geometry was impractical). The Monsanto crystal was lapped and polished as received. It was cleaved along crystal planes into six smaller pieces, each shape approximating an equilateral triangle. One of these pieces was etched in 50% HF—50% HNO_3 prior to deposition of metal film. This somewhat slower etch than hot aqua regia appears to result in a more uniform, smooth surface. Other pieces to be used for optical and electrical measurements were left as received.

The Stanford crystal had not been lapped or polished. One side was fairly rough, but was flat on the average. The other side was smooth, but was somewhat wavy. The rough side of the crystal was next to the substrate during growth so it was taken as the reference side. The crystal was slightly wedge-shaped, so the initial lapping was done on the smooth side to make it parallel with the rough side. The rough side was then lapped smooth and both sides were polished. It was noticed that the originally rough side did not polish as well as the other side. This is presumably due to the differences in the crystal faces. Visual inspection of this crystal after polishing revealed some inhomogeneities. The density of the inhomogeneities was not great, but a few rather large areas of different color were observed. The possible effects of these on future results remain to be determined.

Lapping and polishing operations on GaP are accompanied by the release of phosphine gas. This condition is associated with any mechanical abrading process, which apparently enhances the formation of poisonous phosphorus compounds through catalytic action. Phosphine gas is very high in toxicity and the maximum allowable concentration is 0.05 ppm. Concentrations well below the maximum are easily detected, as phosphine has a strong characteristic odor which becomes noticeable at very low concentration levels. Because of the toxic qualities of the lapping and polishing products, all mechanical operations must be done in a fume hood with a flow rate sufficient to maintain concentrations below the maximum allowable values.

c. Measurements

During the final quarter, more emphasis was placed on determining some of the basic properties of the GaP materials. To obtain complete quantitative information on the various materials available would require a separate research program; however, sufficient measurements have been made so that a qualitative picture of the materials is now available.

The Monsanto and Stanford University crystals were large enough so that optical transmission measurements could be made. Transmission vs. wavelength data have been obtained on both of these crystals using the Perkin Elmer spectrometer and the tungsten source as set up previously for photo-excitation tests on cathodes (see Figs. 3 and 4). While this measurement is not the most sensitive to changes in crystal constitution, it is the least involved method from which a reasonable amount of information can be obtained.

Figure 5 shows the relative absorption constant for the Monsanto crystal; Fig. 6 shows the same data for the Stanford crystal. These absorption constants are calculated by assuming that the absorption is 100 percent at photon energies greater than 2.3 ev. This technique is subject to some criticism as the reflectance of the crystals has not been taken into account; however, as the crystals used were fairly thick and the reflectance is not anticipated to be large, it is considered a reasonable first approximation. The absorption constant for GaP is expected to be at least 100 cm^{-1} at 2.3 ev photon energy and since the thickness of the crystals used was about 0.050 cm, the unabsorbed radiation at the back of the crystal will be less than 0.7 percent of the incident radiation on the front face after only one pass through the crystal. If the reflectance is a low value as assumed, then corrections for multiple reflections within the crystal would be negligible, and the major reflection loss is due only to the incident light on the crystal.

Electronic transitions across the band gap of GaP must involve the absorption or emission of a phonon in order to conserve crystal momentum.

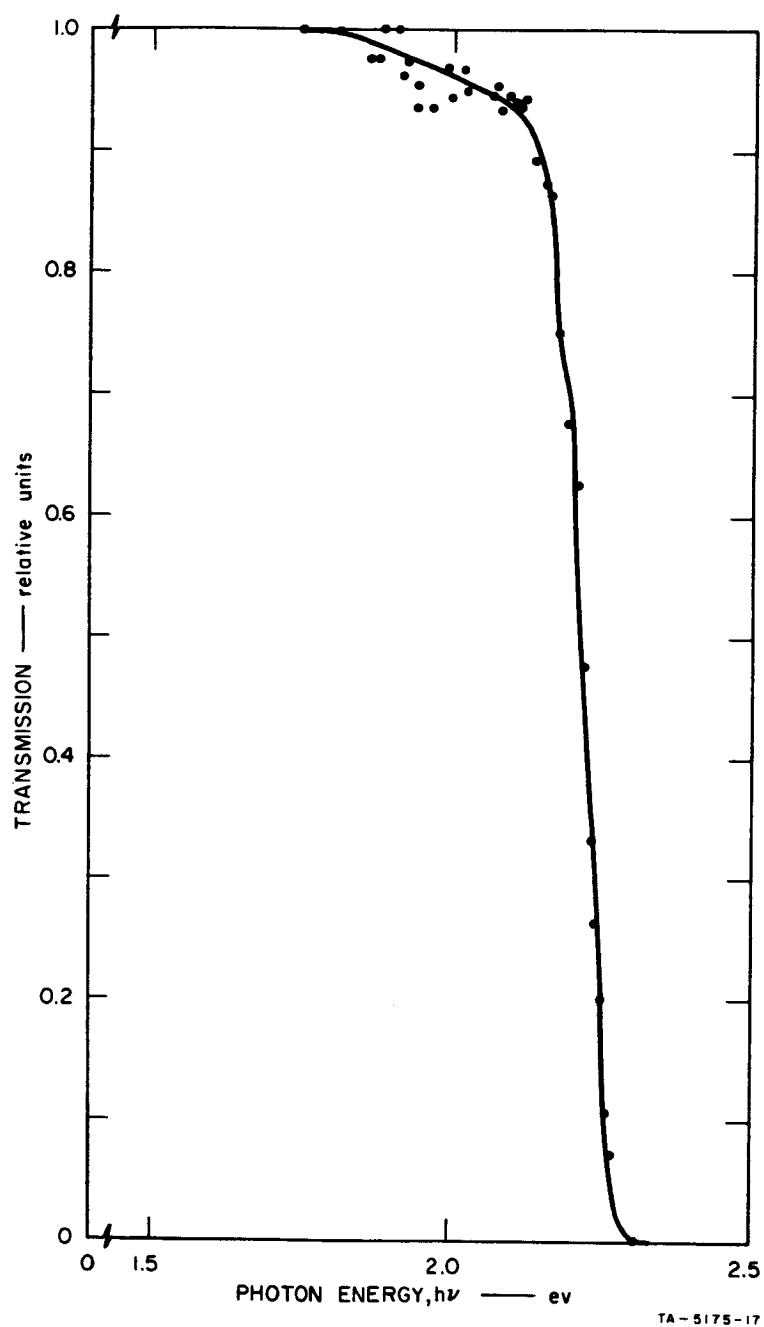


FIG. 3 NORMALIZED TRANSMISSION OF MONSANTO GALLIUM PHOSPHIDE

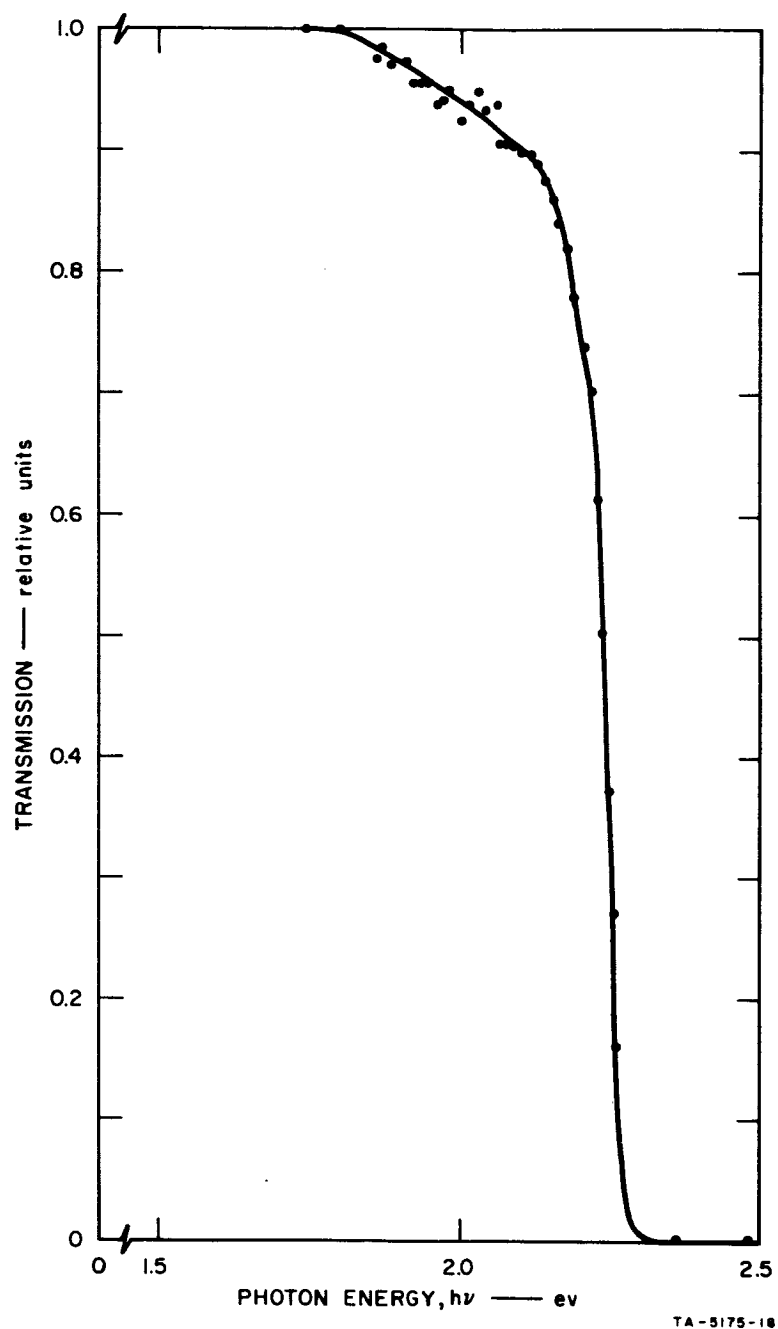


FIG. 4 NORMALIZED TRANSMISSION OF STANFORD GALLIUM PHOSPHIDE

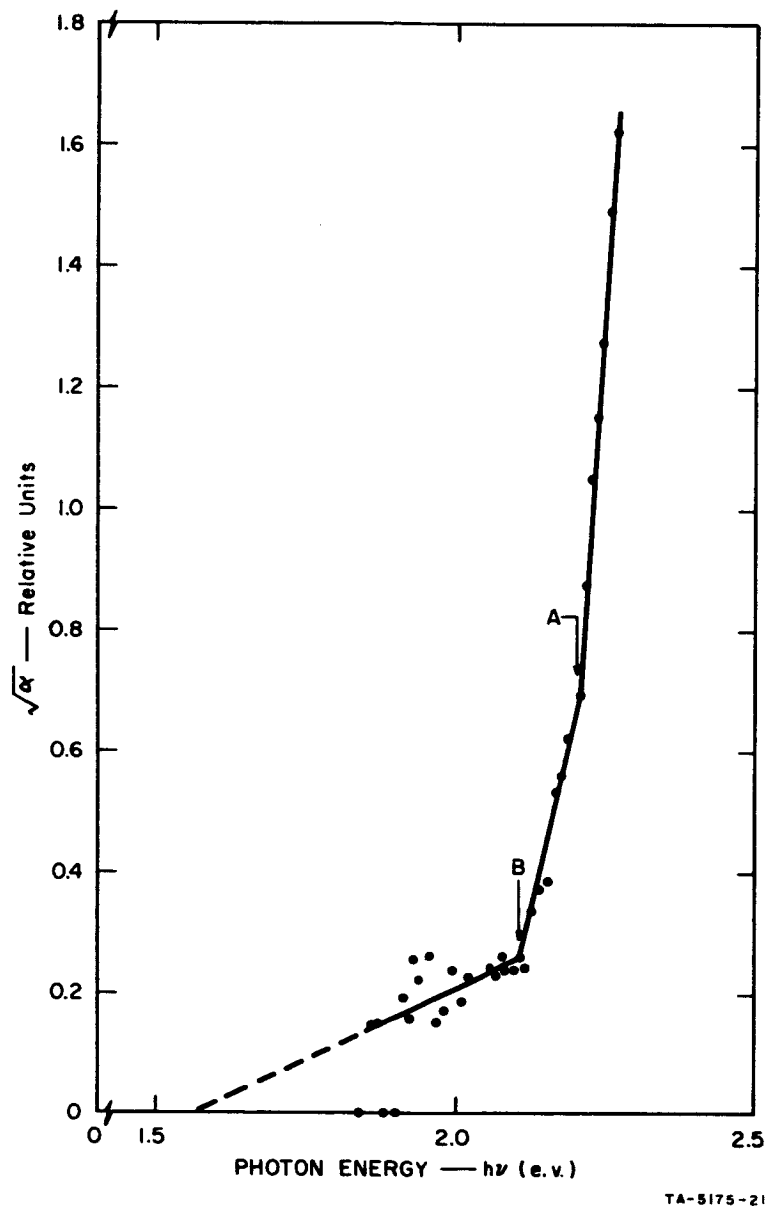


FIG. 5 RELATIVE ABSORPTION OF MONSANTO GALLIUM PHOSPHIDE

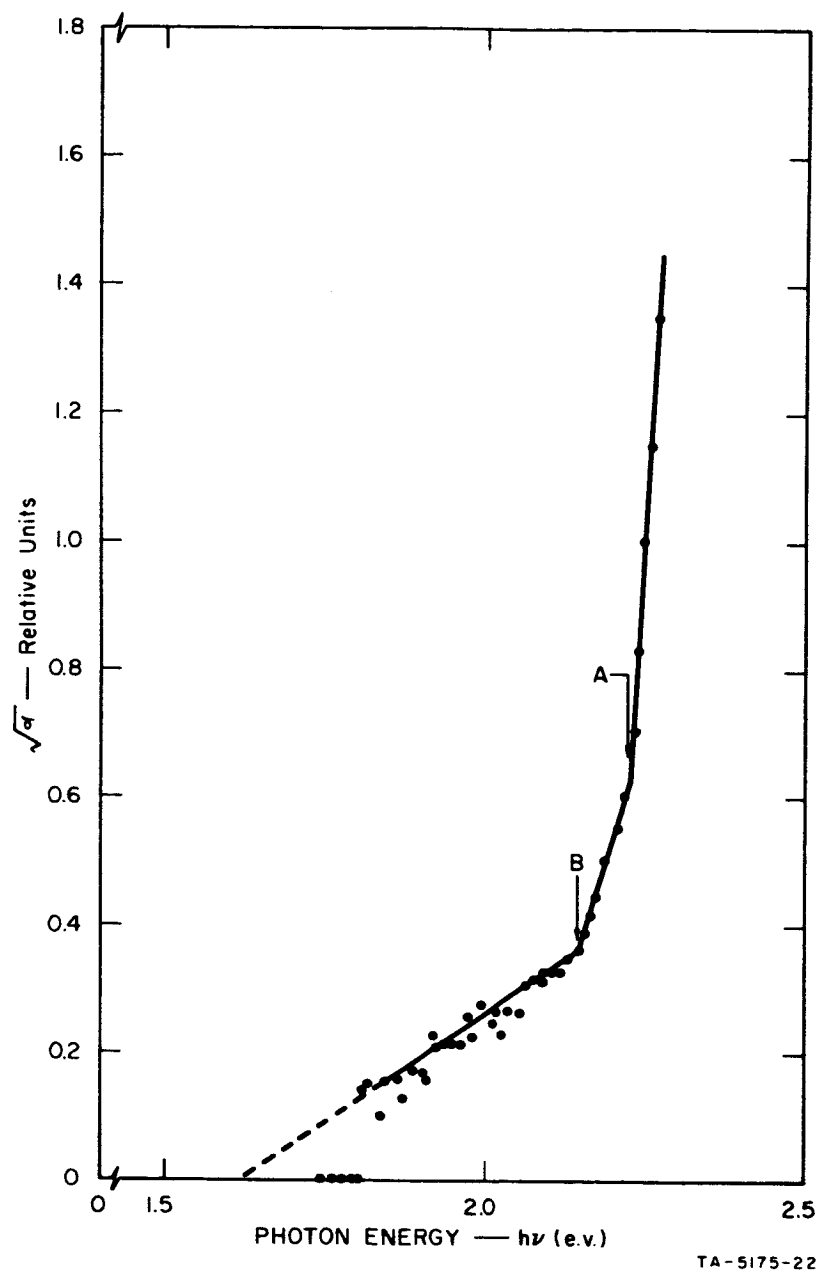


FIG. 6 RELATIVE ABSORPTION OF STANFORD GALLIUM PHOSPHIDE

For this situation the absorption constant is related to the absorbed photon energy as

$$\alpha = C \left\{ \frac{(E_p + E_s - E_g)^2}{\exp(E_s/kT) - 1} + \frac{(E_p - E_s - E_g)^2}{1 - \exp(E_s/kT)} \right\} \quad (1)$$

$$= \alpha_+ + \alpha_-$$

where:

E_p is the photon energy

E_s is the energy of the phonon involved in the transition

E_g is the forbidden band gap

k is Boltzmann's constant

T is the temperature in degrees Kelvin

C is a constant

α is the absorption coefficient.

The first term in Eq. (1) can be considered as optical absorption resulting in the simultaneous absorption of a phonon (α_+) and the second term can be considered as the optical absorption resulting from the emission of a phonon (α_-). If more than one phonon is involved, additional terms must be added for each phonon. From the experimental data, the two components of the absorption can be separated and the strength of the phonons and the band gap of the material can be determined from the relationships:

$$E_g = 1/2(E_+ + E_-) \quad (2)$$

$$E_s = 1/2(E_+ - E_-) \quad (3)$$

where

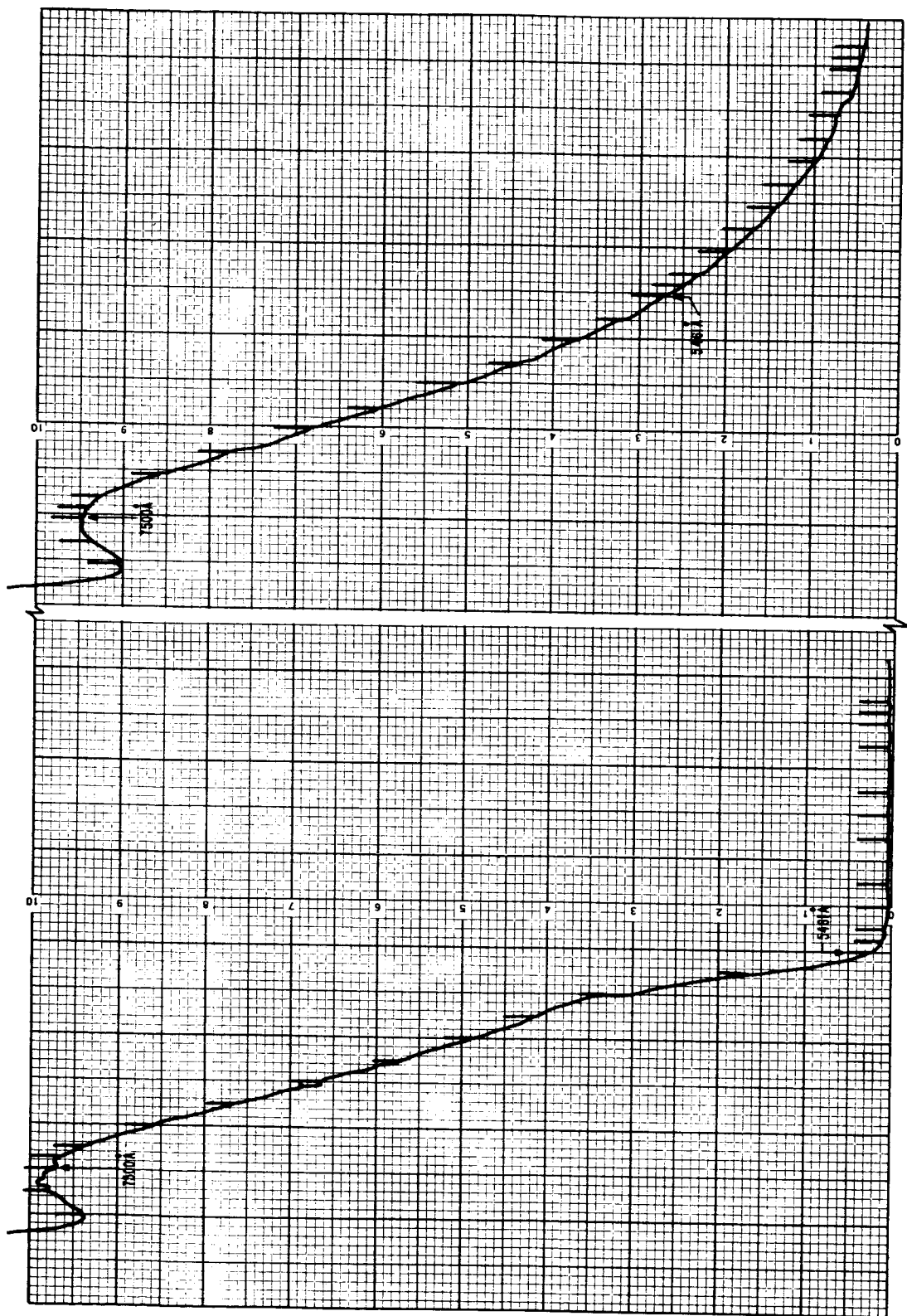
E_+ is the $\alpha_+ = 0$ intercept

E_- is the $\alpha_- = 0$ intercept

Figures 5 and 6 both show the effects of phonon absorption and emission; however, there is evidence that two prominent phonons are involved rather than one, as anticipated. Presumably, breakpoint A on the curves is indicative of the effects of the higher-energy phonon, and breakpoint B indicates the effects of a lower-energy phonon. In order to separate the effects of these two phonons, an additional breakpoint should occur at a lower photon energy than breakpoint B. Since the data become badly scattered at low absorption coefficients, this breakpoint is not obvious and exact values of the band gap are not determinable. From the data obtained, it appears that the band gap should lie between 2.15 and 2.22 ev for both the Monsanto and Stanford crystals at the temperature of the measurements.

Experimental difficulties that contribute to the scatter in the data at low absorption levels are primarily the result of the black-body characteristic of the light source. It turns out that the absorption edge of GaP lies on the short-wavelength side of the black-body radiation curve for tungsten where the radiant energy output varies rapidly with wavelength. Figure 7 is a reproduction of the raw spectrometer data and shows the effects of the tungsten source. In order to normalize the transmission data for GaP, the spectrometer readings must be divided by the output curve of the source. The absorption coefficient is then proportional to the logarithm of the quotient. This is tantamount to subtracting the logarithm of the amplitudes of the two curves. If any uncertainty exists in the values of the curves, its effect will be greatest when the absorption is small and the transmission is near unity where the two curves approach the same values. This effect shows up in a spread of the reduced data in Figs. 5 and 6 and is the primary reason that the structure of the absorption curve cannot be resolved at low values of the absorption coefficient.

Based on the experience outlined above, it appears that in order to obtain the resolution required, a light source with a flat intensity vs. wavelength characteristic extending from about 0.5 to 0.7 micron would be necessary. A number of suitable sources are available in the



TA-5175-23

(b) RESPONSE OF TUNGSTEN SOURCE

(a) TRANSMISSION DATA ON MONSANTO GaP

FIG. 7 TRACING OF SPECTROMETER DATA

form of various high-pressure arc lamps, but the intensity of the output in the wavelength range of interest is low compared to that of the tungsten source. To compensate for the lower intensity, it would be necessary to use a photomultiplier detector. This approach has not been pursued, however, since considerable additional effort would be required to make the necessary modifications to the spectrometer. At this time it is not felt that the extra effort in this direction is warranted.

Another characteristic of GaP that should be considered in cathode fabrication is the ability of the material to withstand a tube-processing environment. Two sets of data were considered in preparing the plot of phosphorus pressure vs. temperature in Fig. 8. The values from Johnston⁴ were measured by the Knudsen effusion method for the dissociation of GaP into gallium and phosphorus. He states that most of the gallium does not leave the heated region of the cell and he has corrected the phosphorus pressure for the small amount of gallium detected. It is not known if the data from Willardson and Goring⁵ for the higher temperatures have been similarly corrected.

Johnston developed an empirical relationship for the phosphorus pressure as a function of temperature:

$$\log p \text{ (mm)} = \frac{-18,870}{T^{\circ}\text{K}} + 13.60$$

for the temperature range 781°C - 1005°C.

Extrapolating to 600°C results in a phosphorus pressure of 1×10^{-8} torr, so it seems reasonable to state that the GaP could withstand processing environments up to this temperature.

C. SURFACE FILM

1. Summary of Requirements

The primary requirement on the metal surface film in the proposed cathode structure is that the barrier height ϕ_b of the resultant surface barrier be higher than the metal work function ϕ'_m after activation. As will be discussed in Part D below, the lower bound on ϕ'_m for BaO activated metal films seems to be about 1.35 eV; the barrier height ϕ_b must therefore

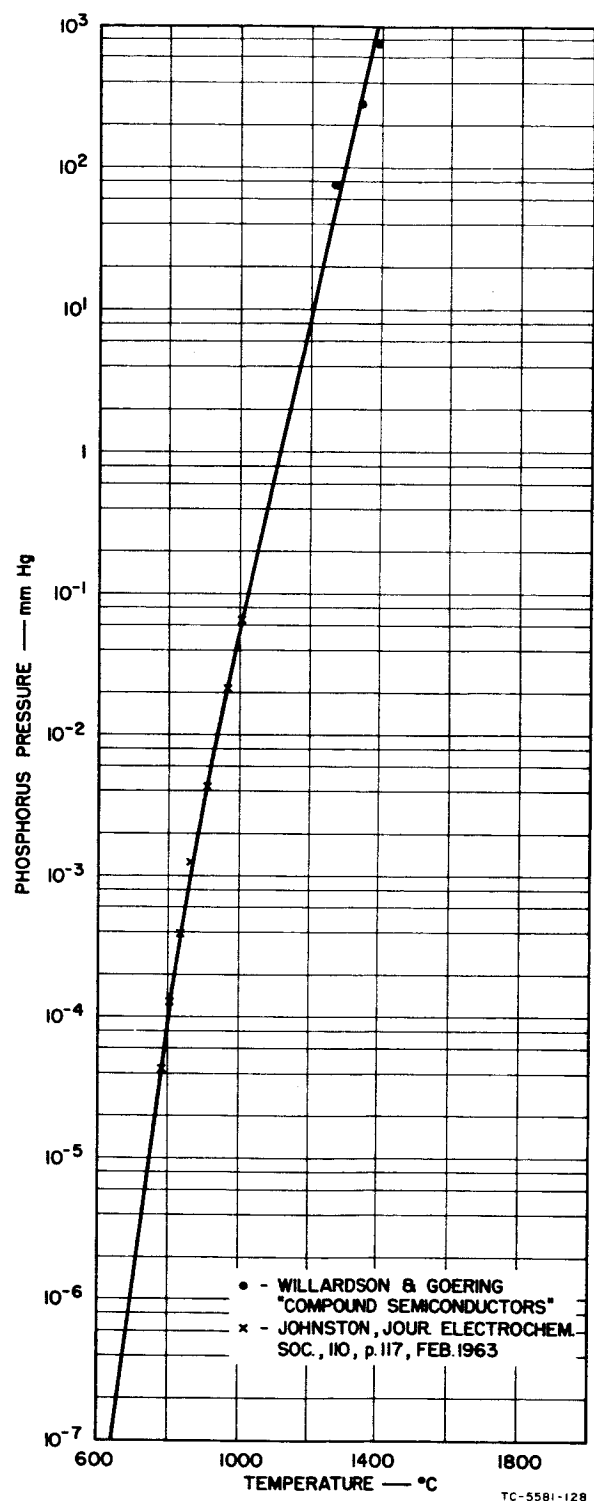


FIG. 8 DISSOCIATION PRESSURE
OF GALLIUM PHOSPHIDE

be greater than this value. As will be discussed in more detail in Part D, almost all theoretical and experimental evidence points to the fact that higher metal/semiconductor surface barriers are correlated with higher work functions for the metal used to form the contact. This places fairly severe restrictions on the metal, for as will be discussed later, it is only the highest work function metals that produce surface barriers exceeding the minimum acceptable height of 1.35 ev.

The thickness of the metal surface film is important in that it determines, for a given hot electron energy, the fraction of electrons that reach the metal/vacuum interface after being emitted over the metal/semiconductor surface barrier. This fraction is equal to $\exp(-t/L)$, where L is the attenuation length for electrons in the particular metal, and t is the film thickness. The attenuation length L is energy-dependent, and is of course different for each metal. Recent measurements in the range of energies 1.2-1.6 ev indicate that L is in the range 200-400Å for most of the metals of interest in this study. If the fraction of electrons reaching the metal/vacuum interface is to be appreciable, the film thickness must not be much larger than the electron attenuation length; it is preferable that it be somewhat smaller than L , in fact.

The lateral conductivity of the surface film must be good in order to avoid excessive lateral voltage drop. This is not expected to be a severe requirement, in view of the fact that most metal films a few hundred angstroms in thickness have sheet resistivities of the order of 1Ω per square. In the event that it becomes desirable to use much thinner films, the lateral conductivity problem can easily be overcome by the evaporation of a somewhat thicker grid of metal over the surface film, as discussed in the First Quarterly Report¹ for the project.

A further requirement on the metal surface film is that it must not tend to agglomerate, as do some metals, e.g., silver, in very thin films. From the standpoint of surface barrier height and ease of activation, however, it appears that one of the refractory metals, e.g., platinum, tantalum, or tungsten, will be used to form the surface film; agglomeration is not usually a problem with these metals.

2. Metal/Semiconductor Contacts

The relation of surface barrier height in metal/semiconductor diodes to the physical parameters of the semiconductor and metal has been the subject of intensive study over the past 30 years. It is only recently, however, that this research has begun to yield quantitative theoretical results, due mainly to the fact that in past years reliable and reproducible experimental data with which to compare theory were not available. In recent years, as a result of significant advances in both vacuum technology and crystal growth techniques, a large number of metal/semiconductor combinations have been carefully studied. Out of these studies have grown several theories relating barrier height to metal and semiconductor properties.

The well-known Schottky theory⁶ predicts that the barrier height will be equal to the difference between metal work function and semiconductor electron affinity. In general, it is observed that the variation of ϕ_b with ϕ_m is monotonically increasing, but much less rapidly than predicted by Schottky theory, and it has been proposed by Bardeen⁷ that this can be explained by the presence of localized electronic states in the forbidden gap at the semiconductor surface. Theories based on Bardeen's model for semiconductor "surface states" have been moderately successful in predicting the variation of ϕ_b with ϕ_m .⁸ The importance of barrier height theories in the present work stems mainly from the desirability of being able to predict the barrier height of a particular metal/semiconductor combination. Consequently, some of the research effort during this program has been directed at the refinement of existing barrier height theories.

The experimental work on Schottky barriers is briefly summarized in the following paragraphs.

a. Tantalum Oxide, Niobium Oxide, and Silicon Oxide

Before the initiation of the present program, the semiconductors tantalum oxide (Ta_2O_5), niobium oxide (Nb_2O_5), and silicon oxide (SiO_2) were investigated as possible candidates for the fabrication of the Schottky barrier cathode. The difficulty in fabricating reproducible

structures from these semiconductors led to their eventual abandonment in favor of semiconducting ZnO.

b. Zinc Oxide

Barriers formed by vacuum evaporation of silver onto ZnO at first appeared to be greater than 2 ev. Later experiments cast doubt on this value, and ZnO was subsequently abandoned. Studies of semiconducting TiO_2 were undertaken at this time.

c. Titanium Dioxide

A large effort was devoted to the study of TiO_2 Schottky barriers. Capacitance measurements seemed to indicate high (~ 2.0 ev) barriers, but this could not be confirmed photoelectrically due to the absence of a photoeffect. Difficulty in fabricating reproducible TiO_2 films, and evidence of instability of the I-V characteristics of TiO_2 diodes in vacuum finally led to the abandonment of this material.

d. Gallium Phosphide

Gallium phosphide has been most recently studied in connection with this program. Published results of other workers⁸ indicate barriers as high as 1.45 ev with platinum films on n-type GaP, and this value has been verified in our laboratory. It is anticipated, on the basis of recent measurements on W/GaP ($\phi_b \simeq 1.40$ ev as indicated in Fig. 9) and experimental results on the work function of W/BaO surfaces,⁹ that a successful cathode might be obtained by BaO activation of a thin film of tungsten on GaP. Time did not permit the experimental evaluation of this structure during the present program, however.

D. ACTIVATION

1. Summary of Requirements

The major requirement in activating the cathode surface is to produce a work function into the vacuum that is lower than the height of the metal/semiconductor barrier. The activated surface should be stable in a good vacuum and should be capable of withstanding the processing schedule for the assembled tube. In addition, the process should be relatively simple so that it can be reproduced without difficulty.

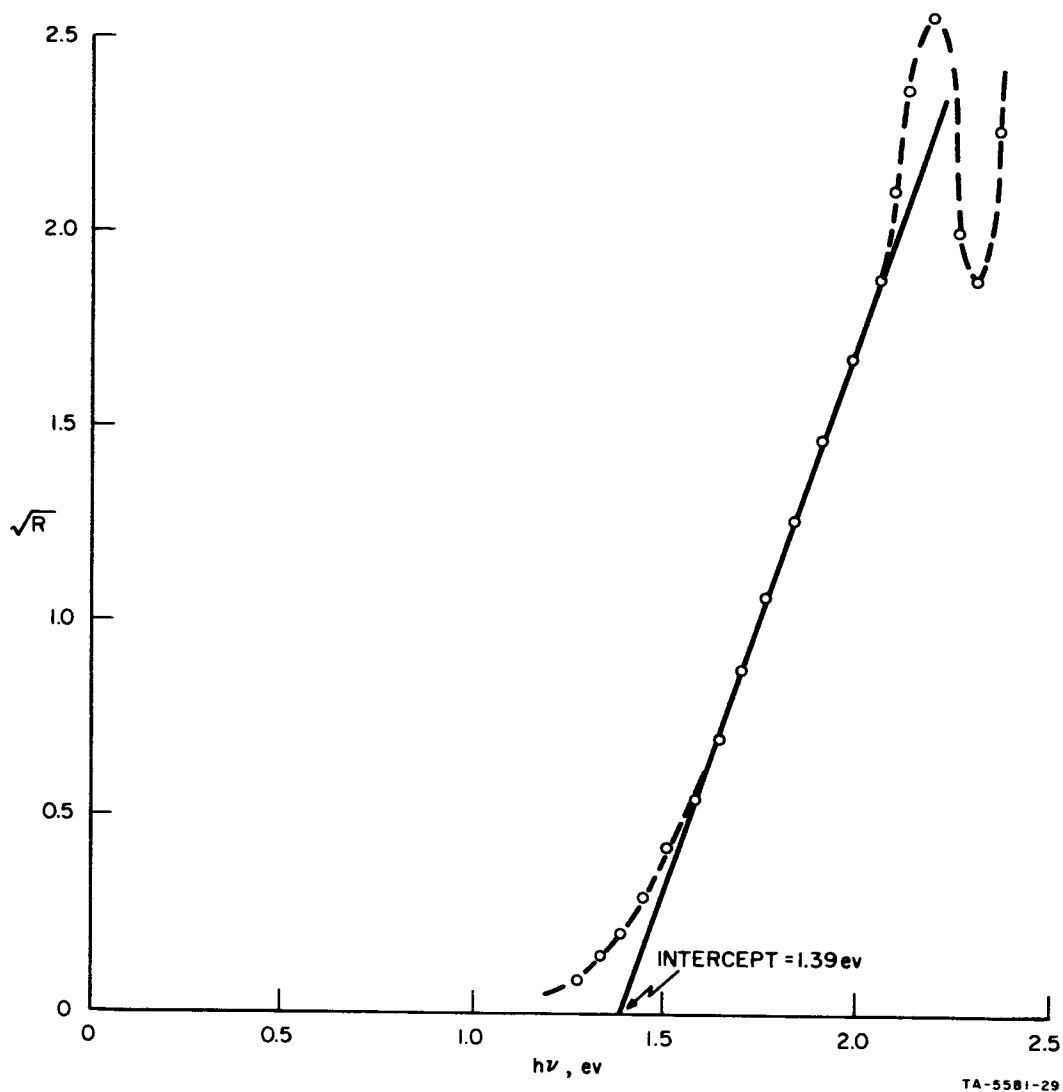


FIG. 9 SQUARE ROOT OF PHOTORESPONSE vs. PHOTON ENERGY
FOR GALLIUM PHOSPHIDE/TUNGSTEN DIODE

2. Measurements

In work prior to this program, cesium was used for activation and an evaluation of some rare-earth hexaborides [gadolinium hexaboride (GdB_6) and lanthanum hexaboride (LaB_6)] was made. During the course of this investigation, thin films of evaporated barium oxide (BaO) were used exclusively. A number of phototubes were fabricated in which BaO was evaporated on various metals. Photoelectric measurements were made using a PE112 spectrometer, from which the vacuum barriers were determined.

The experimental procedure in activating with BaO has followed the technique of Moore and Allison,⁹ who report thermionic work functions as low as 1.0 ev with 10 to 30 monolayers of BaO on Molybdenum. They did not measure BaO on platinum but they obtained 1.9 ev with one monolayer of strontium oxide (SrO) on platinum.

The results of the measurements in this laboratory are summarized in Table I. One of the lowest values obtained was 1.35 ev on evaporated silver, and this was measured some nine months after an initial measurement of 1.44 ev. The actual decrease in the value of ϕ is not as significant as the fact that a low value of ϕ can be maintained over a period of time in a good vacuum. The actual pressure in this phototube cannot be determined, but the tube is gettered with barium and the pressure is estimated to be of the order of 10^{-9} torr.

Unfortunately silver is not a suitable metal for the surface film of the cathode structure because it agglomerates at relatively low temperatures. A number of measurements were made on evaporated platinum but the lowest value obtained was 1.55 ev. The results of two different methods of analyzing the data from the last phototube are shown in Figs. 10 and 11. (For a comparison of these two methods, see Appendix A in Ref. 10.) As indicated in Part C above, vacuum barrier values for BaO on platinum in excess of 1.45 ev, the metal/semiconductor barrier for platinum on GaP, preclude the use of platinum in this structure. Consequently, the most recent work was concerned with measuring the vacuum barrier of BaO on evaporated tungsten, which has not been completed.

E. EXPERIMENTAL RESULTS

Some vacuum emission results were reported in the Third Quarterly Report¹¹ which were attributed to a transverse field phenomena on the surface of the TiO_2 -Pt cathodes. While vacuum emission has not unambiguously been obtained with a Schottky-barrier cathode, it has been demonstrated that surface-barrier structures are extremely stable and are capable of operating for thousands of hours without deterioration. Figure 12 is a photograph of the I-V characteristic on a curve tracer

Table I

SUMMARY OF RESULTS OF BARIUM OXIDE ACTIVATION EXPERIMENTS

Phototube No.	Cathode Material	Measurement of ϕ	Comments
1	Molybdenum Sheet	1.75 ev	Initial measurement after tube was tipped off.
		1.95 ev	Measurement made 3 weeks later after outgassing Molybdenum.
2	Molybdenum Sheet	2.3 ev	Tube incompletely processed.
3	Molybdenum Sheet	1.8 ev	Measurement made with tube on pump.
4	Evaporated Silver	1.44 ev	Initial measurement after processing.
		1.40 ev	Six weeks after initial measurement.
		1.47 ev	Five months after initial measurement.
		1.35 ev	Nine months after initial measurement.
	Evaporated Platinum on TiO ₂ /Ti cathode structure	1.55 ev	
	Evaporated Molybdenum on TiO ₂ /Ti cathode structure	1.75 ev	
5	Evaporated Platinum on sheet Tantalum substrate	1.80 ev	Tantalum substrate was incompletely covered with Platinum. Plots with double intercepts were obtained giving value of 1.32 ev for Tantalum.
6	Evaporated Platinum on Molybdenum substrate	1.58 ev	Two methods of analyzing same data.
		1.625 ev	

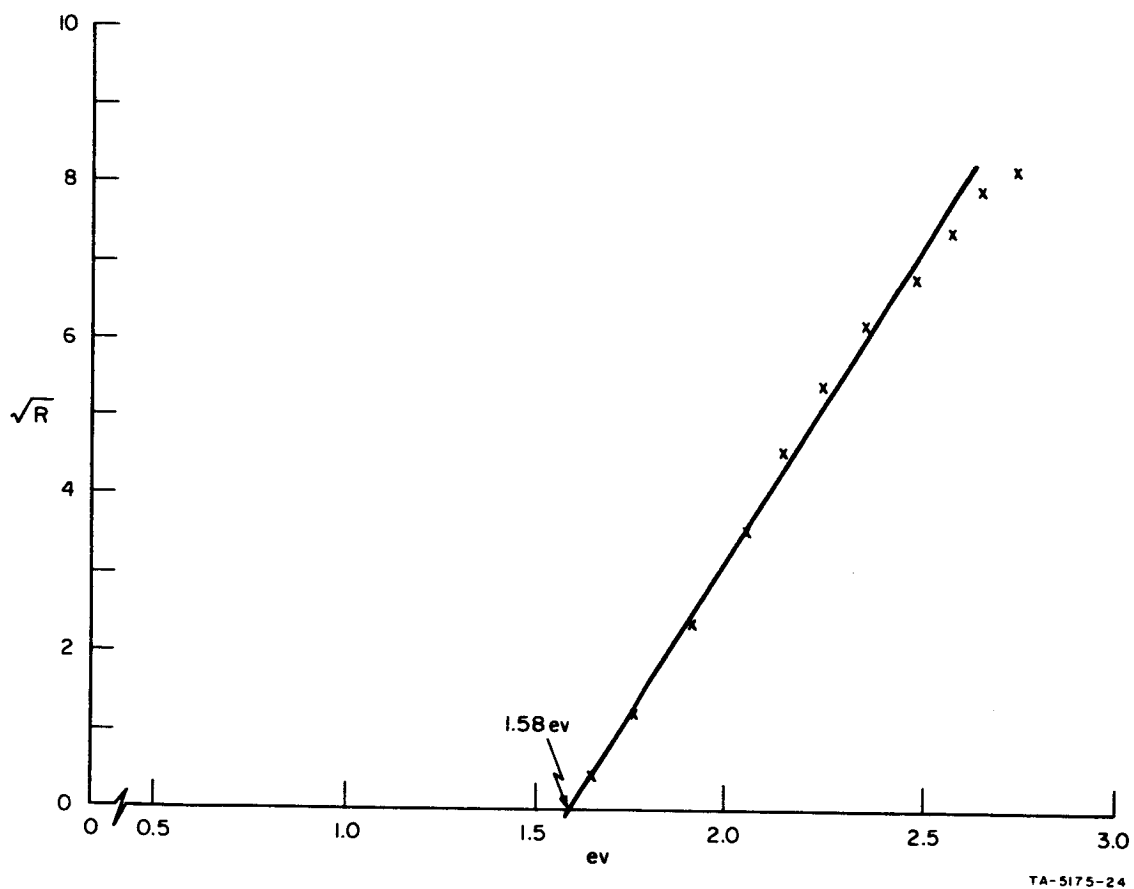
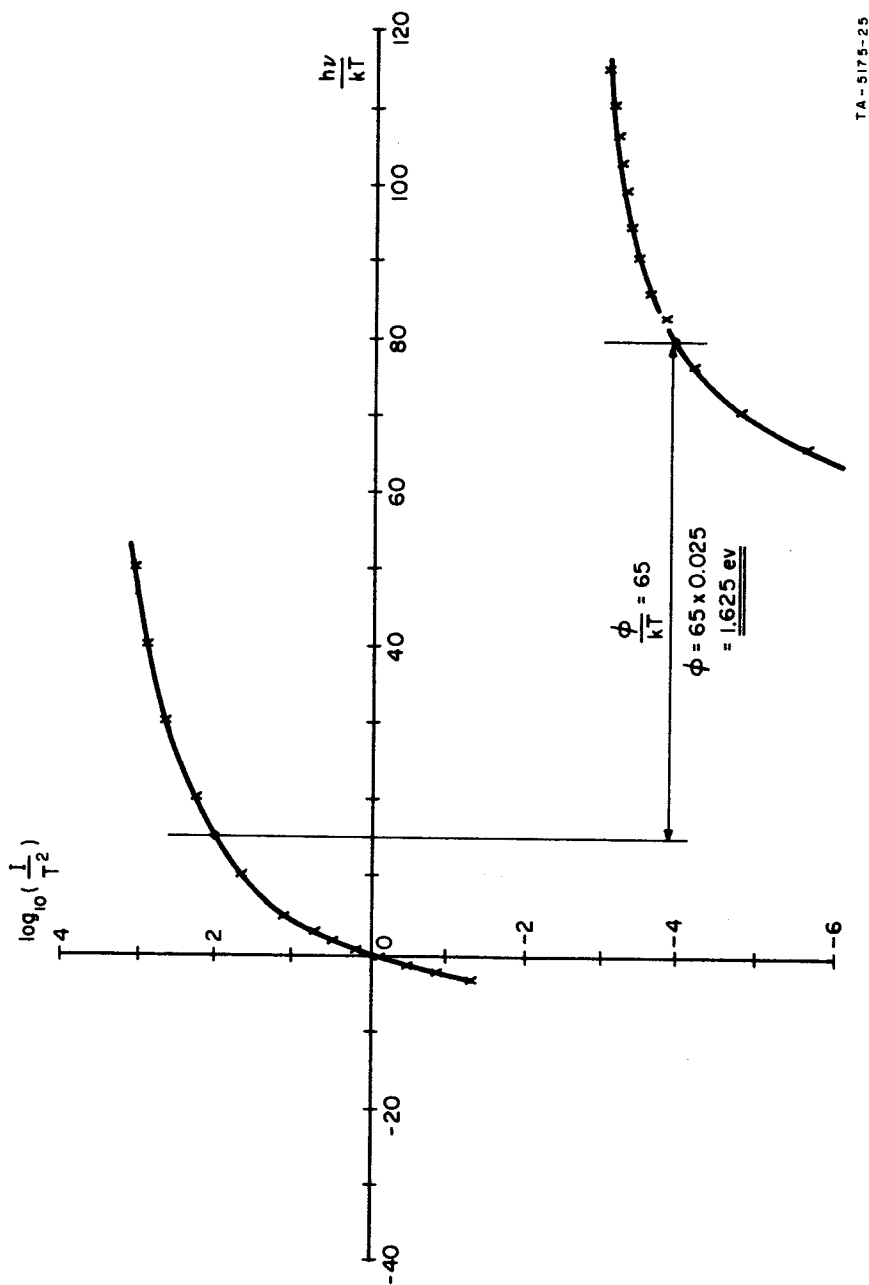


FIG. 10 SQUARE ROOT OF PHOTORESPONSE vs. PHOTON ENERGY
FOR PLATINUM/BARIUM OXIDE PHOTOCATHODE



TA - 5175-25

FIG. 11 FOWLER PLOT FOR PLATINUM/BARIUM OXIDE PHOTOTUBE

of the single-crystal ZnO/silver paint diode that has been operating continuously at 10-ma forward current with 0.95 v applied bias for 7500 hours.

Figure 13 is the same type of photograph for a single-crystal GaP/evaporated-platinum diode that has been on dynamic life test for 2200 hours. A test on a TiO_2/Pt diode was terminated at 1450 hours when the oscilloscope broke down. Figure 14 is typical of the characteristics obtained with TiO_2/Pt diodes.

The stability of BaO-activated surfaces has also been demonstrated (Sec. II-D-2). Their operation in a good vacuum is consistent over a period of at least 6500 hours. Unfortunately the metal/semiconductor barrier heights obtained with the various semiconductors investigated--ZnO, TiO_2 , and GaP--have not been compatible with the vacuum barriers obtained with BaO activation. One of the highest metal/semiconductor barriers measured in this investigation was that obtained with evaporated platinum on single-crystal GaP. Figure 15 is a plot of the square root of the photoresponse vs. photon energy, which resulted in an intercept of 1.4 ev for this diode.

When it was found that a work function for BaO-activated platinum lower than the value of the GaP/Pt barrier could not be obtained, experiments with evaporated-tungsten films were started. Some measurements on GaP/W diodes have been made in addition to the barrier height measurement

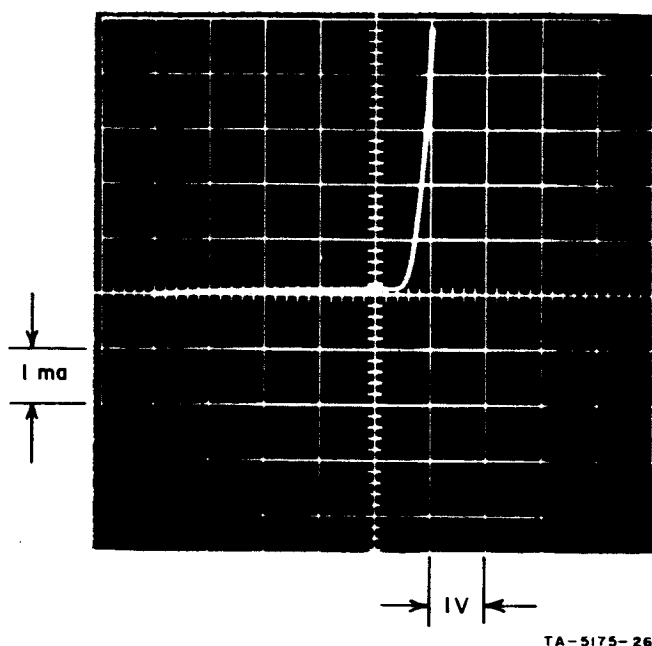
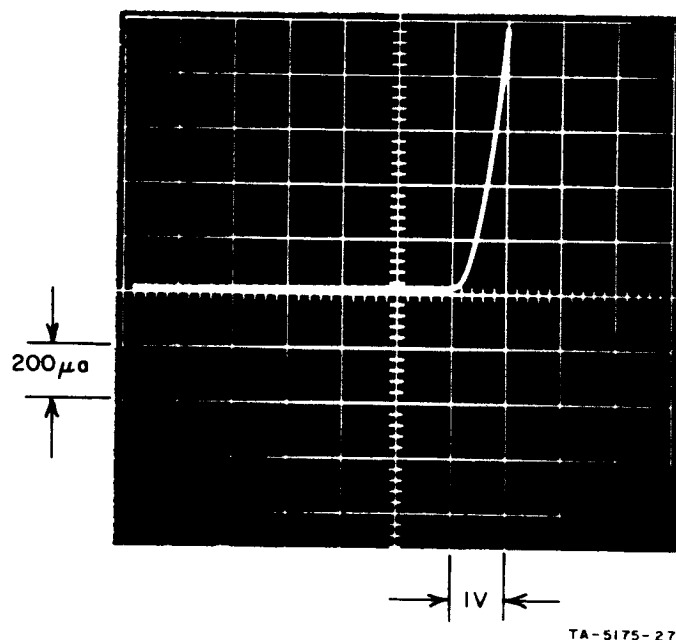
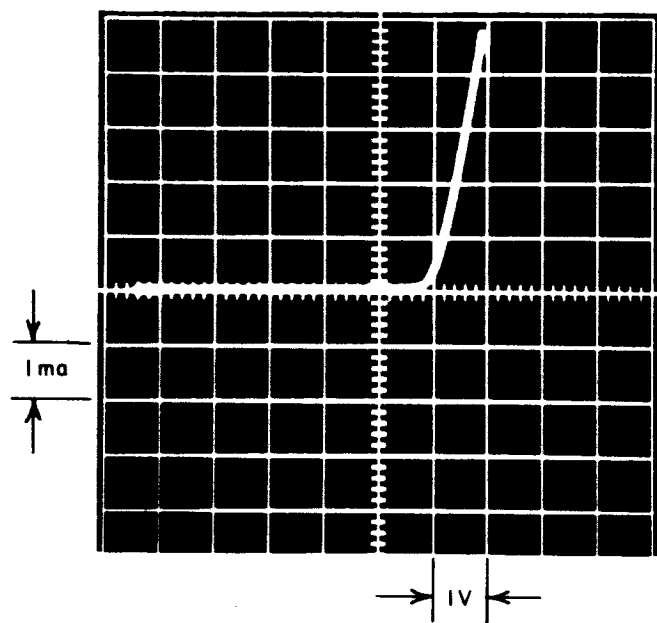


FIG. 12 I-V CHARACTERISTIC OF SINGLE-CRYSTAL ZINC OXIDE/SILVER PAINT DIODE AFTER 7500 HOURS OF OPERATION



TA-5175-27

FIG. 13 I-V CHARACTERISTIC OF GALLIUM PHOSPHIDE/EVAPORATED PLATINUM DIODE AFTER 2200 HOURS OF OPERATION



TA-5175-28

FIG. 14 I-V CHARACTERISTIC OF TITANIUM
DIOXIDE/EVAPORATED PLATINUM DIODE

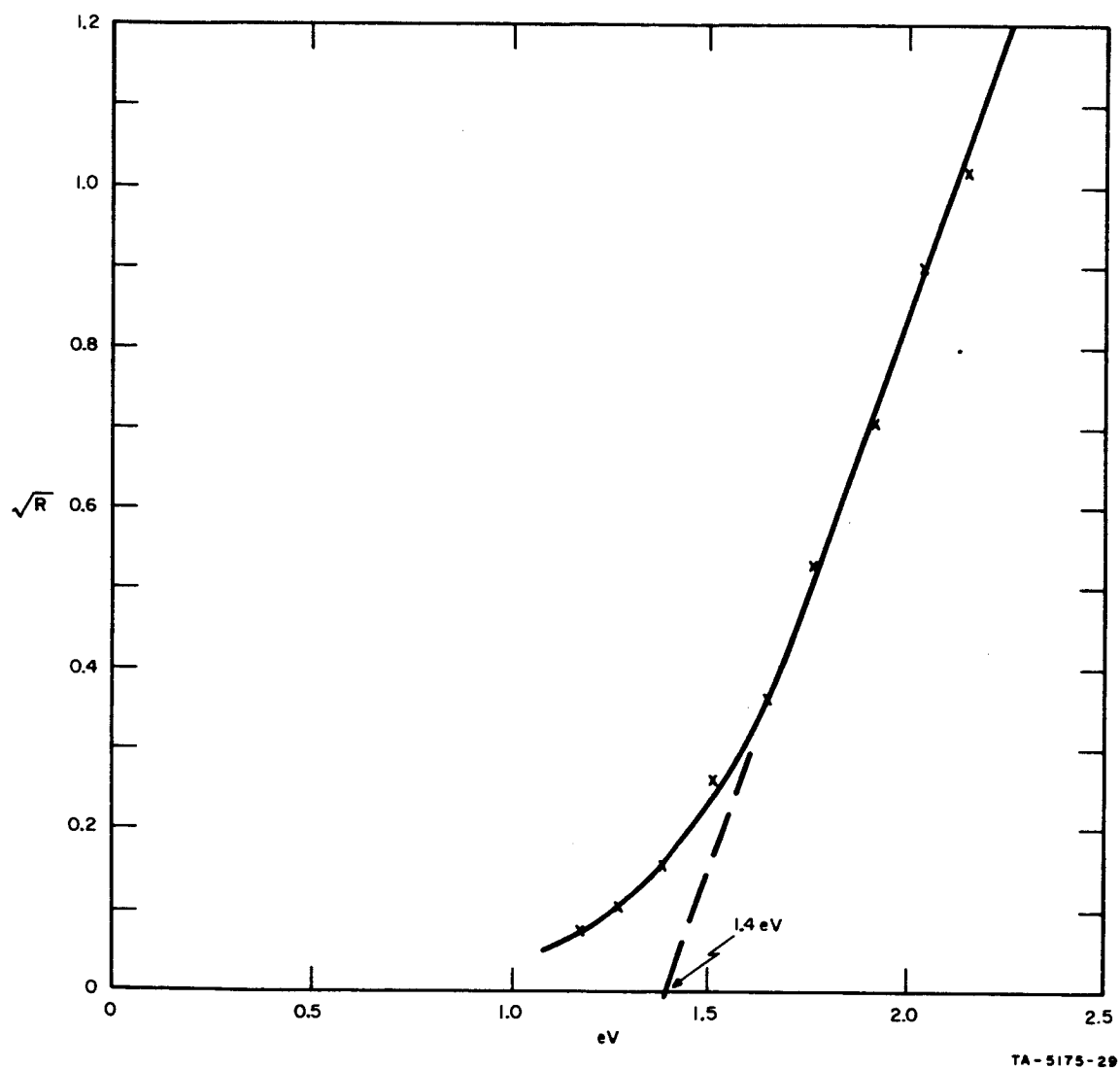


FIG. 15 SQUARE ROOT OF PHOTORESPONSE vs. PHOTON ENERGY FOR GALLIUM PHOSPHIDE/EVAPORATED PLATINUM DIODE

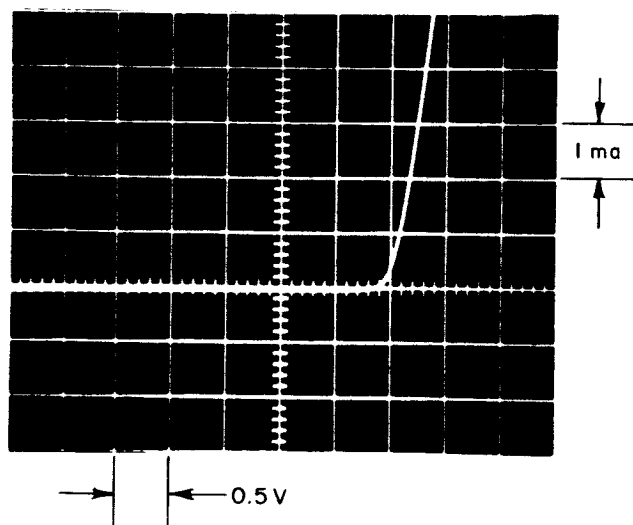
reported in Sec. II-C-2.

Figure 16 is a photograph of an I-V characteristic and Fig. 17 is a log I vs. V plot from one of the diodes. The nonlinear portion at low current levels is probably due to surface leakage. In the linear portion, $n \approx 1.7$ in the expression:

$$J = J_0 \exp \left(\frac{qV}{nkT} \right),$$

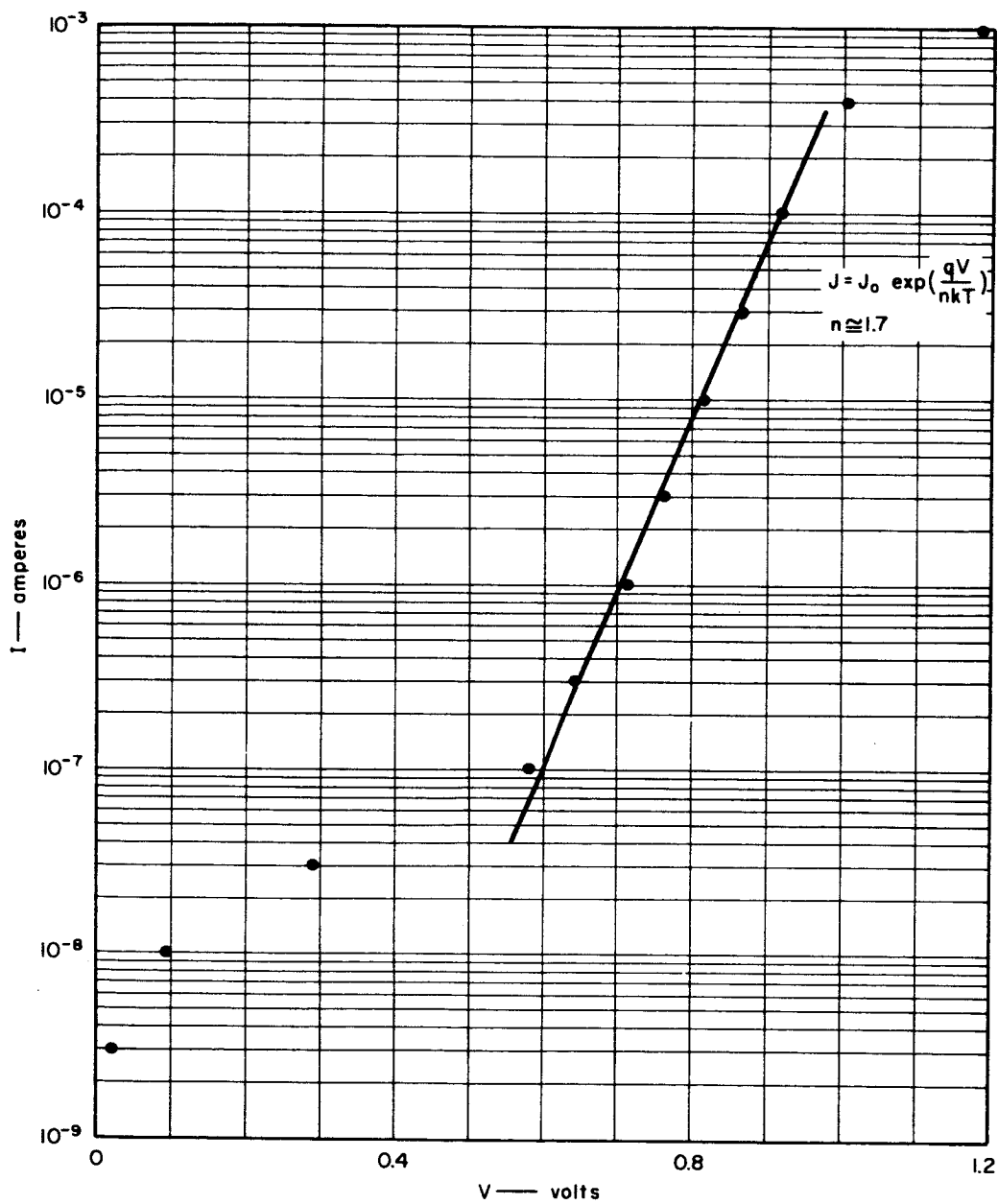
which indicates the possibility of some recombination occurring in the vicinity of the metal/semiconductor junction.

With regard to the results obtained with evaporated platinum and tungsten on GaP, it should be noted that the evaporations were carried out in a recently-assembled, oil-free vacuum system (Fig. 18). It has been demonstrated that erroneous results can be obtained when metal/semiconductor barriers are fabricated in an oil-pumped system. A monolayer of pump oil has the effect of producing higher barriers as measured by $1/C^2$ vs. V plots. Each port on this system is equipped with an optical window for spectrometer measurements, and small electron-beam evaporators fit into the manifold for depositing the refractory-metal films.



TA-5581-30

FIG. 16 I-V CHARACTERISTIC OF GALLIUM PHOSPHIDE/EVAPORATED TUNGSTEN DIODE



TA-5581-6

FIG. 17 LOG I vs. V PLOT FOR GALLIUM PHOSPHIDE/EVAPORATED TUNGSTEN DIODE

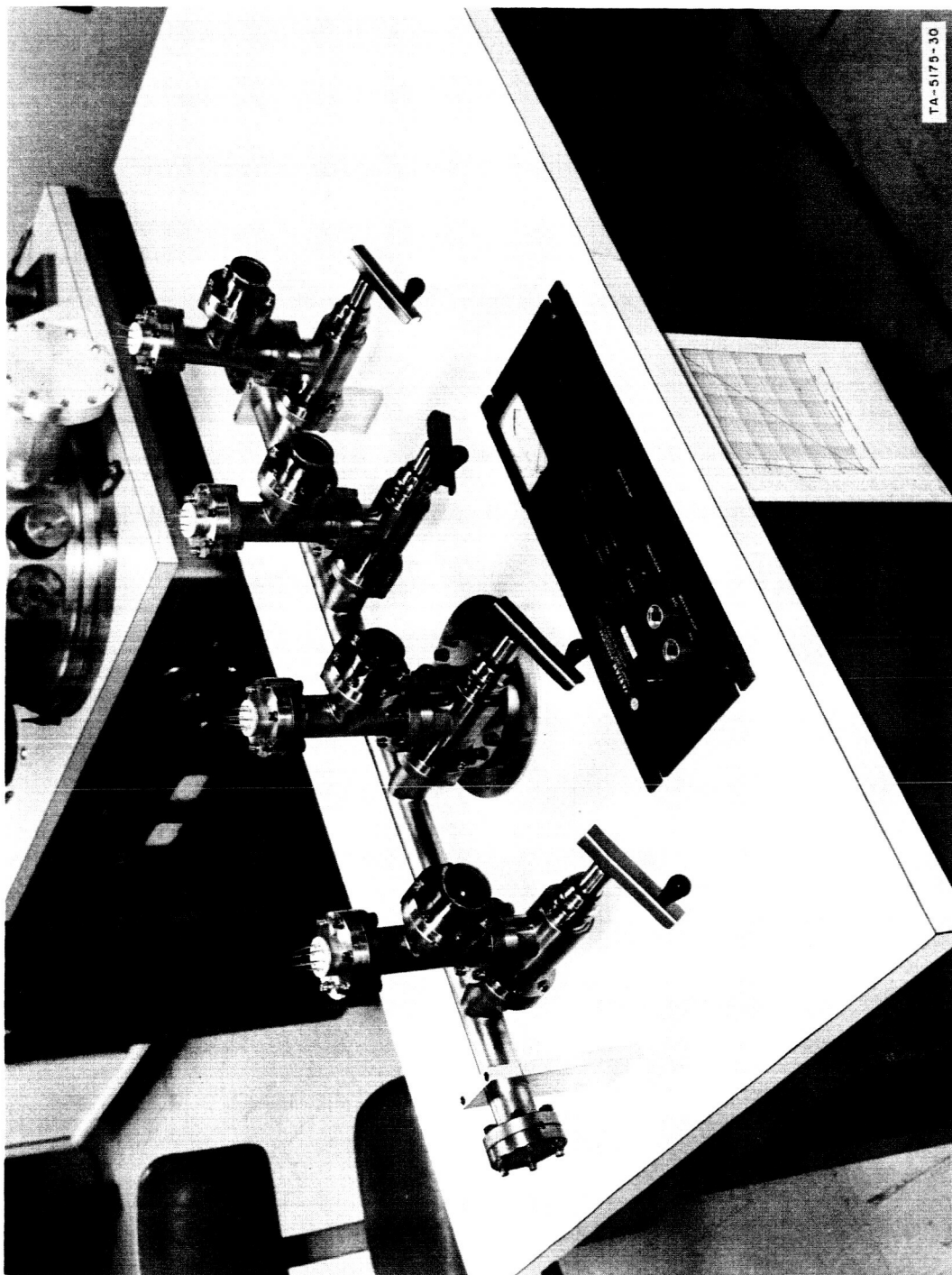


FIG. 18 PHOTOGRAPH OF MULTI-PORT, OIL-FREE VACUUM STATION

III SUMMARY AND CONCLUSIONS

Major progress was made towards the ultimate objectives during the course of the program. The accomplishments can be summarized as follows:

(1) A satisfactory refractory metal/ceramic substrate was developed that can be incorporated into metal/ceramic traveling-wave tube guns to replace the conventional thermionic cathode.

(2) Metal/semiconductor diodes were intensively studied using various metals on the semiconductors ZnO, TiO_2 , and GaP. Reproducible surface barriers as high as 1.45 ev can be achieved with GaP.

(3) The theory of metal/semiconductor contacts has been extended and refined so that it is now beginning to be possible to predict barrier heights with some degree of confidence (to within about ± 0.1 ev in typical cases).

(4) It has been demonstrated that vacuum work functions down to about 1.3 ev can be obtained by evaporating a thin layer of BaO onto a suitable metal substrate.

(5) Long dynamic life (thousands of hours) has been demonstrated for ZnO/Ag and GaP/Pt hot-electron diodes. Very long life has been demonstrated for evaporated BaO photosurfaces.

In conclusion, the work to date has not uncovered any obstacle that would prevent achievement of the objective of developing a practical surface-barrier cathode to replace the thermionic cathode in traveling-wave tubes and other vacuum tubes.

Appendix A

DETAILS OF TiO_2 INVESTIGATION

The investigation of TiO_2 started in December 1964 following a procedure reported by Komolova and Nasledov.¹² The details of the initial process were as follows:

- Cut A55 grade sheet titanium, 0.032-inch thick, into small squares
- Perform superficial polishing with SiC abrasive paper
- Vapor degrease in trichlorethylene
- Dip 15 sec in Globe Cleaning Solution
- Rinse and oxidize in steam at 750°C for 3 hours
- Anodize at 35v rms in a 5 percent NaOH solution for 2 hours
- Sandblast corners and weld nickel leads to the titanium
- Apply surface electrodes of silver paint or evaporated platinum.

The diode characteristics with silver paint were usually better than those with evaporated platinum. The characteristic always deteriorated when the test piece was mounted and sealed into a vacuum envelope. Attempts to measure barrier heights were unsuccessful.

The oxidation temperature was reduced to 650°C after some experimentation and considering data published by Breckenridge and Hosler¹³ at the National Bureau of Standards. Some problems were encountered in the anodizing process but these were largely due to electrical contacts and the freshness of the NaOH solution.

Pellets were punched from the titanium sheet to fit on the cathode substrate. These were deburred and oxidized by the processes described above. Platinum was evaporated on the surface to form a grid, overlaid with a thin film of the same metal, plus a thick annular deposit to contact the top hat. Short circuits developed at the edge of the lip

on the top hat during emission tests. Deburring the inner surface of the top hat and adding an annular deposit of Al_2O_3 on top of the TiO_2 did not help. Some hot-electron emission was detected but it was masked by the thermionic emission resulting from the heating in the region of the shorts.

Following a meeting on February 10 with representatives from MEC and NASA, a modified substrate design was adopted for the purpose of evaluating the TiO_2 . This comprised a titanium pin and platinum pin beaded closely together with G-12 glass. The bead was cut and polished to expose the ends of the two pins. Titanium dioxide was formed on the titanium by the processes previously described. Platinum was evaporated on the surface and emission tests were carried out. In one test emission was obtained in the vicinity of 2 v bias, but most of these cathodes operated as transverse field emitters due to fissures developing in the platinum surface film.

Early in April some high-purity metal (99.9999% titanium) was obtained. An analysis of the A55 grade material revealed a 0.2% iron content so it was decided to use the high-purity metal in all subsequent experiments.

About this time it was also found that the surface preparation of the titanium prior to oxidation was a significant factor in the operation of the TiO_2 diodes. A number of polishing compounds and techniques were tried, as well as various etching solutions. Apparently the sheet stock had a very tenacious oxide on it, which could be removed by abrasion and polishing. Some of the techniques tried introduced secondary problems, such as silicon and aluminum residues from the polishing compounds, and copper from the mounting block holding the pellets. These effects were detected in spectrographic analyses of the polished titanium and were eliminated. Following is an outline of the procedure that was found to produce the best diode characteristics.

Punch high-purity titanium, 0.020-inch thick, into pellets 0.076-inch in diameter. (The use of lubricants in punching was eliminated.)

Anneal in an argon atmosphere for 2 hours at 750°C.

Cement pellets on a holder and rough-grind using SiC papers. Semi-finish using emery paper. Perform initial polishing with 6 μ diamond compound using a silk cloth on a Buehler wheel, followed by a final polish with No. 2 Alpha polishing alumina on a soft microcloth.

Remove pellets from the holder and degrease in acetone. Etch in the following solution^{11,14} for 15 sec:

400 cc 70 percent HNO₃
100 gm ammonium bifluoride
200 cc hydrofluorosilicic acid (48%)/H₂O to make
one litre

Immediately after etching, place the pellets in the furnace and oxidize in steam at 650°C for 3 hours.

After oxidation, sandblast the unpolished surface of the pellets to expose the titanium metal.

Apply surface electrodes.

Several significant features in the procedure should be explained.

The annealing step following punching was included to relieve any strains set up in the metal. It was observed that better diode characteristics were obtained on the sheet from which the pellets were punched than on the pellets themselves.

Chloride solvents were discontinued for degreasing.

The anodizing step was omitted since good characteristics were obtained without it. It is believed that the anodic oxide is a thin layer on the surface of the thermal oxide, and easily punctured during assembly. This may be related to some of the earlier failures of the cathodes during emission tests.

REFERENCES

1. D. V. Geppert and B. V. Dore, "Cold Cathodes for Low-Noise TWT Applications," First Quarterly Report, Contract SRI 010165, SRI Project 5175, Stanford Research Institute, Menlo Park, California (October 1964).
2. C. A. Mead and W. G. Spitzer, Phys. Rev. **134**, p. A713 (1964).
3. D. A. Wright, Proc. Phys. Soc. London **60**, pp. 13-22 (January 1948).
4. W. D. Johnston, J. Electrochem. Soc. **110**, No. 2, pp. 117-119 (February 1963).
5. R. K. Willardson and H. L. Goering, Compound Semiconductors, p. 476, (Reinholdt Publishing Corp., New York, New York 1962).
6. H. K. Henisch, Rectifying Semiconductor Contacts, Ch. 7, (Oxford University Press, New York, 1957).
7. J. Bardeen, Phys. Rev. **71**, p. 717 (1947).
8. See, for example, A. M. Cowley and S. M Sze, paper to be published in J. Appl. Phys. (October 1965).
9. G. E. Moore and H. W. Allison, Phys. Rev. **77**, p. 246 (15 January 1950).
10. D. V. Geppert, "Research on Cold Cathodes," First Quarterly Report, Contract NAS 5-9581, SRI Project 5511, Stanford Research Institute, Menlo Park, California (August 1965).
11. D. V. Geppert and B. V. Dore, "Cold Cathodes for Low-Noise TWT Applications," Third Quarterly Report, Contract SRI 01065, SRI Project 5175, Stanford Research Institute, Menlo Park, California (March 1965).
12. T. I. Komolova and D. N. Nasledov, Radio Eng. & Electronics **4**, p. 175 (April 1960).
13. R. G. Breckenridge and W. R. Hosler, J. Res. Nat. Bureau of Standards **49**, p. 65 (August 1952).
14. J. G. Beach, U.S. Patent No. 2,711,364 (June 21, 1955).

STANFORD
RESEARCH
INSTITUTE

MENLO PARK
CALIFORNIA

Regional Offices and Laboratories

Southern California Laboratories
820 Mission Street
South Pasadena, California 91031

Washington Office
1000 Connecticut Avenue, N.W.
Washington, D.C. 20006

New York Office
270 Park Avenue
New York, New York 10017

Detroit Office
1025 East Maple Road
Birmingham, Michigan 48011

Chicago Office
103 S. Stone Avenue
La Grange, Illinois 60525

Huntsville, Alabama
4810 Bradford Drive, N.W.
Huntsville, Alabama 35800

European Office
Pelikanstrasse 37
Zurich 1, Switzerland

Japan Office
Nomura Securities Building
1-1 Nihonbashidori, Chuo-ku
Tokyo, Japan

Retained Representatives

Toronto, Ontario, Canada
Cyril A. Ing
67 Yonge Street, Room 710
Toronto 1, Ontario, Canada

Milan, Italy
Lorenzo Franceschini
Via Macedonio Melloni, 49
Milan, Italy